

Zero-Sequence Currents in High-Voltage Power Systems During Normal Operation

Citation for published version (APA):

Nauta, S. (2021). *Zero-Sequence Currents in High-Voltage Power Systems During Normal Operation*. [Phd Thesis 1 (Research TU/e / Graduation TU/e), Electrical Engineering]. Technische Universiteit Eindhoven.

Document status and date:

Published: 20/12/2021

Document Version:

Publisher's PDF, also known as Version of Record (includes final page, issue and volume numbers)

Please check the document version of this publication:

- A submitted manuscript is the version of the article upon submission and before peer-review. There can be important differences between the submitted version and the official published version of record. People interested in the research are advised to contact the author for the final version of the publication, or visit the DOI to the publisher's website.
- The final author version and the galley proof are versions of the publication after peer review.
- The final published version features the final layout of the paper including the volume, issue and page numbers.

[Link to publication](#)

General rights

Copyright and moral rights for the publications made accessible in the public portal are retained by the authors and/or other copyright owners and it is a condition of accessing publications that users recognise and abide by the legal requirements associated with these rights.

- Users may download and print one copy of any publication from the public portal for the purpose of private study or research.
- You may not further distribute the material or use it for any profit-making activity or commercial gain
- You may freely distribute the URL identifying the publication in the public portal.

If the publication is distributed under the terms of Article 25fa of the Dutch Copyright Act, indicated by the "Taverne" license above, please follow below link for the End User Agreement:

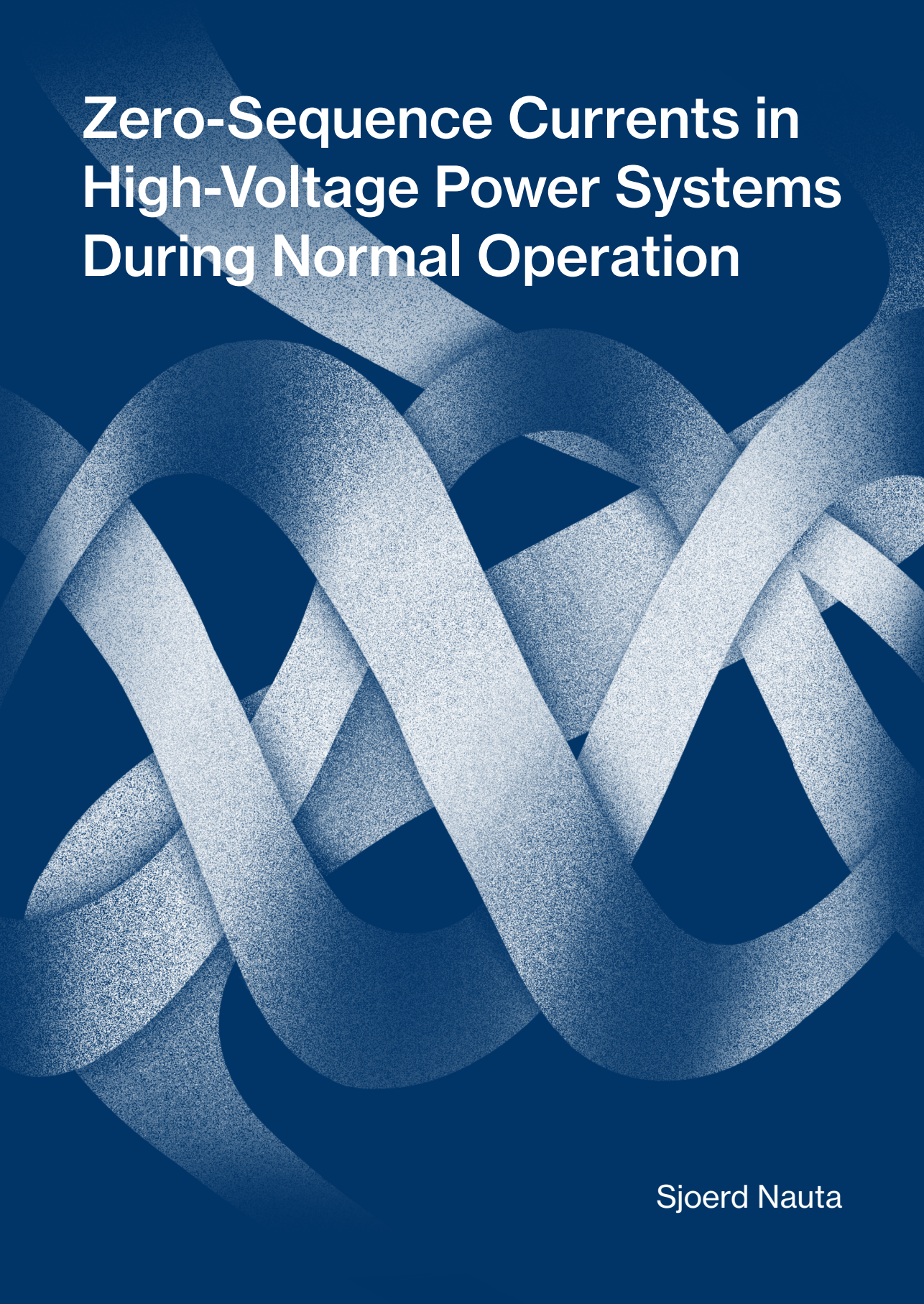
www.tue.nl/taverne

Take down policy

If you believe that this document breaches copyright please contact us at:

openaccess@tue.nl

providing details and we will investigate your claim.



Zero-Sequence Currents in High-Voltage Power Systems During Normal Operation

Sjoerd Nauta

Zero-Sequence Currents in High-Voltage Power Systems During Normal Operation

PROEFSCHRIFT

ter verkrijging van de graad van doctor aan de Technische Universiteit Eindhoven, op gezag van de rector magnificus prof.dr.ir. F.P.T. Baaijens, voor een commissie aangewezen door het College voor Promoties, in het openbaar te verdedigen op 20 december 2021 om 11:00 uur

door

Sjoerd Nauta

geboren te Delft

Dit proefschrift is goedgekeurd door de promotoren en de samenstelling van de promotiecommissie is als volgt:

voorzitter:	prof.dr.ir. M. Misch	
1e promotor:	prof.dr.ing. A.J.M Pemen	
co-promotor:	dr. R. Serra	
leden:	prof.dr.ir. J.F.G. Cobben	
	prof.dr.ir. F.B.J. Leferink	Universiteit Twente
	dr.ir. M. Popov	Technische Universiteit Delft
adviseur:	ir. W.F. van den Akker	
	dr.ir. J.B.M. van Waes	

Het onderzoek of ontwerp dat in dit proefschrift wordt beschreven is uitgevoerd in overeenstemming met de TU/e Gedragscode Wetenschapsbeoefening.

This work was made possible by the support of Alliander.

Printed by Ipskamp Printing, Enschede
Cover design by Yuan Valk

A catalogue record is available from the Eindhoven University of Technology Library

ISBN 978-90-386-5423-2
NUR 959

Copyright © 2021 by Sjoerd Nauta.
All Rights Reserved.

Voor mijn ouders.
Voor jullie onvoorwaardelijke liefde.

Summary

Zero-Sequence Currents in High-Voltage Power Systems During Normal Operation

Infrastructure is the backbone of modern society. Many of society's needs are fulfilled by a mostly invisible web of systems, which are becoming increasingly complex and interconnected. Besides a constant development of infrastructures to cope with these needs, there is an increasing tendency to bundle infrastructures together to efficiently make use of the available space. This is in particular the case in a small and densely populated country such as the Netherlands. It is pivotal that infrastructures can be operated as intended without negative impact from other nearby systems. One of the ways in which infrastructures can be impacted is through electromagnetic interference. This dissertation focuses on the electromagnetic compatibility between the high voltage infrastructure of the electrical power grid and other infrastructures in its vicinity. In particular, it focuses on one important aspect of electromagnetic interference, which is interference of systems by magnetic fields generated by zero-sequence current unbalance during steady-state conditions in high voltage infrastructure. Relative to positive-sequence currents and negative-sequence currents, zero-sequence current generate a relatively large magnetic field due to the absence of the compensating effect of phase shift between the different phase currents. There is however little literature available on the levels of zero-sequence currents that one can expect during normal operation. Furthermore, when levels are presented, for example by means of measurement, the uncertainty levels of those measurements are currently not available in literature. The aim of this dissertation

is to observe the dynamical behavior of zero-sequence currents in high voltage systems during steady-state conditions by means of field measurements.

The current state of the art in literature concerning zero-sequence current behavior during steady-state conditions shows that there are two main causes of zero-sequence currents in high voltage systems: firstly, by a geometric unbalance between conductors in transmission lines, which can be either overhead or underground; secondly, zero-sequence currents can be caused by the presence of unbalanced loads. A distinction can be made between circulating and through zero-sequence currents in transmission lines that consist of multiple parallel circuits. The way that zero-sequence currents propagate between voltage levels depends on the design of the power transformers that are utilized in the network. Furthermore, the meshed nature of high voltage systems complicates the behavior of zero-sequence currents because of the large number of possible paths through which the zero-sequence current can close.

Since zero-sequence currents during steady-state conditions are small in proportion to positive-sequence currents, it is challenging to perform measurements, because zero-sequence current levels can be of the same order as the measurement uncertainty of the instruments that are used to perform the measurement with. To gain insight into measurement uncertainty under these circumstances, three practically applicable measurement strategies are analyzed in this dissertation using two complementary methods of analysis. The outcome of these analyses is that the most precise strategy of measuring zero-sequence currents by simultaneously measuring the combination of the three phase leads. The developed models for measurement uncertainty are validated by means of laboratory measurements.

The developed methods for measuring zero-sequence currents during steady state operation are applied to several field measurement campaigns in the grid. The goals of these measurement is to analyze the dynamical behavior of zero-sequence currents during steady state conditions - including the analysis of measurement uncertainty - and to provide a general description of phenomena that were observed during these measurements. The specific conclusions associated with these measurements relate to the observed behavior during these field measurements. Care must be taken if one wants to generalize these conclusions in a different scenario. In principle, the results from the field measurements are only pertinent to the observed scenarios.

The first case study entails a measurement campaign in two coupled and transposed hybrid 150 kV branches. These branches consist out of a combination of overhead lines and underground cables with transpositions and shows that a nonzero zero-sequence current is present in the branches, taking into account the measurement uncertainty of the measurement system. During the measurement campaign, several modes of operation were observed: daily fluctuations, the effect of one of the measured branches being brought out of service and the effect of large and sudden load fluctuations due to external causes. During daily fluctuations, it was observed that the dynamic range of the zero-sequence current signal is smaller than the dynamic range of the positive-sequence current. While one of the branches was out of service, the zero-sequence current in the remaining branch increased significantly due to the increased load in a third parallel branch. Finally, while large and sudden load fluctuations were observed in the positive-sequence current, these fluctuations were not observed in the zero-sequence current.

Several sets of measurement data that were obtained by Phasor Measurement Units (PMUs) in 380 kV branches were studied in the second set of case studies, where the measurement accuracy of the measurement system was also taken into account. The first situation that is studied entails an untransposed double-circuit overhead transmission line. A decomposition of the measured zero-sequence currents in the transmission line shows that the ratio of the circulating zero-sequence current to the total positive-sequence current is stationary within the measurement accuracy of the measurement system. The ratio of the through zero-sequence current to the total positive-sequence current is found not to be stationary. In the second situation, the effect of a newly built substation within an existing meshed network of high voltage branches is studied. Here it was found that after commissioning of the substation, the ratio of the circulating zero-sequence current to the total positive-sequence current is not stationary. A possible explanation of this nonstationarity is that the parallel branches that are connected to the substation need not be connected to the same busbars at both ends, which means that the 'circulating' zero-sequence currents take a more convoluted path through the meshed network.

Samenvatting

Homopolaire stromen in hoogspanningssystemen tijdens normale bedrijfssituaties

Infrastructuur is de ruggengraat van de moderne maatschappij. Veel maatschappelijke behoeftes worden vervuld door een veelal onzichtbaar web van systemen, dat steeds complexer en meer onderling verbonden wordt. Naast een constante ontwikkeling van infrastructuren om te voldoen aan deze behoeftes is er een toenemende trend om infrastructuren samen te bundelen om efficiënt gebruik te maken van de beschikbare ruimte. Dit is met name het geval in kleine en dichtbevolkte landen zoals Nederland. Het is van groot belang dat infrastructuren hun taak kunnen uitvoeren zoals bedoeld zonder dat deze negatief worden beïnvloed door nabije systemen. Eén van de manieren waarop infrastructuren kunnen worden beïnvloed is als gevolg van elektromagnetische interferentie. Dit proefschrift richt zich op de elektromagnetische compatibiliteit tussen de hoogspanningsinfrastructuur van het elektriciteitsnetwerk en andere infrastructuren in de nabijheid. In het bijzonder richt het proefschrift zich op één belangrijk aspect van elektromagnetische interferentie, namelijk de interferentie met andere systemen als gevolg van magneetvelden die worden veroorzaakt door homopolaire stromen gedurende normale bedrijfssituaties in het hoogspanningsnet. In verhouding tot de directe- en inverse component veroorzaken homopolaire stromen relatief hoge magneetvelden als gevolg van het

ontbrekende dempende effect van faseverschuiving tussen de fasestroomcomponenten. Er is echter weinig literatuur beschikbaar die beschrijft hoe groot de homopolaire stromen zijn die kunnen worden verwacht tijdens normale bedrijfssituaties. Daarnaast worden er, daar waar niveaus worden beschreven, die bijvoorbeeld zijn verkregen door middel van metingen, geen uitspraken gedaan over de meetnauwkeurigheid die geassocieerd is met de betreffende metingen. Het doel van dit proefschrift is om het dynamisch gedrag van homopolaire stromen gedurende normale bedrijfssituaties te observeren door middel van metingen in het veld.

De huidige stand van de techniek in de wetenschappelijke literatuur met betrekking tot homopolaire stromen gedurende normale bedrijfssituaties laat zien dat er twee hoofdoorzaken zijn voor de aanwezigheid van homopolaire stromen in hoogspanningssystemen: ten eerste worden homopolaire stromen veroorzaakt door geometrische onbalans tussen geleiders in hoogspanningsverbindingen, die zowel bovengronds als ondergronds kunnen zijn; ten tweede worden homopolaire stromen veroorzaakt door ongebalanceerde belastingen. Er kan onderscheid worden gemaakt tussen circulerende en doorgaande homopolaire stromen in hoogspanningsverbindingen die uit meerdere circuits bestaan. De propagatie van homopolaire stromen tussen verschillende spanningsniveaus is afhankelijk van het ontwerp van vermogenstransformatoren in het netwerk. Daarnaast leidt het vermaasde ontwerp van hoogspanningsnetten ertoe dat homopolaire stromen op een geconvolueerde manier door het netwerk worden getransporteerd, vanwege het grote aantal mogelijke paden waarlangs de homopolaire stroom kan lopen.

Aangezien homopolaire stromen tijdens normale bedrijfssituaties klein zijn in verhouding tot de directe stroomcomponent is het uitdagend deze te meten. Homopolaire stromen kunnen namelijk van dezelfde orde van grootte zijn als de meetonzekerheid van de instrumenten waarmee wordt gemeten. Om inzicht te verkrijgen over de meetnauwkeurigheid onder deze omstandigheden worden in dit proefschrift drie praktisch toepasbare meetmethodes geanalyseerd door gebruik te maken van twee complementaire analysemethodes. De uitkomsten van deze analyses zijn dat de meest nauwkeurige meetmethode gebruikt maakt van een enkel meetinstrument dat de drie fasecomponenten simultaan meet. De ontwikkelde modellen voor de analyse van de meetonzekerheid zijn gevalideerd door middel van metingen in een laboratoriumopstelling.

De ontwikkelde methoden voor het meten van homopolaire stromen tijdens normale bedrijfssituaties zijn toegepast op meerdere veldmetingen in het hoogspanningsnet. Het doel van deze metingen betreft het analyseren van het dynamische gedrag van homopolaire stromen tijdens normale bedrijfssituatie - inclusief de analyse van de meetnauwkeurigheid - en het op hoofdlijnen beschrijven van fenomenen die tijdens de metingen zijn geobserveerd. De specifieke conclusies hieronder zijn verbonden aan de observaties tijdens de veldmetingen. Daarom moet zorg worden betracht indien men de conclusies wil toepassen op andere scenario's. De resultaten van de veldmetingen zijn in principe alleen van toepassing op de veldmetingen.

De eerste gevalstudie betreft een meetcampagne in twee gekoppelde en getransponeerde hybride 150kV-verbindingen. De verbindingen bestaan uit een combinatie van bovengrondse lijnen en ondergrondse kabels. De gevalstudie laat zien dat er een eindige homopolaire stroom aanwezig is in de verbindingen, rekening houdend met de meetnauwkeurigheid van het meetsysteem. Tijdens de meetcampagne zijn verschillende operatiemodi gevonden: dagelijkse fluctuaties, het effect van het uit bedrijf nemen van één van de gemeten verbindingen en grote fluctuaties als gevolg van externe invloeden. Tijdens de dagelijkse fluctuaties is vastgesteld dat het dynamisch bereik van het homopolaire stroomsignaal kleiner was dan dat van het directe stroomsignaal. Terwijl één van de verbindingen buiten bedrijf was, bleek dat de homopolaire stroom in de overgebleven verbinding significant toenam vanwege de toegenomen belasting in een derde circuit dat parallel loopt aan de twee bemeeten verbindingen. Ten slotte werden de grote en plotselinge fluctuaties van de belasting wel waargenomen in het directe stroomsignaal, maar niet in het homopolaire stroomsignaal.

Verschillende datasets met meetdata die zijn vastgelegd door middel van *Phasor Measurement Units* (PMUs) in 380kV-verbindingen zijn geanalyseerd in de tweede verzameling gevalstudies. Ook hier is rekening gehouden met de meetnauwkeurigheid van het toepaste meetsysteem. De eerste bestudeerde situatie betrof een niet getransponeerde bovengrondse lijn die bestaat uit twee parallelle circuits. De decompositie van de gemeten homopolaire stromen in de verbinding laat zien dat de verhouding tussen de circulerende homopolaire stroom en totale directe stroom stationair is. De verhouding tussen de doorgaande homopolaire stroom en de totale directe stroom is niet stationair. Bij de tweede bestudeerde situatie is het effect bestudeerd dat het in bedrijf nemen van een nieuw onderstation in een bestand

vermaasd netdeel heeft gehad op de aldaar voorkomende circulerende en doorgaande homopolaire stromen. De uitkomst van deze tweede gevalstudie is dat na de inbedrijfname van het nieuwe onderstation de gemeten verhouding tussen de circulerende homopolaire stroom en de totale directe stroom niet stationair is. Een mogelijke verklaring voor het niet stationair zijn van de circulerende homopolaire stroom is dat de parallelle circuits niet zijn aangesloten op dezelfde onderstationrails aan beide zijden van de verbinding, waardoor de 'circulerende' homopolaire stroom een gecompliceerd pad volgt door het vermaasde netwerk.

Contents

Summary	vii
Samenvatting	xi
1 Introduction	1
1.1 Electromagnetic Compatibility	2
1.2 Infrastructures and EMC	3
1.3 Sequence currents and magnetic fields	6
1.4 Problem statement	7
1.5 Aim and scope of this dissertation	8
1.6 Dissertation outline	9
2 Zero-sequence current unbalance during normal operation	11
2.1 The method of symmetrical components	12
2.2 Transmission line impedance	19
2.3 Earth return currents	23
2.4 Zero-sequence current unbalance in overhead lines	31
2.5 Zero-sequence current unbalance in cable systems	37
2.6 Zero-sequence current propagation between voltage levels	43
2.7 External sources of zero-sequence current unbalance	46
2.8 Zero-sequence currents in radially connected networks	47
2.9 Magnetic fields due to zero-sequence currents	48
2.10 Summary and conclusions	51

3	Zero-sequence current measurement uncertainty during normal operation	53
3.1	Introduction	53
3.2	Zero-sequence current measurement techniques	56
3.3	Measurement uncertainty analysis of secondary current measurements	62
3.4	Analytical approach to error analysis	65
3.5	Error analysis using Monte Carlo simulations	69
3.6	Comparison between the analytical method and the MC simulation method	72
3.7	Validation measurements and simulations	75
3.8	Summary and conclusions	78
4	Zero-sequence current measurements in the 150 kV grid using the direct method	81
4.1	Introduction	81
4.2	A hybrid transposed transmission line in a meshed network	82
4.3	Measurement setup	84
4.4	Measurement chain accuracy	86
4.5	Measurement results and analysis	88
4.6	Summary and conclusions	98
5	Zero-sequence currents and unbalance factors: two case studies	101
5.1	Introduction	101
5.2	Measurement setup	102
5.3	Measurement chain accuracy	103
5.4	Circulating and through zero-sequence currents in parallel circuits .	105
5.5	A newly included substation in the existing network	110
5.6	Summary and conclusions	115
6	Conclusions, contribution and further research	117
6.1	Conclusions	118
6.2	Dissertation contribution	120
6.3	Recommendations for future research	121
6.4	Practical recommendations for measurement and modeling of zero- sequence currents	122

Appendices	125
A OHL zero-sequence impedance expressions for several situations	125
B Earth return currents according to Carson	129
C Earth return currents according to Pollaczek	133
D Carson series definitions	135
E EMTP model of parallel circuit transmission line	137
F Error propagation in unbalance factors	141
Bibliography	143
List of Publications	155
Acknowledgements	157
Curriculum Vitae	161

Chapter 1

Introduction

Infrastructure is the backbone of modern society. Many of society's needs are fulfilled by a mostly invisible web of systems, which are becoming increasingly complex and interconnected [1]. Examples of such infrastructures are the electric power grid, gas infrastructure and road and rail infrastructures. Furthermore, societies undergo constant change and, consequently, their needs change as well. With society's needs changing, infrastructures also need to change to cope with these changing needs. Examples of such changes are the increasing world population and climate change, which requires society to switch to more sustainable carbon-neutral sources of energy (i.e. the renewable energy transition [2]–[4]).

The development and operation of infrastructures is however faced by many challenges. For example, in a small and densely populated country like the Netherlands, the available space for infrastructure is limited. This leads to a tendency to bundle different types of infrastructure together [5]. However, it is pivotal that the different infrastructures can operate as intended without negatively being impacted by other nearby systems. One of the ways in which infrastructure can be negatively impacted by other (nearby) systems is through electromagnetic interference.

This dissertation focuses on the electromagnetic compatibility between the high voltage infrastructure of the electrical power grid and other infrastructures in its vicinity, such as railway infrastructure or gas infrastructure. In particular, this dissertation focuses on one important aspect of electromagnetic compatibility, which

is the electromagnetic interference of systems by magnetic fields generated by zero-sequence currents in high voltage infrastructure.

This introductory chapter will first treat the concepts of electromagnetic compatibility, which is the study of the capability of a system to operate according to its intended use in the presence of electromagnetic interference by other systems in its vicinity without introducing too much disturbance to other systems (Section 1.1). Next, examples of relevant infrastructures will be described with respect to their electromagnetic properties in Section 1.2. Furthermore, an important concept in three-phase high voltage systems is the unbalance between phase currents and voltages, which can be described by means of the method of symmetric components, which is introduced in section 1.3. Section 1.4 introduces the problem statement that this dissertation aims to address. Next, the aim and scope of the dissertation are presented in section 1.5 and an outline of the dissertation is given in section 1.6.

1.1 Electromagnetic Compatibility

To properly operate a given system in an electromagnetic environment, it is important that this system is sufficiently *immune* to external sources of disturbance and that it does not *emit* too much electromagnetic interference into its surroundings [6], [7]. The discipline of electromagnetic compatibility (EMC) studies these system properties and aims to ensure that all systems are sufficiently compatible to operate in each other's vicinity [6]. EMC is a field of research that spans from small spatial scales (e.g. on the IC level [8]) to much larger scales (e.g. on the level of infrastructures [9]).

The ability of a system not to be disturbed by electromagnetic signals up to a certain level is indicated by the system's *immunity* [6]. The ability of a system to not disturb its surroundings above a certain level is indicated by the system's *emission* [6]. Levels can be determined that indicate the minimum immunity (i.e. the immunity level) and the maximum emission (i.e. the emission limit). In general, these levels are dependent on the frequency content of a disturbing electromagnetic signal. For many types of equipment, emission and immunity levels are formalized in international norms, such as the IEC 61000-series [10].

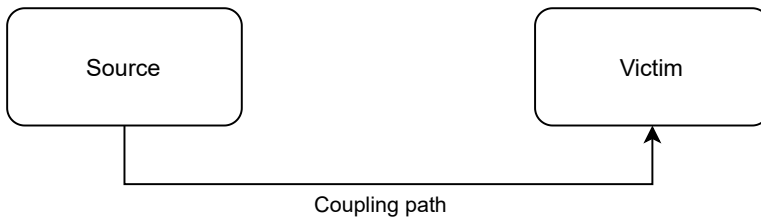


Figure 1.1: A general model for electromagnetic interference, including a source, a coupling path and a victim.

A general heuristic for the way systems behave in an EMC context is shown in figure 1.1. A *source* (the emitter) may emit a disturbing signal, which is coupled to a *victim* (a possibly susceptible system) through a *coupling path*. Several modes of electromagnetic coupling can be identified [6]: coupling through direct electrical connections (conductive coupling), coupling through the magnetic field (inductive coupling), coupling through the electric field (capacitive coupling) and coupling through radiation (radiative coupling). The difference between inductive and capacitive coupling on one hand and radiative coupling on the other hand is determined by the electrical distance between source and victim expressed in units of wavelength. For example, a 50 Hz power frequency electromagnetic wave has a wavelength in vacuum of $\lambda = \frac{c}{f} = 6000$ km, where c^1 is the speed of light. Whereas inductive and capacitive interference is concerned with inter-system distances smaller than or approximately equal to the wavelength, radiative coupling is associated with distances much larger than the wavelength of the signal. This dissertation is concerned with phenomena at low frequencies (e.g. 50 Hz, as this is the AC power system frequency in Europe and many other countries around the world) and therefore only the first three coupling modes of coupling will be considered.

1.2 Infrastructures and EMC

As was introduced in the preceding sections, infrastructures can also be subject to EMC issues and it is therefore important that the different types of infrastructure can function in each other's vicinity without being unacceptably disturbed. This section will go into more detail on the specific properties of several important types of infrastructures with respect to EMC.

¹299 792 458 m/s in vacuum.

Electrical transmission and distribution power systems

The purpose of electrical transmission and distribution power systems is to transport and deliver electrical energy from a generator to a load. This is done through an intricate and heavily interconnected network of components and systems, such as power transformers, overhead transmission lines and underground cables. Moreover, an important feature of the electricity grid is that many generators and loads are connected through often intricately meshed networks. These generators and loads, as well as the network itself, continually change in time, which makes the dynamic behavior of load flows highly complex. An important and relatively recent trend in the electrical power grid is the shift from unidirectional power flows (i.e. from centralized sources of generation towards the different loads) to a bidirectional power flows. In the latter case, many dispersed generators contribute to the whole system [11] and a decreasing amount of redundancy is allotted to accommodate generation of renewable electrical energy [12]. To accommodate to such grid behavior, grid operators modify their networks by including an increasing amount of so-called smart components and systems into the network [13]. However, these smart components can also bring along particular EMC issues [13], [14], such as issues concerning power electronic interfaces, smart meters and power line communication [13] and possible interference of short circuit currents with the correct operation of remote measurement and control electronics [14].

The issues mentioned above are *intra*-system electromagnetic interference issues [7], meaning that the issues concern EMC within the electricity infrastructure under investigation. The electricity grid can however also experience *inter*-system EMC issues, due to the electromagnetic fields that are inherently associated with the voltages and currents in the electricity grid. The next two subsections will go into more detail on the risks associated with inter-system electromagnetic interference between the electricity grid and two important infrastructures: the pipeline infrastructure and the railway infrastructure.

Pipeline infrastructure

Pipeline infrastructure fulfills different roles in transporting bulk materials such as water (both drinking water as well as heated water), oil or oil-derived products

and gases (both natural gas as well as synthetically produced gases such as hydrogen gas). Due to the desirable mechanical characteristics of certain metallic materials, such as steel, pipeline infrastructures are often built out of metallic (and thus conductive) materials. An example of this is the high-pressure gas infrastructure in the Netherlands, which is fully operated with steel pipelines. To protect these pipelines, the steel pipes are usually protected by a non-conducting outer layer, such as polyethylene (PE), in combination with cathodic protection to protect against unwanted corrosion of the steel.

A downside of using conductive pipeline infrastructures is the fact that this type of infrastructure can be sensitive to electromagnetic interference from outside sources, such as inductive coupling with nearby high voltage infrastructure [15]. Two main types of risk are associated with this interference: firstly, due to the inductive coupling, an unacceptably high voltage may be induced on the pipeline, which could lead to a hazard to personnel carrying out maintenance work on the pipelines [15]; secondly, when isolation defects are present on the pipeline, induced alternating voltages can cancel out the applied cathodic protection voltage for certain parts of the cycle of the alternating voltage. This last phenomenon is known as AC corrosion [16].

In practice, electromagnetic interference calculations are carried out according to established standards² to assess the possible risks associated with the interference prior to the construction of new electricity infrastructure or pipeline infrastructure. If the outcome of these calculations is such that the analyzed risks are unacceptable, preventive measures are proposed to mitigate the risks.

Railway infrastructure

Electrified railways are another type of infrastructure that can be associated with electromagnetic interference within itself and between itself and the electricity grid. Railway infrastructure consists of several systems that might be compromised by EM interference issues, such as signalling and telecommunication systems or step-and touch voltages [17].

As an example, the railway infrastructure in the Netherlands is for a large part operated with a 1500 V DC traction system, which is controlled by an GRS track

²In the Netherlands, the mutual interference between pipeline infrastructure and electrical infrastructure is described in the national standard NEN 3654.

relais system that operates in the majority of cases in the Netherlands at 75 Hz. The GRS system is characterized by certain immunity levels, which are dependent on time, current, the presence of currents in neighbouring tracks and the type of relay that is installed locally [17]. The immunity level is also dependent on the number of tracks through which the return current of the GRS system is allowed to pass (single or double track return), where the single track return has lower immunity levels [17].

Several possible sources of EM interference on railway infrastructure can be identified [18], [19]: rolling stock (i.e. trains on the track), which can contain noisy power electronics; signaling equipment; (DC) substations for tractions; or external sources, such as nearby high voltage infrastructure.

For situations where railway infrastructure and high voltage infrastructure are constructed in each other's vicinity, electromagnetic interference studies are also carried out to assess the possible risks and to determine the necessary preventive mitigating measures³.

1.3 Sequence currents and magnetic fields

In perfectly balanced three-phase power systems during normal operation⁴, all three phases are equal in amplitude and the phase angle difference between phase voltages and currents is exactly 120° . In reality however, phase voltages and/or phase currents are in general not equal in amplitude and the phase angle differences are not exactly 120° . This unbalance between phase voltages or phase currents within a three-phase power system can be described by the method of symmetrical components [20], giving rise to the definitions of the positive-sequence, negative-sequence and zero-sequence voltages and currents (see (2.2)). Symmetrical components can be constructed for both three phase voltages as well as currents. While the mathematical description of symmetrical components is further elaborated in Chapter 2, the significance of this decomposition with respect to the resulting electromagnetic

³In the Netherlands, the mutual interference between railway infrastructure and electrical infrastructure is described in the railway guideline RLN00398.

⁴Normal operation or steady state conditions in this dissertation is understood as the situation in which the high voltage systems operates normally, i.e. not during (asymmetric) short-circuit conditions or other faulty or transient conditions.

fields and therefore the EMC with other systems in the vicinity of a high voltage three phase transmission line is demonstrated in this section.

From the definition of symmetrical components, it follows that the vectorial sum of the positive-sequence phase components⁵ and negative-sequence phase components of a three-phase system are equal to zero, since these phase components are symmetric and therefore share the same magnitude and have a phase angle difference of $\frac{2\pi}{3}$. The sum of zero-sequence phase components however is not equal to zero by definition: since the zero-sequence components of each phase share the same phase angle, the sum of the zero-sequence components is only equal to zero when the magnitude of the respective zero-sequence phase components is equal to zero. This property of the zero-sequence current components has a profound effect on the magnetic field of a high voltage transmission line that carries a zero sequence current.

The presence of a - relatively small - zero-sequence current can have a profound influence on the resulting magnetic field surrounding a transmission line. The contributions to the total magnetic field for a symmetrical current distribution (e.g. a positive-sequence current) cancel out at a larger distances, since the distance between conductors becomes negligible at a greater distance from the transmission line. However, this effect of mutual cancellation is not present with zero-sequence currents, since the zero-sequence components in each conductor share the same phase angle. The result is a more gradual decay of the magnetic field as a function of the distance to the transmission line.

1.4 Problem statement

The presence of zero-sequence currents around transmission lines in three-phase power systems leads to magnetic fields surrounding the transmission line and therefore may lead to unwanted inductive interference with nearby infrastructures. During normal operation - which in this dissertation is understood to be the situation in which the high voltage system operates in steady state conditions at nominal frequency (50 Hz in case of the Netherlands), i.e. not during short-circuit conditions, or other faulty or transient circumstances - zero-sequence currents are expected to be relatively small with respect to positive-sequence currents. The exact levels that

⁵E.g. I_{A1} for the positive-sequence current phase component of phase A, etc.

are to be expected in different situations are however not described extensively in literature. Moreover, where zero-sequence current levels are reported in literature, only single values at the maximum operating current of the system are given and the dynamical behavior of zero-sequence currents with respect to positive-sequence currents in time is lacking. One of the ways in which more insight could be gained on the dynamical behavior of zero-sequence currents during normal operation is through measurements.

When performing measurements, it is important to know the associated measurement uncertainty to be able to draw the right conclusions about the measurement outcomes. The relatively low levels of zero-sequence currents with respect to positive-sequence currents during normal operation make it challenging to perform accurate zero-sequence current measurements, taking into account the respective accuracies of the measurement instruments inside the measurement chain that is designed to measure these zero-sequence currents. A thorough analysis of measurement accuracy of zero-sequence currents during normal operation in three-phase power systems for such measurement chains is currently not available in literature.

1.5 Aim and scope of this dissertation

The main goal of this dissertation is to provide more insight into the dynamical behavior of zero-sequence currents during normal operation. This goal is achieved by means of the following interconnected subgoals:

- To provide an overview of the current state of the art in literature concerning the presence and behavior of zero-sequence currents in three-phase power systems during normal operation.
- To develop and validate methods to determine the measurement uncertainty of zero-sequence currents during normal operation for several measurement methods that can be and are applied to measurements in practice.
- To apply the methods to determine zero-sequence current measurement uncertainty, in order to observe the dynamical and time-dependent behavior of zero-sequence currents during steady-state conditions in field measurements in two scenarios:

- Using a dedicated setup to measure zero-sequence currents through the secondary currents of the current transformers present at a high voltage substation in two hybrid transposed high voltage branches.
- In several high voltage transmission lines where existing Phasor Measurement Units (PMUs) are installed.

As was stated above, the scope of this dissertation are zero-sequence currents during steady state conditions (non-short circuit circumstances). Since zero-sequence currents during short-circuit situations are much larger relative to positive-sequence currents, the relative measurement accuracy is better in these situations. The developed methods could, in principle, also be applied to these situations.

1.6 Dissertation outline

The chapters in this dissertation are built up in the following manner:

Chapter 2: Zero-sequence current unbalance during normal operation provides an overview of the current state of the art in literature concerning zero-sequence currents during normal operation. An extensive overview of the current state of the art with regards to this topic is currently not available in literature and Chapter 2 aims to address this gap.

Chapter 3: Zero-sequence current measurement uncertainty during normal operation provides novel methods to assess the measurement uncertainty associated with zero-sequence current measurements during normal operation, by means of a mathematical analysis of the measurement equations as well as Monte Carlo simulations of the respective measurement chains. As was stated in Section 1.4, no such methods are currently available in literature. In this chapter, the measurement uncertainty for these measurements is developed for three measurement strategies that could be used in practice. The Monte Carlo simulations and analytical expressions are also validated by means of laboratory measurements.

Chapter 4: Zero-sequence current measurements in coupled 150 kV transmission lines presents a case study in which two 150 kV transmission lines were measured for a period of approximately ten days. The results obtained in Chapter 3 were used to assess the measurement uncertainty for the measurement series.

Chapter 5: PMU measurements in 380 kV transmission lines presents two case studies of 380 kV transmission line in which existing Phasor Measurement Units were installed. The results from Chapter 3 were also applied in these cases to assess the measurement uncertainty related to these measurement series.

Chapter 6: Conclusions, contribution and further research summarizes the conclusions and contributions from the different chapters and provides recommendations for measurement practice and further research.

Chapter 2

Zero-sequence current unbalance during normal operation

During normal operation, zero-sequence currents can be present in power systems. As was discussed in the opening chapter of this dissertation, zero-sequence current unbalance can lead to a number of issues, such as undesired electromagnetic interference with nearby infrastructure. This chapter provides an overview of the state-of-the-art of knowledge on zero-sequence currents during normal operation and introduces the concepts, notation and terminology used in the remaining chapters of this dissertation.

Section 2.1 introduces the methods of symmetrical components and provides the necessary tool to understand zero-sequence current unbalance. The impedance matrix concept is also introduced. The contents of the impedance matrix is then elaborated upon in section 2.2. An important concept in the treatment of zero-sequence currents are currents returning through Earth. Section 2.3 gives an overview of the models that describe earth return currents for both overhead and underground transmission systems. Two important applications in which zero-sequence currents are caused and play an important role are overhead lines (section 2.4) and underground cable systems (section 2.5). These applications are treated in the mentioned sections. Zero-sequence currents can propagate between voltage levels through power transformers, depending on the winding and earthing of the transformer. This propagation is described in section 2.6. Section 2.7 outlines the ways in which

zero-sequence currents can be caused by external sources. Finally, section 2.9 describes the effect of zero-sequence currents on magnetic fields around transmission lines.

2.1 The method of symmetrical components

A sinusoidal signal that is described by an amplitude and a phase angle (with respect to a given reference) is called a phasor. A phasor can describe the behavior of different parameters of interest, such as a phase current or a line voltage. An arbitrary combination of a phasor triplet at the same frequency (such as the three phase currents within a single circuit of a transmission line) can be broken down into an equivalent system of three components called symmetrical components. This was shown in 1918 by C.L. Fortescue [20]. The method of symmetric components uses a matrix transformation to transform a set of three phasors into its symmetric components.

A three phase system, such as three phase voltages or three phase currents, can be described by six independent degrees of freedom: three amplitudes and three phase angles with respect to an arbitrary reference. The phase voltages or phase currents can be described in vector form by defining a 1×3 -vector:

$$\begin{bmatrix} I_A \\ I_B \\ I_C \end{bmatrix} = \begin{bmatrix} |I_A| \cdot e^{j \cdot \arg I_A} \\ |I_B| \cdot e^{j \cdot \arg I_B} \\ |I_C| \cdot e^{j \cdot \arg I_C} \end{bmatrix}. \quad (2.1)$$

This current (or voltage) vector can be transformed into its respective symmetric components by means of the following transformation matrix T :

$$T = \begin{bmatrix} 1 & 1 & 1 \\ 1 & \alpha^2 & \alpha \\ 1 & \alpha & \alpha^2 \end{bmatrix},$$

where alpha is defined as $\alpha = e^{j \cdot \frac{2\pi}{3}}$, i.e. a phasor rotation over an angle of $\frac{2\pi}{3}$, or 120° . The symmetrical components of a set of phase currents or phase voltages is calculated by multiplying the phase vector by the transformation matrix, which

uses the inverse of the transformation matrix T :

$$\begin{bmatrix} I_0 \\ I_1 \\ I_2 \end{bmatrix} = \frac{1}{3} \begin{bmatrix} 1 & 1 & 1 \\ 1 & \alpha^2 & \alpha \\ 1 & \alpha & \alpha^2 \end{bmatrix} \begin{bmatrix} I_A \\ I_B \\ I_C \end{bmatrix}. \quad (2.2)$$

The inverted transformation T^{-1} allows us to reconstruct a set of three phasors out of its symmetrical components:

$$\begin{bmatrix} I_A \\ I_B \\ I_C \end{bmatrix} = \begin{bmatrix} 1 & 1 & 1 \\ 1 & \alpha & \alpha^2 \\ 1 & \alpha^2 & \alpha \end{bmatrix} \begin{bmatrix} I_0 \\ I_1 \\ I_2 \end{bmatrix}. \quad (2.3)$$

The result of the transformation are three symmetric components of the three-phase signal: the positive sequence current I_1 , the negative sequence current I_2 and the zero sequence current I_0 . Each phase current can therefore be written as a sum of three subterms, e.g. $I_A = I_{A0} + I_{A1} + I_{A2}$.

The positive sequence and negative sequence components of the phasor triplet have in common that both are symmetric, i.e. the three phase components in these sequences are equal in amplitude and are exactly $\frac{2\pi}{3}$ out of phase. When summing the three subterms of I_1 or I_2 , the factor $1 + \alpha + \alpha^2$ appears, which is equal to zero¹. The difference between the positive sequence and negative sequence is the order of the phases². The zero-sequence component is not symmetric. All three zero-sequence components of a phasor triplet have the same amplitude, but they also share the same phase angle. The sum of the three zero-sequence subterms therefore does not equal zero.

Example: Reconstruction of phase currents from symmetrical components.

Using the methods described above, we can reconstruct the three independent phase currents with different amplitudes and phases from their corresponding symmetrical components. For example, if we have the following combination of I_0 , I_1 and I_2 :

¹E.g. from ((2.3)): $I_{A1} + I_{B1} + I_{C1} = I_1 + \alpha I_1 + \alpha^2 I_1 = (1 + \alpha + \alpha^2) I_1 = 0$

²E.g. the positive sequence is ordered $A \rightarrow B \rightarrow C$ and the negative sequence is ordered $A \rightarrow C \rightarrow B$.

- $I_0 = 10/60^\circ$ A
- $I_1 = 100/90^\circ$ A
- $I_2 = 10/45^\circ$ A

This leads to the following phasor plot and corresponding phasor summations:

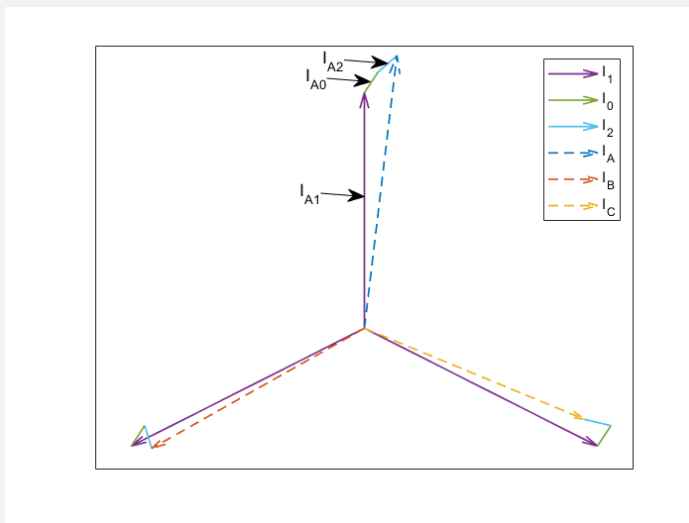


Figure 2.1: Graphical representation of the construction of phase vectors out of symmetrical components. Note that the vectors for I_1 (purple) and I_2 (light blue) are at an angle of 120° with each other and that the vectors associated with I_0 (green) all point in the same direction. The subterms for I_A are shown as an example.

The phasors I_A , I_B and I_C appear as follows in the time domain:

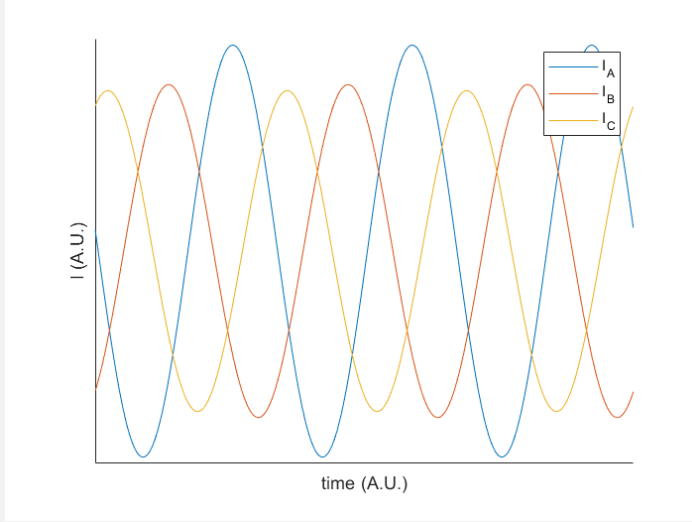


Figure 2.2: The current signals for I_A , I_B and I_C in the time domain.

2.1.1 Unbalance factors

For a given set of symmetrical components, one can define several unbalance factors that describe the relative value of the components. These unbalance factors express the amplitude of the zero-sequence current and negative-sequence current as a percentage of the amplitude of the positive-sequence current. During normal operation, these factors are generally smaller than 100%.

For the zero-sequence components in a single three-phase transmission circuit, the zero-sequence unbalance factor m_{I_0} is defined as follows:

$$m_{I_0} = \left| \frac{I_0}{I_1} \right| \times 100\%. \quad (2.4)$$

The negative-sequence unbalance factor can be defined in a similar fashion:

$$m_{I_2} = \left| \frac{I_2}{I_1} \right| \times 100\%. \quad (2.5)$$

In this dissertation, we shall mainly focus on zero-sequence unbalance.

For a transmission line that consists of multiple parallel circuits, one may also define the *circulating* unbalance factor [21]:

$$m_{c0} = \left| \frac{I_0^I - I_0^{II}}{I_1^I + I_1^{II}} \right| \times 100\%, \quad (2.6)$$

and the *through* unbalance factor [21]:

$$m_{t0} = \left| \frac{I_0^I + I_0^{II}}{I_1^I + I_1^{II}} \right| \times 100\%. \quad (2.7)$$

In these equations, the superscripts refer to the particular circuit in which a certain positive-sequence or zero-sequence current is present, as defined in figure 2.3. The circulating unbalance factor describes the zero-sequence current that circulates within the transmission line: its phase angle is opposite to the phase angle in the other circuit. Since the circulating zero-sequence current is not present outside of the transmission line, it is also referred to as the *internal* unbalance. The through unbalance is equal in phase in both circuits and passes through the entire transmission line.

Similarly to current unbalance factors, voltage unbalance factors can be defined. International norms are available that define limits to the maximum negative-sequence voltage unbalance factors as a function of the voltage level of the system under consideration (medium voltage, high voltage or extra high voltage) [22]. Such limits however do not exist for zero-sequence current unbalance levels.

2.1.2 The impedance matrix

The impedance matrix describes the relation between voltages and currents in a system. In a high voltage system, this consists of terms describing both the phase conductors and the ground conductors, if present. The relation between voltages and currents in a single-circuit transmission line with ground return with three phase conductors (r, s, t) and two ground conductors (v, w) is given by the following

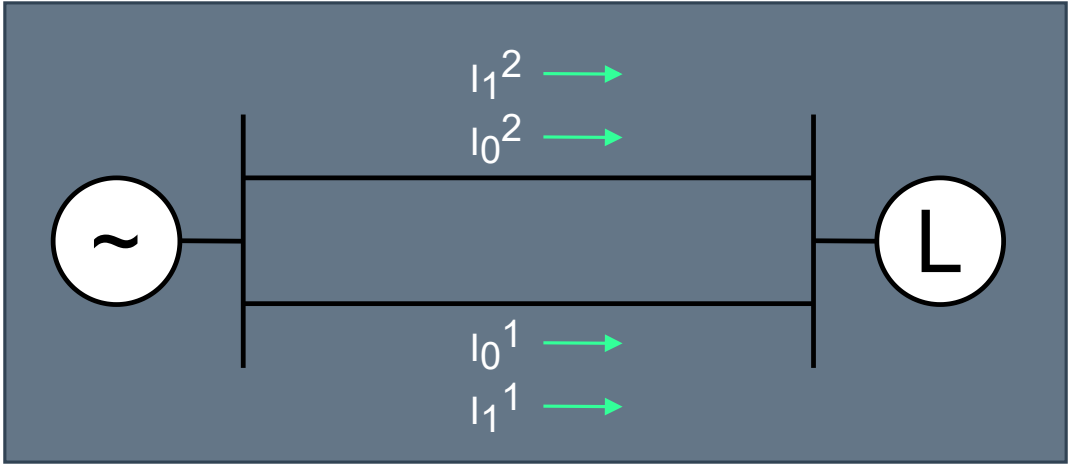


Figure 2.3: A schematic overview of a transmission line that consists of two parallel three-phase circuits. The respective positive-sequence current and zero-sequence current in circuit 1 are I_1^1 and I_0^1 . These components are also defined for circuit 2.

(5×5)-matrix [23]:

$$\begin{bmatrix} \Delta V_a \\ \Delta V_b \\ \Delta V_c \\ \Delta V_v \\ \Delta V_w \end{bmatrix} = \begin{bmatrix} Z_{aa-g} & Z_{ab-g} & Z_{ac-g} & Z_{av-g} & Z_{aw-g} \\ Z_{ba-g} & Z_{bb-g} & Z_{bc-g} & Z_{bv-g} & Z_{bw-g} \\ Z_{ca-g} & Z_{cb-g} & Z_{cc-g} & Z_{cv-g} & Z_{cw-g} \\ Z_{va-g} & Z_{vb-g} & Z_{vc-g} & Z_{vv-g} & Z_{vw-g} \\ Z_{wa-g} & Z_{wb-g} & Z_{wc-g} & Z_{wv-g} & Z_{ww-g} \end{bmatrix} \begin{bmatrix} I_a \\ I_b \\ I_c \\ I_v \\ I_w \end{bmatrix}. \quad (2.8)$$

Where ΔV_x is the voltage difference between the beginning and end of the transmission line, I_x are the conductor currents and Z_{xy} are the impedances between conductor x and y . A repeated index signifies a self-impedance (e.g. Z_{aa-g}) and an index with unequal term relates to a mutual impedance (e.g. Z_{ab-g}). A ground return current equal to the sum of all conductor currents is present to close the circuit. When the ground conductors are connected to earth on both ends, the respective voltages ΔV_v and ΔV_w are zero and the matrix may be reduced to a (3×3)-matrix [23]: Z_{ABC} . The expressions above can also be extended for transmission lines that consist of multiple circuits (in practice a high voltage transmission line consists out of two or three parallel circuits) [24]. The impedance matrix of a two-circuit transmission line with two ground conductors is the following:

$$\begin{bmatrix} \Delta V_a \\ \Delta V_b \\ \Delta V_c \\ \Delta V_d \\ \Delta V_e \\ \Delta V_f \\ \Delta V_v \\ \Delta V_w \end{bmatrix} = \begin{bmatrix} Z_{aa-g} & Z_{ab-g} & Z_{ac-g} & Z_{ad-g} & Z_{ae-g} & Z_{af-g} & Z_{av-g} & Z_{aw-g} \\ Z_{ba-g} & Z_{bb-g} & Z_{bc-g} & Z_{bd-g} & Z_{be-g} & Z_{bf-g} & Z_{bv-g} & Z_{bw-g} \\ Z_{ca-g} & Z_{cb-g} & Z_{cc-g} & Z_{cd-g} & Z_{ce-g} & Z_{cf-g} & Z_{cv-g} & Z_{cw-g} \\ Z_{da-g} & Z_{db-g} & Z_{dc-g} & Z_{dd-g} & Z_{de-g} & Z_{df-g} & Z_{dv-g} & Z_{dw-g} \\ Z_{ea-g} & Z_{eb-g} & Z_{ec-g} & Z_{ed-g} & Z_{ee-g} & Z_{ef-g} & Z_{ev-g} & Z_{ew-g} \\ Z_{fa-g} & Z_{fb-g} & Z_{fc-g} & Z_{fd-g} & Z_{fe-g} & Z_{ff-g} & Z_{fv-g} & Z_{fw-g} \\ Z_{va-g} & Z_{vb-g} & Z_{vc-g} & Z_{vd-g} & Z_{ve-g} & Z_{vf-g} & Z_{vv-g} & Z_{vw-g} \\ Z_{wa-g} & Z_{wb-g} & Z_{wc-g} & Z_{wd-g} & Z_{we-g} & Z_{wf-g} & Z_{wv-g} & Z_{ww-g} \end{bmatrix} \begin{bmatrix} I_a \\ I_b \\ I_c \\ I_d \\ I_e \\ I_f \\ I_v \\ I_w \end{bmatrix}, \quad (2.9)$$

where d, e, f are the conductors of the second circuit. The other elements are equal for the single-circuit case.

The impedance matrix of a transmission line is determined by the physical properties and positions of the conductors and surrounding dielectric media. Because of the complexity of determining the full impedance matrix this is often done by means of specialised software. Section 2.2 goes into further detail to understand the contents of the elements in the impedance matrix.

The reduced impedance matrix of phase currents can be transformed into symmetrical components through the following equation [23]:

$$Z_{012} = T^{-1}Z_{ABC}T. \quad (2.10)$$

This transformed matrix determines the relation between voltage and current in symmetrical components for a given three-phase system:

$$\begin{bmatrix} \Delta V_0 \\ \Delta V_1 \\ \Delta V_2 \end{bmatrix} = \begin{bmatrix} Z_{00} & Z_{01} & Z_{02} \\ Z_{10} & Z_{11} & Z_{12} \\ Z_{20} & Z_{21} & Z_{22} \end{bmatrix} \begin{bmatrix} I_0 \\ I_1 \\ I_2 \end{bmatrix}. \quad (2.11)$$

The inverse of this matrix is called the *admittance matrix* and gives the following relationship [25]:

$$\begin{bmatrix} I_0 \\ I_1 \\ I_2 \end{bmatrix} = \begin{bmatrix} y_{00} & y_{01} & y_{02} \\ y_{10} & y_{11} & y_{12} \\ y_{20} & y_{21} & y_{22} \end{bmatrix} \begin{bmatrix} \Delta V_0 \\ \Delta V_1 \\ \Delta V_2 \end{bmatrix}. \quad (2.12)$$

In a system where there is no zero-sequence or negative-sequence voltage (thus only positive-sequence voltage), this relationship simplifies to [25]:

$$\begin{bmatrix} I_0 \\ I_1 \\ I_2 \end{bmatrix} = \begin{bmatrix} y_{01} \\ y_{11} \\ y_{21} \end{bmatrix} \Delta V_1. \quad (2.13)$$

This relationship can be used to determine the unbalance factors in terms of sequence impedances [25]:

$$m_{10} = \frac{I_0}{I_1} = \frac{y_{01}}{y_{11}} = \frac{Z_{02}Z_{21} - Z_{01}Z_{22}}{Z_{00}Z_{22} - Z_{20}Z_{02}} \approx -\frac{Z_{01}}{Z_{11}}. \quad (2.14)$$

since $Z_{22} \gg Z_{02}, Z_{21}$ [21]. As will be discussed further on in this chapter, in case of a symmetric conductor arrangement there is no relation between the positive sequence and zero sequence, therefore $Z_{01} = 0$ and $m_{10} = 0$.

2.2 Transmission line impedance

The impedance of a transmission line is determined by four parameters: the resistance and the inductance (that together make up the series impedance of the transmission line) on one hand and the capacitance and the conductance (that together make up the admittance of the transmission line) [24]. During normal operation, two main modes of coupling between conductors can be distinguished: inductive coupling and capacitive coupling [24]. When the geometric spacing of conductors is not symmetric to one another, this will lead to current unbalance due to asymmetric mutual coupling. This is called the *inherent* asymmetry of a transmission line [26].

2.2.1 Inductive coupling

Inductive coupling is the coupling between conductors through the magnetic field: due to the current flowing in one conductor, a magnetic field will exist around that conductor. This magnetic field will induce a voltage in a different conductor. Inductive coupling depends on: the characteristics of the conductor (or conductor bundle); the distance to the secondary conductor; conductor length; and properties

of the medium between conductors. For three-phase systems, expressions can be found that define the system impedances as symmetric components.

As an example, the positive-sequence inductance of a single-circuit three-phase overhead transmission line is given by [27]:

$$L_1 = \frac{\mu_0}{2\pi} \left(\ln \frac{D_M}{r_B} + \frac{1}{4n} \right). \quad (2.15)$$

where L_1 is the per-unit positive-sequence inductance [H/m]; μ_0 is the vacuum magnetic permeability ($= 4\pi \cdot 10^{-7}$ H/m); D_M is the geometric mean distance³ between conductors [m]; r_B is the bundle conductor equivalent radius [m] (equal to the conductor radius r for a single conductor); and n is the number of conductors per bundle.

The geometric mean distance for a three-phase circuit is given by:

$$D_M = \sqrt[3]{D_{12} \cdot D_{23} \cdot D_{31}}, \quad (2.16)$$

where D_{nm} is the distance between the center of the conductor or conductor bundles n and m . The corresponding per-unit positive-sequence inductive reactance is given by: $X_1 = \omega L_1$. For overhead lines that contain more than one parallel three-phase circuits, the expressions for positive-sequence inductance and positive-sequence inductive reactance change slightly [27], [28].

Whereas the positive-sequence inductance is only dependent on the properties of the transmission line itself (i.e. the conductor properties and the geometric configuration of the conductors), the zero-sequence impedance is also dependent on the properties of the media surrounding the transmission line. In particular, since the earth is conductive, there will be an interaction between the currents in the transmission line and the earth itself since part of the zero-sequence current can close through earth. To model this, the earth return current is assumed to return as a mirrored conductor under the earth's surface. This model is discussed in detail in section 2.3.

³The geometric mean distance is defined as the harmonic mean of the distances between the conductors of the circuits [24].

In general, the self-impedance per unit length for an above-ground conductor with earth return is given by [28]:

$$Z_{self} = R + j \frac{\mu_0 \omega}{2\pi} \ln \frac{2h}{r} + \frac{\mu_0 \omega}{\pi} (P + jQ), \quad (2.17)$$

and the mutual impedance per unit length with other conductors is given by [28]:

$$Z_{mutual} = j \frac{\mu_0 \omega}{2\pi} \ln \frac{\bar{d}}{d} + \frac{\mu_0 \omega}{\pi} (P + jQ). \quad (2.18)$$

Here, Z_{self} and Z_{mutual} are the self- and mutual impedances respectively; R is the conductor resistance per unit length; ω is the radial frequency; h is the height above ground; r is the conductor radius; d is the distance between conductors; and \bar{d} is the distance between one conductor and the other conductor's mirror image. The functions $P(p, \theta)$ and $Q(p, \theta)$ account for the contribution of the earth return current to the total impedance. These functions can be expressed as indefinite integrals and approximations are given by Carson [29], which are further discussed in section 2.3.

For zero-sequence inductive impedance the following approximating expression is valid for a single-circuit line without earth wires:

$$Z'_0 = \frac{R'_1}{n} + \frac{3}{4} \frac{\mu_0 \omega}{\pi} + j \frac{\mu_0 \omega}{2\pi} \left(3 \cdot \ln \frac{\delta}{\sqrt[3]{r_B D_M^2}} + \frac{\mu_T}{4n} \right). \quad (2.19)$$

where R'_1 is the resistance per unit length of a single conductor in a bundle, ω is the radial frequency, μ_T is the relative permeability of the conductor material (= 1 for conductors made of non-ferromagnetic materials, e.g. aluminium or copper) and $\delta = \frac{1.85}{\sqrt{\mu_0 \omega / \rho}}$ is the return depth of the earth current [27]. The return depth is dependent on the frequency and the specific resistivity of the earth below the transmission line. For higher frequencies, the return depth decreases and for higher resistivities the return depth increases. Therefore, a higher specific resistivity of the earth will lead to an increased zero-sequence impedance of the transmission line. Adding one or more earth wires will change the zero-sequence impedance of the transmission line, since the return path for the zero-sequence current changes. Adding ground wires will decrease the zero-sequence impedance, *ceteris paribus*.

2.2.2 Capacitive coupling

Capacitive coupling is the coupling between conductors through the electric field. The capacitance between line and neutral in an overhead line with equilaterally spaced conductors is given by [23], [24]:

$$C_n = \frac{2\pi\epsilon_0}{\ln D/r}. \quad (2.20)$$

where ϵ_0 is the permittivity of vacuum ($\approx 8.85 \cdot 10^{-12}$ F/m), D is the spacing between phase conductors and r the radius of the conductor. In a balanced system, the line-to-neutral capacitance is equal to twice the line-to-line capacitance [24]. For instance, $C_n = C_{an} = C_{bn} = 2C_{ab}$. For systems in which conductors are not equilaterally spaced or systems that consist out of more than one circuit, the expression is more extensive and involves the distance between conductors and their mirror images below ground [23].

For a general three phase line, the following capacitance matrix can be constructed [23]:

$$C_{abc} = \begin{bmatrix} C_{aa} & -C_{ab} & -C_{ac} \\ -C_{ba} & C_{bb} & -C_{bc} \\ -C_{ca} & -C_{cb} & C_{cc} \end{bmatrix}. \quad (2.21)$$

In a symmetrical line, all diagonal elements are equal (denoted by C) and off-diagonal components are also equal (denoted by C'). Using (2.10), we can transform this matrix into symmetrical components [23]:

$$C_{012} = T^{-1}C_{abc}T = \begin{bmatrix} C - 2C' & 0 & 0 \\ 0 & C + C' & 0 \\ 0 & 0 & C + C' \end{bmatrix}. \quad (2.22)$$

This shows that for a equilaterally spaced, single-circuit overhead transmission line, there is no coupling between the positive-sequence and zero-sequence, since all off-diagonal terms are equal to zero⁴. In overhead lines that consist of more than one circuit, the distances between conductors need not be the same everywhere and there may be off-diagonal terms in the total capacitance matrix.

⁴It is also worthwhile to express C and C' as a function of C_0 , C_1 and C_2 in this case. Rearranging the equations for C_0 , C_1 and C_2 then gives: $C = \frac{1}{3}(C_0 + C_1 + C_2)$ and $C' = \frac{1}{3}(C_1 - C_0)$.

Since high-voltage underground cable systems have grounded conductors around each cable, there will be a negligible electric field outside of the grounded conductor. Therefore, there is no capacitive coupling between different cables present in high-voltage underground cable systems. In this case C' is equal to zero, since there are no off-diagonal capacitance terms. In this case, $C_1 = C_0$. The lack of capacitive coupling is valid for systems that consist out of single-phase cables as well as systems that consist of three-phase cables.

2.3 Earth return currents

Since the Earth has a finite electrical resistance, the current returning through earth should also be taken into account when describing an unbalanced three phase system. Two models that are used to describe the interactions between conductor currents and the current in the earth are the equations by Carson [30] and Pollaczek [31]: Carson's equations describe the interaction for conductors above ground, Pollaczek's equations describe the interaction between conductors above ground and underground. Both Carson and Pollaczek start with the same differential equation for the electric field in the vicinity of a transmission line with ground return:

$$\Delta \vec{E} + k^2 \vec{E} = \vec{0}, \quad (2.23)$$

where \vec{E} is the electric field vector; Δ (the Laplace operator); and $k^2 = -j\mu\omega(\sigma + j\omega\epsilon)$. Here, μ is the magnetic permeability, ω is the angular velocity, σ is the earth conductivity ($= 1/\rho_{earth}$) and ϵ is the electrical permittivity.

Both Carson and Pollaczek use a number of assumptions to solve the partial differential equation (2.23):

1. All media surrounding the conductors (i.e. the air and the earth) are homogeneous, which means that the components of electric and magnetic fields follow the wave equation (2.23).
2. The conductors are assumed to be dimensionless, i.e. the conductor radius is assumed to be zero. This means that there is no magnetic field present inside the conductor.

3. There is no damping in the longitudinal direction of the conductors. The derivative in the z -direction (direction of the conductors) is therefore equal to 0 and the problem can be stated in a two-dimensional problem in the plane perpendicular to the direction of the conductors (i.e. the resulting magnetic field component in the z -direction (of the conductors) is zero).
4. The displacement current is assumed to be much smaller than the conductive current in the earth. The relative permeability of the earth is assumed to be equal to 1. Therefore, the constant k can be assumed to be $k^2 = -j\omega\mu_0\sigma$. This factor can be regarded as the inverse of the complex skin depth p of the earth ($k = 1/p$).
5. The air is assumed to be a perfect isolator ($\sigma_{air} = 0$). The relative permeability and relative permittivity of the earth are assumed to be equal to 1.
6. All components of electric and magnetic fields can be written as harmonic functions, i.e. of the form $Ae^{j\omega t}$.

The expressions from both Carson and Pollaczek give impedances that have an imaginary component as well as a real component. This means that although the earth current is induced through the magnetic field, there also is a resistive part in the impedance expression. Therefore, the coupling is described as a mutual impedance with both real and imaginary parts instead of mutual inductance (which would consist of only an imaginary part).

It should be noted that assumption 3) above does not hold for transmission lines of finite length. In reality, near the end points of a transmission line, the problem can no longer be assumed to be a 2D-problem and the effects at the transmission line terminations need to be taken into account and a more sophisticated model is needed in these situations. An in-depth discussion of this effect can be found in [9, section 1.2, Appendix A].

2.3.1 Carson's equations

John R. Carson [30] described the impedances with earth return of conductors placed above ground, both their self-impedance as well as mutual impedance. This chapter presents an example of the outcome of an analysis of an overhead line based on

Carson's work. The background concerning Carson's equations may be found in appendix B.

Example: Impedance between two overhead conductors according to Carson

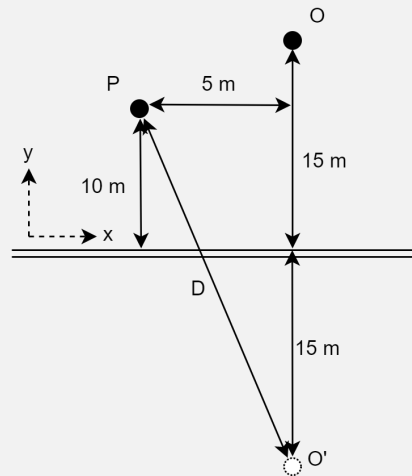


Figure 2.4: Conductor geometry used in this example.

The self- and mutual impedances of two overhead conductors can be determined by using Carson's equations. In this example, we will study two conductors that are closer than $r = 1/4$ together, see figure 2.4.

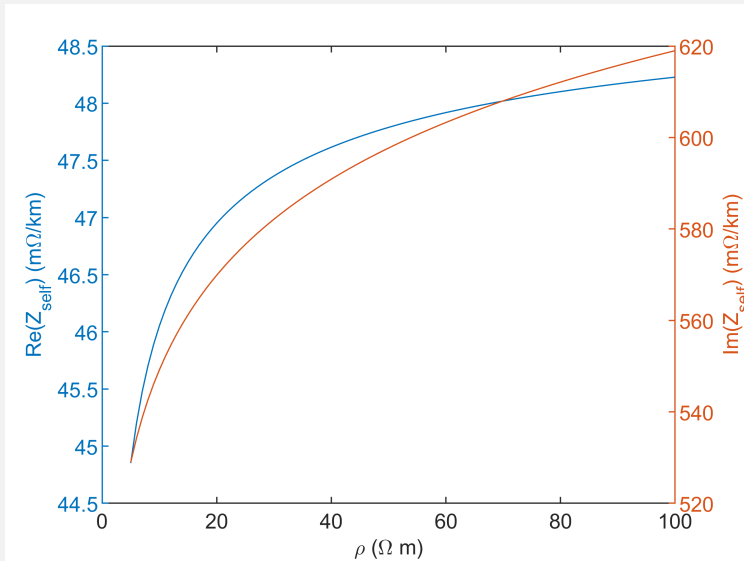


Figure 2.5: Self impedance of conductor P as a function of ground resistivity.

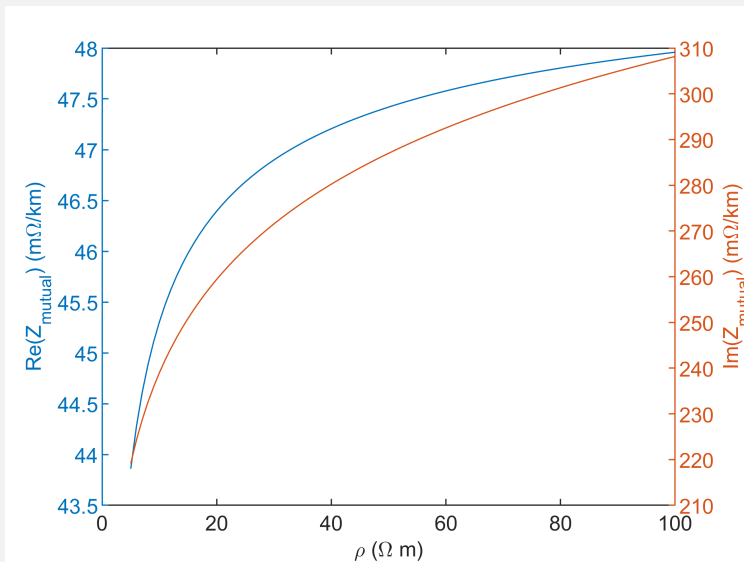


Figure 2.6: Mutual impedance between conductors P and O as a function of ground resistivity.

For the example, ground resistivity is varied between $\rho = 5\Omega m$ and $100\Omega m$, which correspond to r -values between 0.22 and 0.05 and which are typical values

for ground resistivities found in the Netherlands. The frequency is held constant at 50 Hz. For the sake of the example, the internal impedance of the conductor (z) is neglected.

Figures 2.5 and 2.6 show the behaviour of the real and imaginary part of the impedance as a function of ground resistivity. All impedances increase with increasing ground resistivity, however the rate of increase diminishes. Also observe that while the real part of the impedances are approximately equal, the imaginary part of the mutual impedance is approximately twice as large as the imaginary part of the self impedance. This can be explained by the fact that the real part of the impedance is associated with the properties of the earth, whereas the imaginary part is largely determined by the distance between the conductor and the respective image conductor.

2.3.2 Pollaczek's equations

The calculation of impedances with earth return related to underground cables is treated by Felix Pollaczek [31], [32]. Three cases were treated in these works:

1. the self-impedance with ground return for underground cables;
2. the mutual impedance between two separate underground cables;
3. the mutual impedance between an underground cable and an overhead conductor.

The full expressions for each of these cases is further discussed in appendix C. This chapter presents an example concerning several underground cables using Pollaczek's expressions.

Example: Impedance between two underground cables

As an example, we will study the mutual impedance between two underground cables (i.e. the underground-underground model). Since we are interested in the impedance at a relatively low frequency (50 Hz), we can use the approximating expressions by Saad et al. [33] for self- and mutual impedance:

$$Z_{self} = \frac{j\omega\mu_0}{2\pi} \left[K_0 \left(\frac{R}{p} \right) + \frac{2}{4 + R^2/p^2} \cdot e^{-\frac{2h}{p}} \right], \quad (2.24)$$

$$Z_{mutual} = \frac{j\omega\mu_0}{2\pi} \left[K_0 \left(\frac{d}{p} \right) + \frac{2}{4 + x^2/p^2} \cdot e^{-\frac{h_1+h_2}{p}} \right]. \quad (2.25)$$

The geometry used in this example are shown in figure 2.7.

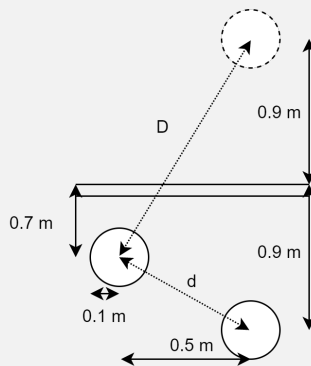


Figure 2.7: Dimensions as used in this example.

Figures 2.8 and 2.9 show the behavior of the real and imaginary part of the cable self-impedance and mutual-impedance respectively, as a function of ground resistivity. As can be observed from the graphs, the real part (the resistive component) of the impedance decreases with increasing resistivity, and the imaginary part (the reactive component) increases with increasing ground resistivity.

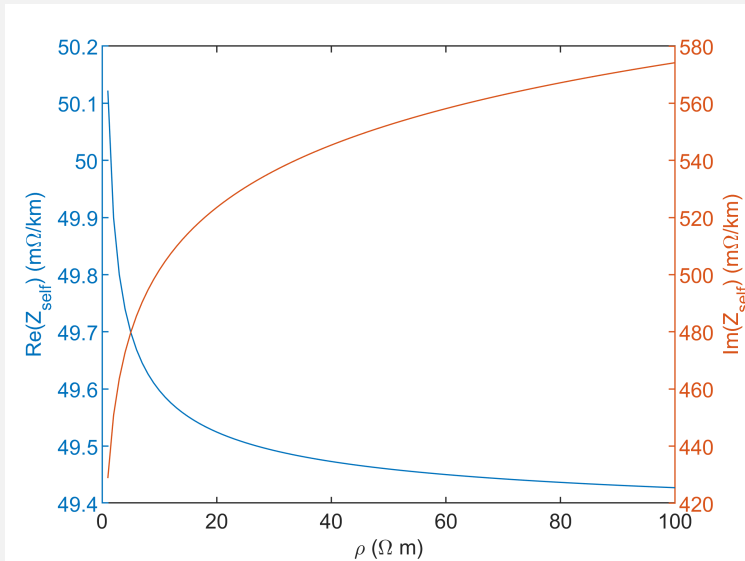


Figure 2.8: Cable self-impedance with earth return as a function of earth resistivity.

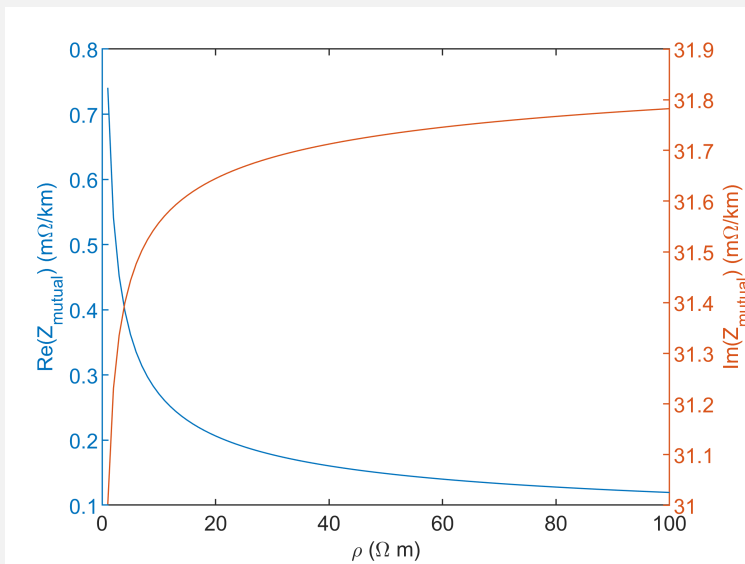


Figure 2.9: Cable mutual-impedance with earth return as a function of earth resistivity.

2.3.3 Earth return current distribution

The models given by Carson and Pollaczek give insight into the behaviour of earth return currents. It is worthwhile to study how these currents behave in practice. Given the expression for the electric field strength in the underground, the distribution of the earth current density can be deduced from the following constitutive relation between electric field strength and current density: $\vec{j} = \sigma \vec{E}$. The assumption here is that the soil resistivity is linear and isotropic.

According to the assumption Carson makes that only the z -component of the electric field is present, the current density also only has a z -component. This means that the direction of the earth current density is opposed to the exciting current in the conductors.

Woodhouse et al. [34], [35] provide several expressions for the solution of Carson's equations to the electric field and therefore the current density underground. The exact solution of the current density depends on the particular solution to the partial differential equation (2.23) that one chooses to use.

Carson [30] gives the following solution for the electric field due to the earth return current:

$$E_z = - \int_0^{\infty} F(s) \cdot e^{y\sqrt{s^2-k^2}} \cdot \cos xs ds, \quad (2.26)$$

cf. the first term in (B.1). The minus sign in front of the integral indicates that the earth return current is opposite in phase to the direction of the exciting current.

Woodhouse [34] makes a different assumption with respect to the symmetry around x (i.e. the horizontal direction perpendicular to the direction of the conductor carrying the exciting current): where Carson does not state that the earth current distribution should be symmetric to the left and right of the conductor, Woodhouse argues that the solution should in fact be symmetric about the x -axis. Therefore, when separating variables to solve the partial differential equation, Woodhouse replaces x by $|x|$ and ends up with the following expression [34]:

$$E_z = - \int_0^{\infty} F(s) \cdot e^{y\sqrt{s^2-k^2}} \cdot e^{-|x|s} ds. \quad (2.27)$$

Figures 2.10 and 2.11 show the solutions as presented by Woodhouse et al. [35]. These solutions show that Carson's solution for the earth current density is clearly different from the solution by Woodhouse. At the surface ($y = 0$), Carson's solution

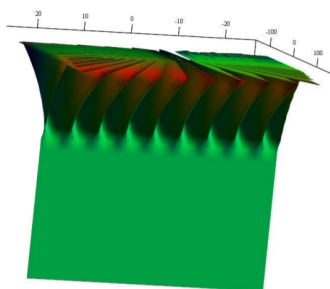


Figure 2.10: Solution to the earth current distribution (2.26) according to Carson. Figure from [35].

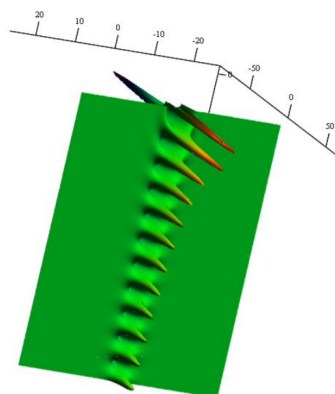


Figure 2.11: Solution to the earth current distribution (2.27) according to Woodhouse et al. Figure from [35].

oscillates, but it does not decay with increasing distance in the horizontal direction. In the vertical direction, Carson's solution decays. Woodhouse's solution on the other hand does decay with horizontal distance and shows decaying oscillatory behaviour in the vertical direction [35].

Both solutions show that the earth current density is highest directly under the exciting AC current. Note that this effect only applies to time-varying currents, not for DC currents, and the contraction effect increases with increasing frequency. Therefore, the earth current will "follow" the path of the exciting current in the opposite direction, as is shown by Rudenberg [36], see figure 2.12.

2.4 Zero-sequence current unbalance in overhead lines

Overhead lines are used to transport electrical energy between high-voltage substations. Overhead lines consist of phase conductors which are attached to towers via insulators. In a three phase system, the number of phase conductors is always a multiple of three. Often, multiple circuits or branches are present in the same right-of-way of an overhead line. In most cases in the Netherlands, two three-phase circuits per tower are present. Overhead lines in the Netherlands are operated at

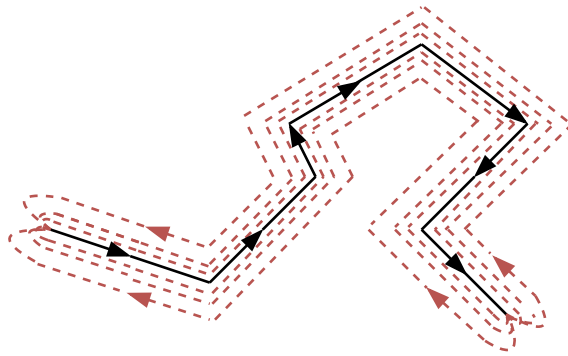


Figure 2.12: Example of the earth current distribution relative to the exciting current based on [36]. The current density (J) of the earth current follows the profile of the exciting current (I), as to minimize the total enclosed loop. The exciting current flows from the left side of the figure to the right side and the earth current flows in the opposite direction.

voltages of 50 kV or higher (up to 380 kV). In other countries, overhead lines are also operated at lower voltages.

Overhead line systems consist of the following main parts: the phase conductors, lightning wires, insulators and towers (or pylons) [27].

Phase conductors are bare conductors (i.e. without insulation), which are installed by means of suspended insulators under the tower's horizontal struts. In some tower designs, insulators are installed directly on the vertical tower structure (such as the Wintrack design as used by TenneT).

Besides phase conductors, one or more conductors connected to ground are present. These conductors are called lightning wires⁵ and are present to conduct lightning current to ground in case of a lightning strike or to provide a predetermined return path for the return current in case of a phase-to-ground short circuit fault. To be able to shield the phase conductors from lightning impact, earth wires are installed above the phase conductors. The exact geometrical configuration of the lightning wires is determined by the Basic Insulation Level (BIL) of the overhead line. The BIL also determines the length of the insulator chains of the phase conductors. In some overhead line designs, grounded wires are also present *below*

⁵In literature other terms for these wires are encountered such as: earth wires, grounded wires or shield wires.

the phase conductors. This is done to decrease the exposure to magnetic fields in the vicinity of the overhead line.

Insulators are used to insulate conductors from the grounded structure (i.e. the towers). The insulator length depends on the Basic Insulation Level of the overhead line.

Towers (sometimes named pylons) can be designed in several ways to provide certain geometric configurations of phase conductors. For example, phase conductors can be placed in a triangle configuration or vertical configuration. Besides the geometric configuration of the phase conductors, the order in which the phase conductors are installed is of importance. In some overhead lines, the position of the phase conductors is rotated through the length of the overhead line to ensure that every phase conductors has the same average distance to ground over the length of the line. This is called a *transposed line* [24]. Chapter 4 will discuss zero-sequence current measurements in a transposed system of high voltage branches that partly consists out of overhead lines.

Another important aspect of the tower are the connections to ground. The grounding design of a tower should be such that when a short circuit current enters the ground at the tower, touch and step voltages comply with the set safety levels [27].

Figure 2.13 shows a schematic example of an overhead line with two circuits and two lightning wires. The phase conductors are installed in a "delta"-configuration, where each circuit of phase conductors is installed as a equilateral triangle.

The geometric configuration of an overhead line determines the induced zero-sequence current in each circuit within the line. For a double-circuit overhead line with a balanced load and balanced source, the zero-sequence current in one circuit is equal in amplitude and opposite in phase to the zero-sequence current in the other circuit ("circulating zero-sequence unbalance", see section 2.1.1) [21]. The net zero-sequence current through the line in this case is relatively low with respect to circulating current [25]. Hesse [21], [37] shows that for an untransposed double circuit line in flat formation, the circulating unbalance can be a factor ten times larger than the through unbalance. The circulating current in an untransposed line consisting of two or more circuits is caused by the fact that the geometric distance (and therefore the mutual inductance) from one conductor to the conductors in the opposing circuits is not equal. Figure 2.14 shows this schematically.

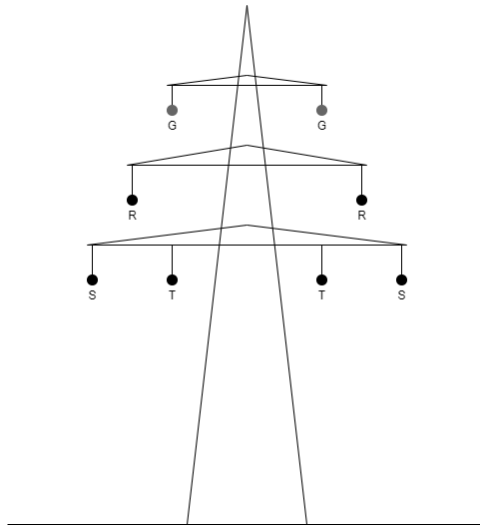


Figure 2.13: Schematic depiction of an overhead line where the conductors are arranged in a "delta"-configuration. The lightning wires are denoted by G, the phase conductors by R, S and T, respectively. Note that the two parallel circuits on the tower are installed as mirror images of each other (i.e. the left circuit is arranged as R, T, S in clockwise direction and the right circuit is arranged as R, S, T). Note that whereas the phase conductors R, S and T are connected to the tower through phase conductors, the lightning wires are usually electrically bonded to the tower structure.

Kalyuzhny and Kushnir [26] studied the influence of phase arrangement in a transmission system that consists of a double circuit line by using computer simulations. The paper shows that whilst the circulating zero-sequence current unbalance is independent of line length (in the paper, Kalyuzhny and Kushnir studied two lengths: 4 km and 50 km), the through unbalance is dependent on the length of the line. A longer line will have a higher through unbalance, since for short lines the through unbalance is limited by the system impedances on the sending and receiving ends of the line. Since the circulating zero-sequence current unbalance is unaffected by these system impedances, it is only dependent on the per-unit-length impedances of the double-circuit line itself and it is therefore independent of the length of the line. This behaviour is also confirmed by Li et al. [38]. Several other authors performed similar analyses on different double-circuit systems to estimate unbalanced currents [39]–[42].

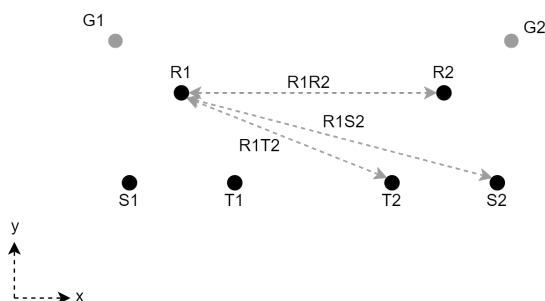


Figure 2.14: As an example, when in both circuits conductors are installed in triangle formation in an overhead line, the distances from one conductor to the conductors in the other circuits are not equal. For clarity, only the distances between one conductor in circuit 1 and the conductors in circuit 2 are plotted and the construction of the pylon is not shown.

Li et al. [38] identified the following main factors that contribute to the unbalance of a multicircuit transmission system:

- Phase arrangement
- Height above ground
- Spacing between circuits
- Conductor properties

Gönen and Haj-Mohamadi [43] investigated the influence of "overhead ground wires" (earth wires) - among other factors - on the unbalance in both transposed and untransposed overhead lines by performing computer simulations. This research found that the inclusion of earth wires decreases the zero-sequence current unbalance. The decrease however diminishes with an increasing number of earth wires: adding another earth wire will not decrease the unbalance factors as much as the preceding earth wire did.

In several papers, Ehrenberger and Švec [44], [45] discuss the problem of current unbalance in meshed systems. In a meshed system, transmission lines do not connect a single source to a single load, but the network is more complex. An example of a simple meshed network is shown in figure 2.15. Ehrenberger and Švec

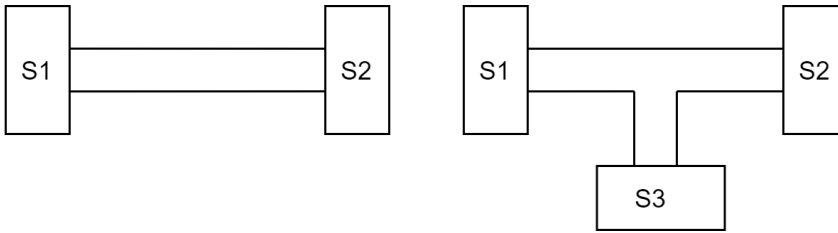


Figure 2.15: Example of a double-circuit point to point branch from substation S1 to substation S2 (on the left) and a meshed configuration (on the right) where substation S3 is installed in one of the circuits.

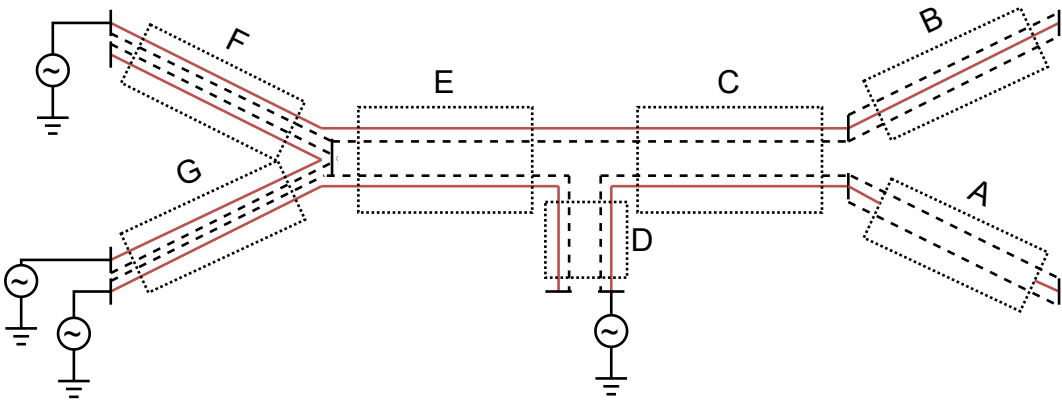


Figure 2.16: An example of a meshed network that was studied by Ehrenberger and Švec [44], [45], figure based on these sources.

propose a method using "virtual shield wires" to reduce the mathematical complexity of the problem. In [45] the authors study a meshed-network case⁶ in which they determine the unbalance factors for several phase permutations in two particular circuits in the network, see figure 2.16. For each of these permutations, the authors determined the unbalance factors m_{10} for the circuits under interest. Note that due to the meshed nature of the circuits, one cannot use the definitions for circulating and through unbalance factors, as defined before.

The zero-sequence impedance of overhead lines for a number of situations according to [27] is given in appendix A.

⁶The addition of a new 400 kV substation in the Czech Republic.

2.4.1 The effect of transposition on zero-sequence unbalance

In a transposed line, each phase conductor will have the same average position with respect to earth and to the other conductors. Therefore, each phase inductance and capacitance over the length of the line will be equal over the full length of the line [24]. For a transposed line, the following relationship between currents and voltages in symmetric components can be given[25]:

$$\begin{bmatrix} \Delta V_0 \\ \Delta V_1 \\ \Delta V_2 \end{bmatrix} = \begin{bmatrix} Z_{00} & 0 & 0 \\ 0 & Z_{11} & 0 \\ 0 & 0 & Z_{22} \end{bmatrix} \begin{bmatrix} I_0 \\ I_1 \\ I_2 \end{bmatrix}. \quad (2.28)$$

One may observe that there is no coupling between symmetric components in this case. Therefore, where are no unbalanced sources or loads present, the unbalance factor is zero (cf. (2.14)). This result also holds for overhead lines with earth wires present [25].

In practice, not all overhead lines are operated as perfectly transposed circuits. Installing a transposed circuit is relatively expensive in comparison to untransposed circuits [25]. Furthermore, transposing an overhead line necessitates the use of transposing towers, which are more complex to construct than non-transposing towers and exhibit higher failure rates [25]. In the Dutch context, many double-circuit overhead line branches are not designed as point-to-point connections, but often have a substation connected to one of the circuits, creating a meshed network (see figure 2.15). Furthermore, due to several causes, overhead lines are sometimes reconstructed as underground cable systems for part of the total length. In Chapter 4, such a system is studied further. In these cases, designing a fully transposed system is practically impossible. Research also shows that zero-sequence currents can be present in meshed networks where transposed branches are present [45].

2.5 Zero-sequence current unbalance in cable systems

Besides overhead lines, high voltage power can also be transported using cable systems. In a high voltage cable, the conductor is insulated from the environment by means of a insulation layer. This means that high voltage cables can be installed underground and that the phase conductors can be placed much closer together than

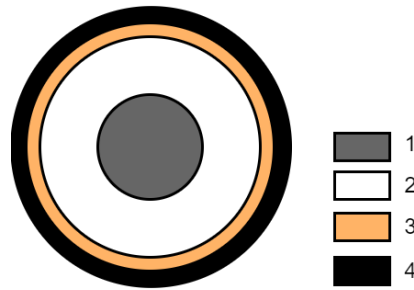


Figure 2.17: Schematic overview of a (single-core coaxial) high voltage cable. The following components are visible: 1. Conductor; 2. Insulation; 3. Earth return conductor; 4. Outer sheath.

in an overhead line (where the conductors are insulated by the air surrounding the conductor). Therefore, high voltage cable systems are often installed in high-density environments, such as urban environments. In this dissertation, we will only consider cable systems that are installed underground, which is the usual practice in the Netherlands.

In general, a high voltage cable is build up coaxially from the following components (see Figure 2.17):

- **The conductor** The purpose of the conductor is to conduct current. The conductor is generally made out of aluminium or copper. Depending on the conductor size, the conductor can be a solid piece or it can be made up out of several wires in a particular configuration.
- **The insulation** Modern cables are insulated by polymeric materials, such as XLPE (cross-linked polyethylene). The purpose of the insulator is to insulate the conductor from its surroundings.
- **The earth return conductor or metallic sheath** The purpose of the earth return conductor is to provide a defined return path for unbalanced currents or short-circuit currents. The earth return current can be a continuous layer of metal (such as lead or aluminium) or it can consist of a wire screen made out of several metal wires (mostly copper)⁷.

⁷In some cases, metallic sheaths are used that are made from a material with a high magnetic permeability, such as steel. This is the case in older armoured paper-insulated cables (PILC) and pipe-type gas pressure cables. In these cases, a larger proportion of the return current will return through the earth return conductor [9, Appendix A]

- **The outer sheath** The role of the outer sheath is to protect the inner components of the cable against outside risks and to insulate the earth return conductor.

Next to these main components, cables consist of several other components, but these are not of interest for the topic of this dissertation.

The cable itself is only part of the larger cable system. A cable system also consists out of joints (which connect the different lengths of cable) and terminations (which allow the cable to be installed to a high voltage installation or transformer). Note that the earth connection at the cable termination has a impedance to earth.

Cable systems can be installed underground in several ways, depending on what the optimal design is. Three single-phase cables are combined in a so-called *circuit*, equivalent to the configuration of an overhead line. The two main configurations in which single-phase cable circuits are installed are triangle (or delta) formation and flat formation. These two configurations are shown in figure 2.18. One of the advantages of triangle formation is that each phase has the same distance to the two other phases. Therefore, the inductive coupling between phases is equal. This configuration also needs the least amount of horizontal space. Since the phases are installed close together, this configuration can have a relatively low current rating with respect to flat formation. In flat formation, cables are spaced further away from each other, which can have a positive effect on the cable's maximum current rating. This is however dependent on the current running through the earth return conductors, since this current is dependent on the distance between phases and the manner in which the earth return conductors are bonded to ground (e.g. single-point bonded, both sides bonded or cross-bonded). Other possibilities to increase the current carrying capacity of a cable system are to increase the conductor diameter, to install a second circuit in parallel or by eliminating currents in the earth return conductors by connected these in a so-called *cross-bonding* configuration [46].

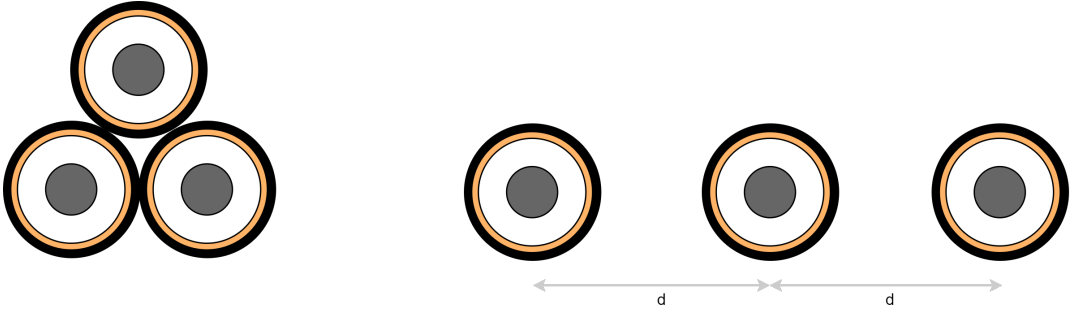


Figure 2.18: Example of cable circuits in triangle formation (on the left) and flat formation with (on the right).

A full electromagnetic cable model is given in [47]. For a single-core coaxial cable, this model consists of an impedance matrix Z and an admittance matrix Y . These matrices relate voltages and currents in the following way:

$$\frac{\partial V}{\partial z} = -Z \cdot I, \quad (2.29)$$

$$\frac{\partial I}{\partial z} = -Y \cdot V. \quad (2.30)$$

These equations are known as the Heaviside's Telegrapher's equations [48].

The impedance matrix of a cable system is given by:

$$Z = Z_i + Z_o, \quad (2.31)$$

where Z_i is the internal cable self-impedance matrix and Z_o is the earth return impedance matrix. The full formulation of Z_i is given in [47]. For a single-core cable consisting of a core and a metal sheath, this matrix is a 2×2 -matrix, which has the following form:

$$Z_{ij} = \begin{bmatrix} Z_{ccj} & Z_{csj} \\ Z_{csj} & Z_{ssj} \end{bmatrix}, \quad (2.32)$$

where for each j th cable, Z_{ccj} is the core impedance, Z_{csj} is the impedance between core and sheath and Z_{ssj} is the impedance of the metal sheath. The internal matrix of a cable system consisting of multiple cable is a diagonal matrix of these submatrices. There are no diagonal terms in the internal impedance matrix.

The earth return impedance matrix Z_o for underground cable systems consists

of the expressions for mutual impedance between underground cable systems with ground return according to Pollaczek (see (C.1) and (C.2), [32]).

The admittance matrix is given by:

$$Y = j\omega P_i^{-1}, \quad (2.33)$$

where P_i is the cable internal potential coefficient matrix [47]. In single-core coaxial cables with an earth-return conductor, there is no coupling through the admittance matrix, since there is a negligible electric field outside of the earth-return conductor. This means that only the diagonal (internal) terms of the potential matrix are nonzero (cf. (2.21) and (2.22)).

For a three-phase cable system consisting of single-phase cables where the metal sheaths are bonded to earth at both ends, the internal impedance matrix can be reduced, since the voltages at both ends of the metal sheaths are zero [49]. Voltages and currents of the main conductors are then related by:

$$V_C = Z_{CN} I_C, \quad (2.34)$$

where V_C and I_C are vectors containing the three phase voltages and currents, respectively and Z_{CN} is the reduced impedance matrix (cf. matrix Z_{ABC} in section 2.1.2). Given this impedance matrix, an impedance matrix of symmetric components can be constructed using (2.10). For a symmetric cable configuration, i.e. when the cables are installed in triangle formation or in three-phase cables, all conductors in the cable system are equidistant. In this case, there will be no off-diagonal terms in the symmetric components impedance matrix and by equation (2.14) the zero-sequence current is equal to zero when there is no unbalanced source or load present. In the case of an asymmetrical cable configuration (e.g. when the cables are laid in flat formation), the mutual terms need not be equal to zero. These mutual terms can be determined by performing computer simulations due to the large number of terms involved [49].

In a study by Nakanishi et al. [50], the behaviour of zero-sequence currents in a system that contains multiple parallel cable circuits was investigated, because a high zero-sequence current level was observed in a cross-bonded cable system. The

study investigates the behaviour of zero-sequence currents in a double-circuit configuration and a four-circuit configuration and looked at different cable arrangements in each of these configurations. Field measurements were performed and these are compared with computer simulations, showing good agreement between each other. In the double circuit configuration, several arrangements were studied. In some arrangements, no or a negligible amount of zero-sequence current was present. In other arrangements, zero-sequence currents are present, but these completely consist of circulating zero-sequence currents, as additional analysis shows. The same observation can be made for the four-circuit configuration. Nakanishi et al. also discuss the influence of crossbonding the cables' metal sheaths on zero-sequence currents. The presence of crossbonding does not influence the zero-sequence current present. Also, an unbalanced crossbonding configuration (i.e. where the CB minor section lengths are not equal), does not influence the zero-sequence current. In their paper, Nakanishi et al. do not discuss the transformer configurations on either end of the cable circuits and the way in which transformer neutrals are grounded.

A number of other papers build upon the work by Nakanishi et al. and also discuss the behaviour of zero-sequence currents in systems consisting of more than one three-phase circuits [51], [52], in particular case studies such as cables installed in a duct that connect to (low voltage) high power convertors [52].

In the following subsections, two special types of cable systems are considered in the context of zero-sequence currents: three-phase cables and pipe-type cables.

2.5.1 Three-phase cables

Three-phase cables are built up such, that three cores are enclosed by a mutual metallic screen. In addition, each core is surrounded by a semiconducting layer at the outside of the primary insulation, which means that the electric field outside this layer is negligible and the capacitive coupling between phase conductors is very small. The advantage of this design is that a whole three-phase circuit is enclosed in a single cable. Developing an analytical closed-form mathematical model for a three-phase cable with a shared metal sheath is a very difficult task. Therefore, numerical methods such as the Finite Element Method are often employed to build numerical models in these cases [53].

2.5.2 Pipe-type cables

Pipe-type cables are cables in which three phase conductors are installed in a mutual metal pipe. In the Netherlands, this type of cables can be found in high-voltage gas-pressure cable systems. The three phases are installed in a common pipe that can be made out of a ferromagnetic material, with a high effective relative magnetic permeability. This means that the skin depth at 50 Hz in the pipe can be smaller than the wall thickness. If this is the case, the wall thickness can be regarded as infinite [47]. For example, for a steel pipe with an effective relative magnetic permeability of 2000, the skin depth at 50 Hz is equal to [48]: $\delta = \sqrt{\frac{2\rho}{\omega\mu}} \approx 0.6$ mm. A typical steel pipe used for gas-pressure cables has a wall thickness in the order of 5 mm, so it can be regarded as an infinitely thick steel pipe.

For a pipe-type cable with a wall thickness that can be regarded infinite, the impedance matrix is given by:

$$Z = Z_i + Z_p, \quad (2.35)$$

where Z_i are the internal impedance matrices of the cores inside the pipe and Z_p is the matrix describing the impedance between the inner conductor with respect to the pipe inner surface.

In a pipe type cable with infinite wall thickness, there is no magnetic field outside of the pipe and therefore no electromagnetic interaction with other objects in its vicinity. When the wall thickness cannot be assumed to be infinite, matrices can be constructed which describe the interaction between the inner wall and outer wall and a matrix for the self earth return impedance of the pipe [47].

2.6 Zero-sequence current propagation between voltage levels

Power transformers determine the propagation of zero-sequence currents between voltage levels. Depending on the type of transformer, zero-sequence currents can or cannot pass through the transformer. The purpose of a transformer is to transfer positive-sequence currents from one voltage level to another voltage level. Therefore all transformer types will pass positive-sequence currents from the primary side to the secondary side (or vice versa). The same is valid for negative-sequence

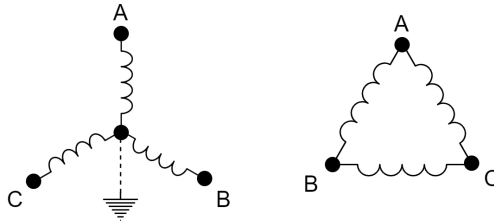


Figure 2.19: Schematic overview of a wye connection (on the left) and delta connection. Note that the neutral point of the wye connection can be either grounded or ungrounded.

currents. Depending on the configuration of the transformer, zero-sequence currents can or cannot pass through the transformer. In the most cases in the Netherlands, networks and transformers are designed such that there is no coupling between the zero-sequence circuits on the primary and secondary side.

There are two types of transformer windings: wye and delta. In a wye configuration, the three phases are connected to a mutual neutral point. This neutral point can be either grounded or ungrounded. In a delta configuration, each phase is connected in series to another phase, forming a "triangle". A schematic overview of the wye and delta connections is given in figure 2.19.

Zero-sequence currents cannot always propagate through transformers. When zero-sequence currents can propagate, a cause of zero-sequence currents on one side (such as an unbalanced load) will lead to the presence of a zero-sequence current on the other side, if and only if there is a source present that can provide zero-sequence currents on this other side. The possibility for zero-sequence currents to pass through is dependent on the primary and secondary connections (and if applicable the tertiary connection) of the transformer. In table 2.1, the behaviour of the propagation of zero-sequence currents of twelve common transformer types is given, according to [54]. For a propagation path to be present, there must be a path for the zero-sequence current to pass from one side of the transformer to the other side. This propagatory path is present when there is a connection to ground from the neutral point on both sides of the transformer [23], [54], [55].

In some cases, transformers can act as a source for zero-sequence currents, which is shown in the third column of table 2.1. This is the case when there is a cause for zero-sequence currents on the side of the transformer (such as an unbalanced load, see section 2.7) where the transformer can act as a zero-sequence current source:

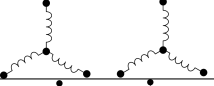
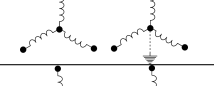
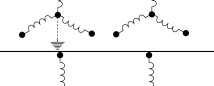
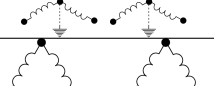


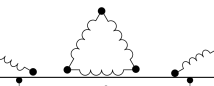
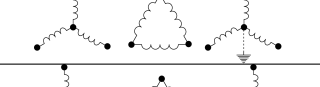
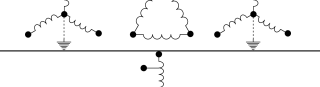
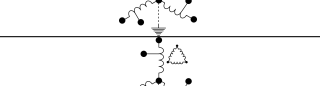
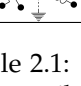
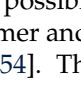
Transformer type Primary Secondary	Zero-sequence current Propagation path	Zero-sequence current Source
	No	No
	No	No
	No	No
	Yes	No
	No	No
	No	Yes →
	No	Yes ←
	No	No
	No	Yes →
	Yes	Yes ← →
	Yes	No
	Yes	Yes ← →

Table 2.1: Overview of transformer connections configurations and the possibility for zero-sequence currents to pass through the transformer and to provide a source for zero-sequence currents according to [54]. The arrows point to the direction in which the transformer can act as a source for zero-sequence currents.

there is a path through which the zero-sequence current can flow from the transformer, through the connected transmission path to the cause of the unbalance, and returning through earth or earth conductors. The primary-sequence current on the other side of the of the transformer is then transformed into a zero-sequence current [54]. In the Netherlands, two-core and three-core transformers where the neutral

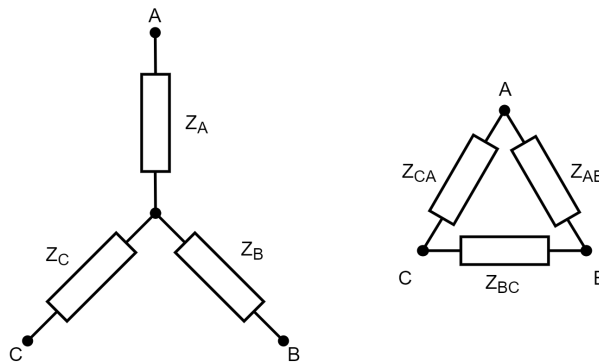


Figure 2.20: Schematic overview of a wye-connected load on the left and a delta-connected load on the right.

points are grounded a both sides are not used (e.g. the fourth and ninth rows in table 2.1). This means that in these cases there is no propagation path between voltage levels present. Furthermore, transformers in most cases are designed such that the zero-sequence networks between the primary and secondary sides are decoupled as much as possible.

2.7 External sources of zero-sequence current unbalance

Zero-sequence currents can also have a cause outside of transmission lines in a high voltage system. Several authors have addressed this issue [56], [57].

Fekih Ahmed [56] determined that the necessary and sufficient condition for load unbalance in a three-phase point-to-point power system is that the load impedances are unequal. If and only if the load impedances are equal, the unbalance power term will be equal to zero. This is valid for both a wye-connected and delta-connected load (see figure 2.20 for an schematic example of a wye-connected and delta-connected load). This unbalance requirement is independent of the fact that the source is balanced. The load is balanced if and only if $Z_A = Z_B = Z_C$ for a wye-connected load and $Z_{AB} = Z_{BC} = Z_{CA}$ for a delta-connected load.

Pokorny [57] gives an example of several unbalanced load configurations and the associated zero-sequence and negative-sequence unbalance factors. In the case that a single-phase load is installed *between* two phases, Pokorny shows that the negative sequence unbalance factor is always equal to zero. This is valid for 1, 2 or

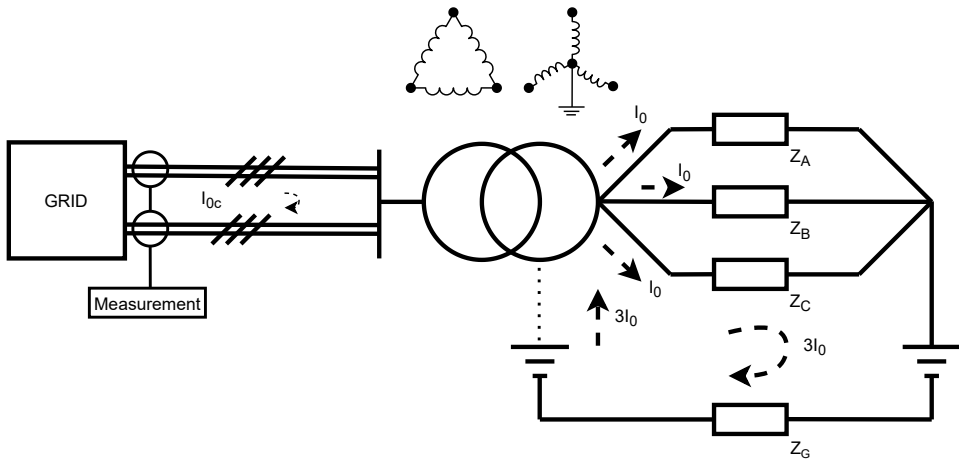


Figure 2.21: Example of a radially connected unbalanced three-phase load with a transformer between the feeding transmission line and the load

3 single phase loads between phases, where these loads in principle can be unequal to each other. In case single phase loads are installed between a phase and neutral, zero-sequence currents can be present. In the case in which there are three equal impedances installed between the three respective phases and neutral, we end up with the delta-connected situation described in [56] and the system will be balanced.

It is highly challenging to model the contribution of external sources of zero-sequence current in extended meshed networks, due to the large number of possible paths through which the zero-sequence current can close and the large number of possible locations of these sources.

2.8 Zero-sequence currents in radially connected networks

Figure 2.21 brings together several concepts that have been discussed in this chapter and shows how these concepts can be applied to analyze zero-sequence currents in a real life situation. In the example, an unbalanced load (in wye-configuration) is present at the secondary side of a delta-wye transformer, of which the neutral has been connected to earth (section 2.6). The combination of the unbalanced load (section 2.7) $Z_A \neq Z_B \neq Z_C$ (which can be designated as the cause) together with the particular transformer type (which can be designated as the source) leads to a

zero-sequence current that will run within the circuit and that will close through earth. The zero-sequence current itself is determined by the earth return impedance Z_G , which depends on geometry, length and properties of the earth return (section 2.3).

The transformer is connected to the grid via a single double-circuit transmission line. This transmission line can be either an overhead line (section 2.4) or an underground cable system (section 2.5). Due to the characteristics of the transformer in this case, the zero-sequence current that is generated at the secondary side of the transformer is not passed to the primary side of the transformer: there is no propagation of zero-sequence currents between voltage levels in this case. Therefore, if one would measure the through zero-sequence current at the “near” side of the transmission line, its value will be zero (within the accuracy of the measurement system). On the other hand, there might be a circulating zero-sequence current present in the transmission line due to the geometric configuration thereof.

We can conclude in this case that in a radial connection where a transformer of the right configuration is present, there will be no through zero-sequence current due to unbalanced loads at the secondary side. If, on the other hand, a different type of transformer – such as an autotransformer with an extra delta winding – is chosen, the zero-sequence current that is caused at the secondary will propagate between voltage levels and a measurable amount of through zero-sequence current may be measured in the transmission line.

2.9 Magnetic fields due to zero-sequence currents

Currents and magnetic field are related through the Ampère-Maxwell law [58]:

$$\nabla \times \vec{B} = \mu_0 \nabla \times \vec{H} = \mu_0 \left(\vec{J} + \epsilon_0 \frac{\partial \vec{E}}{\partial t} \right), \quad (2.36)$$

where \vec{B} is the magnetic flux density (measured in [T]), \vec{H} is the magnetic field strength (measured in [A/m]) and J is the current density (measured in [A/m²]). For our purposes (power frequencies), the latter part of the equation, $\epsilon_0 \frac{\partial \vec{E}}{\partial t}$ (called

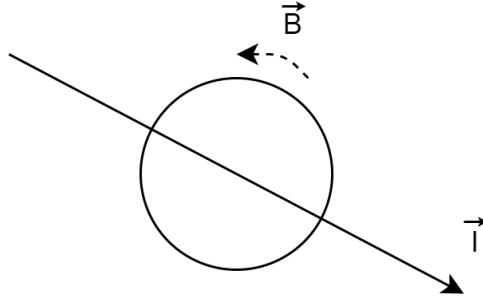


Figure 2.22: Relation between magnetic field direction resulting from a current coming towards the reader.

the *displacement current*) can be assumed to be zero. For a line current I , the expression for the magnetic field is given by the Biot-Savart law [58]:

$$\vec{B}(\vec{r}) = \frac{\mu_0}{4\pi} \int \frac{\vec{I} \times \hat{r}}{r^2} dl', \quad (2.37)$$

where r is the euclidean distance between the current element and the position of interest and \hat{r} is the unit vector pointing from the current element to the position of interest.

For an infinitely long conductor, the Biot-Savart expression can be integrated from $-\infty$ to ∞ , yielding the following expression[58]:

$$\vec{B} = \frac{\mu_0 I}{2\pi r} \hat{\phi}, \quad (2.38)$$

where $\hat{\phi}$ is a unit vector pointing in the direction perpendicular to the direction of the current and the direction from the current to the point of observation, according to the right-hand rule.

2.9.1 Magnetic fields around transmission lines that carry zero-sequence currents

The magnetic field caused by a three-phase transmission line carrying a purely symmetric current distribution (such as a positive-sequence current) will be lower than a three-phase transmission line carrying a zero-sequence current in combination with a symmetric current distribution. Because the three phases in a symmetric

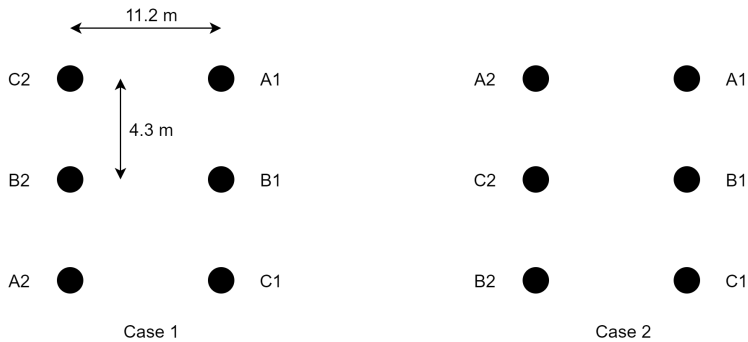


Figure 2.23: Phase arrangements and geometry according to Kalyuzhny and Kushnir [26]. In both cases circuit 1 is on the right and circuit 2 is on the left. The relative phase arrangements differ, however.

three-phase current are 120° out of phase with each other and equal in amplitude, the magnetic field components will cancel each other out at a distance much larger than the separation between the phase conductors.

Kalyuzhny and Kushnir [26] show that the presence of a zero-sequence current due to an unbalanced load can lead to magnetic fields which are 47% larger in that particular case (see figure 2.23 for the geometry of the cases used by Kalyuzhny and Kushnir). To show the influence of phase arrangement on the resulting magnetic field, a plot was made of the absolute magnetic field strength resulting from the currents passing through each phase in figure 2.24 at 1 m height above ground. The figure shows that there is a clear distinction in the behaviour of the magnetic field as a function of the phase arrangement. In the first case, the field decays at a slower rate as a function of the distance from the center of the overhead line, where in the second case the magnetic field is higher in the at the center of the overhead line. Note that the paper by Kalyuzhny and Kushnir does not take into account the current passing through the earth wires and the ground. Adding these currents to the total model will result in a lower resulting magnetic field.

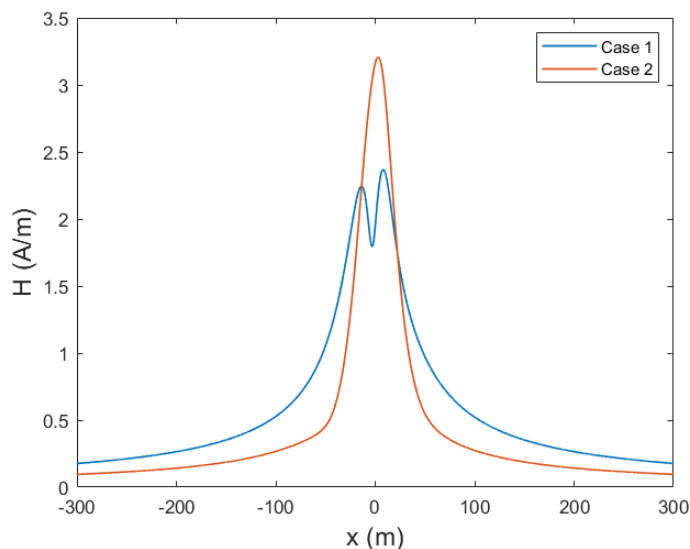


Figure 2.24: Comparison of the resulting absolute H-field at 1 m above ground between two arrangements of a double-circuit line from the paper of Kalyuzhny and Kusnir [26] in two described cases. The magnetic field in case 1 decays much slower as a function of distance due to the presence of inherently caused zero-sequence currents in the transmission line. The difference in field strength can be up to 47%. Note that this paper does not take into account the current running through the earth wires or ground, which will have an influence on the total resulting magnetic field.

2.10 Summary and conclusions

This chapter brings together the current state of the art concerning zero-sequence current unbalance during normal operation. The method of symmetric components can aid in understanding unbalance in three-phase systems. Several key concepts are introduced that are used throughout this dissertation, such as the circulating and through unbalance factors, which describe a decomposition of zero-sequence currents in transmission lines that consist of multiple parallel circuits.

Two main causes of zero-sequence currents during normal operation are identified: geometric unbalance between conductors in transmission lines (both overhead as well as underground systems) and unbalanced loads. In some cases, zero-sequence currents can propagate between different voltage levels. This depends

of the specific design of the transformer that transforms one voltage into another voltage.

The order in which conductors are installed in transmission lines can have a significant influence on the circulating and through zero-sequence currents in a transmission line and therefore on the resulting magnetic field surrounding the transmission line.

Chapter 3

Zero-sequence current measurement uncertainty during normal operation

3.1 Introduction

Zero-sequence currents (ZSC) in high-voltage power systems during normal (non-fault) operation can have a significant influence on nearby conductive structures, such as pipelines or railway infrastructure. This is caused by the fact that magnetic fields of ZSCs decay less quickly as a function of distance from the high-voltage infrastructure than magnetic fields of symmetric three-phase currents [15]. Through inductive coupling, an induced voltage can be present on nearby metallic conductive structures, which can have a detrimental effect on the safety, operation and integrity of these structures. There is a tendency to construct infrastructure systems in each other's proximity, especially in areas with high population density.

Part of the content in this chapter has been published in:
S. Nauta, R. Serra, "Zero-Sequence Current Measurement Uncertainty in Three-Phase Power Systems During Normal Operation" *IET Generation, Transmission & Distribution*. <https://dx.doi.org/10.1049/gtd2.12254>

Although this has obvious spatial advantages, it also increases the risk of undesirable electromagnetic interference (EMI). To achieve electromagnetic compatibility (EMC), several mitigating measures can be employed. Estimations of the amount of EMI are normally performed in order to assess the need and pertinence of suitable applied EMC measures [59]. Furthermore, another important field in which ZSCs can play a role is the performance of distance protection relays during (asymmetric) power swings [60], [61]. During these power swings, ZSC levels can be larger than during normal operation without power swings. These levels and the associated measurement uncertainties are therefore worthwhile to study in order to prevent unnecessary tripping of protection relays [60].

A relatively small body of literature is available on the levels of ZSCs that one may expect during normal operation [26], [37], [40], [45], [50], [57] and this literature is limited to single measurement values or theoretical values of ZSCs. Furthermore, where measurements are presented, little attention is given to the accuracy of the measurements. Meshed networks give rise to an increased challenge to accurately determine the actual flow of zero-sequence currents [45], which is only increased by the complexity of all possible permutations from switching branches on or off within the network. Considering all these permutations in theoretical calculations would result in an impractically large number of calculations. Measurements of ZSCs during normal operation can help to provide increased insight into ZSC levels that are to be expected in addition to theoretical calculations. These measurement could be implemented as online measurements using (existing) PMUs. However, performing those measurements with reasonable accuracy presents a metrological challenge: during normal operation, ZSC levels are much lower than positive-sequence current levels [62].

Zero-sequence currents are determined by transmission line parameters such as the return impedance. This return impedance depends on several variables, in particular the earth return impedance [23], [63]. This is partly determined by the presence of conducting objects in the earth, such as metallic pipelines. Since the presence of these objects is often not known to the modeller, theoretical calculations can depart from the actual situation. Furthermore, the return impedance, as well as other transmission line parameters may not be constant in time. In these cases, measurements can also help to determine accurate parameters.

Several studies address the topic of estimating the uncertainty intervals of transmission line parameters, such as (three-phase) line impedances, using PMUs [63]–[68]. Most of these works are concerned with the reconstruction of single-phase transmission line parameters that can change over time, such as single-phase transmission line impedance. When these methods are extended to the measurement of three-phase transmission line parameters, such as the zero-sequence impedance of a transmission line [63], [69], the measurement uncertainty of zero-sequence currents for the particular measurement strategy needs to be known. Some authors focus on the measurement of positive-sequence components, but not on zero-sequence components [70]. A number of studies take the associated measurement errors into account when reconstructing three-phase transmission line parameters using PMU measurements [71]–[73]. PMU measurements were demonstrated to be of use to calibrate instrument transformers when one highly accurate instrument transformer is present and PMU are installed on both sides of a transmission line [74]. Other authors use PMU measurements in combination with a small number of calibrated instrument transformers to calibrate instrument transformers in the whole network [75]. In [73], a simulation of positive-sequence parameter errors based on Monte Carlo (MC) simulations is presented. A main drawback of this strategy is that performing these simulations for a wide variety of input parameters is computationally and timewise intensive. The development of analytical expressions to determine measurement uncertainty based on the applicable system parameters would therefore be very beneficial. Furthermore, PMU measurements depend on the separate measurement of the three phases, which are later combined to determine the ZSC. Based on its definition, ZSCs can also be measured by using a single probe around the secondary circuits from the current transformers, which may help to decrease the total measurement uncertainty of ZSC measurements.

This research aims to contribute to the existing literature in the following ways:

1. The development of complete analytical expressions of measurement uncertainty for three practically applicable measurement strategies for ZSCs during normal operation.
2. By comparing the uncertainties of the different measurement strategies under consideration. In particular, the difference in measurement accuracy between

measuring ZSCs using one probe on the secondary side and using three independent probes (e.g. in the case of PMU measurements) is studied.

3. Validation of the analytical expressions by means of MC simulations that simulate the measurement chains.
4. Validation of the analytical expressions by means of experimental validation.

The three studied measurement strategies are the (1) direct and (2) indirect measurement of zero-sequence currents using the secondary currents from pre-installed primary current transformers, as well as measurements using (3) PMUs.

This chapter is organized as follows: Section 3.2 gives an overview of three different ZSC measurements strategies under consideration, highlighting the main challenges of measuring ZSC during normal operation. Section 3.3 elaborates on the two methods that are taken to study measurement errors: the analytical method and the MC method, with the respective assumptions and description of the error sources in the measurement chains. Analytical expressions for the measurement errors of the three strategies are derived in section 3.4. Section 3.5 presents the MC simulations. To determine the mutual accordance between the applied methods, section 3.6 compares the outcomes of the methods and discusses their practical applications in measurement. The analytical outcomes were also validated by means of measurements, as described in 3.7. Section 3.8 presents the conclusions.

3.2 Zero-sequence current measurement techniques

Two approaches to measuring ZSCs in high voltage systems during normal operation can be distinguished: by directly probing the currents running in the primary conductors of a transmission line or by making use of the existing current transformers and measuring the secondary currents of these. Both approaches have their particular advantages and disadvantages, which are further explicated in the following sections.

3.2.1 Measurement of primary currents

Currents can be directly measured by installing current probes around or nearby the primary conductors. In high voltage-power systems, it is significantly challenging

to perform direct measurements on zero-sequence currents from the primary conductors due to the constraints posed by the safety distances that need to be taken into account. This chapter will therefore mainly focus on the measurement of secondary currents to determine zero-sequence currents.

When implementing this measurement approach in a high voltage environment, attention needs to be given to the safety aspects of the measurement setup. Therefore the circuit that is to be measured will most likely need to be taken out of service temporarily when installing and removing the current probes. Measuring the zero-sequence current in a three-phase circuit directly poses an additional challenge, since all three phases need to be measured simultaneously. In general, it is not possible to use a current probe at the transformer neutral to measure zero-sequence currents in a particular circuit during normal operation/non-fault conditions due to a number of reasons:

1. A transformer neutral connection is not always available due to the particular earthing arrangement at the substation. For instance, a transformer can have a delta connection at the voltage level of interest. Without the presence of a dedicated earthing transformer, a neutral connection is not available.
2. When the substation which houses the transformer is connected to a meshed network or to more than one other substation, there is no equivalence between the measured current at the transformer neutral and the zero-sequence current in one of the branches connected to the substation.
3. When two high voltage branches (partially) share the same right-of-way, zero-sequence currents will be induced in both branches due to mutual coupling [26]. These zero-sequence currents will be equal in amplitude and in opposite in phase. Therefore, this (inherent) part of the zero-sequence current in a high voltage circuit will not close through ground and will not be measured at the transformer neutral.

One needs to take care of the total conductor arrangement that is enclosed by the current probe. When both the primary conductor and the earth return conductor are enclosed (as is the case in a shielded power cable) and the earth return conductor is grounded at both ends, the resulting magnetic field from both the current in the primary conductor and the earth return conductor is measured. When the earth

return conductor is single-point bonded this is of no concern, since a negligible current will pass through the earthed conductors at short cable lengths.

Several types of current probes can be used to measure currents in high voltage systems: current transformers [76]; Rogowski coils [76]; Remote measurement of the magnetic field using field probes [77].

Current transformers use Faraday's law of induction to transform a (large) primary current into a smaller secondary current. This secondary current is fed through a sense resistor. By measuring the voltage over this resistor, the secondary current can be deduced by Ohm's law [76]. To measure the zero-sequence current in the three phase conductors simultaneously, a current transformer needs to be installed around all three phase conductors. In practice, this would be impossible due to the safety distances around the conductors that need to be taken into account.

Rogowski coils also make use Faraday's law of induction to measure a primary current inside its circumference[76]. Rogowski coils differ with respect to current transformers. A Rogowski coil is inherently linear, since it has an air core[76]. This however also means that a Rogowski coil is less sensitive than a current probe with a magnetic core. Rogowski coils measure the time derivative of the current passing through its interior. An integrator is therefore needed to determine the primary current. An advantage of a Rogowski coil is that it can be constructed flexibly, which increases ease of installation. Rogowski coils can also be installed in series to directly measure the zero-sequence current, which may increase the accuracy of measurement.

Remote measurements that measure the magnetic field distribution around a transmission line could be a third method to directly probe the zero-sequence currents present in that transmission line [78]. In the past years, some efforts were made to solve this problem by using drone measurements around transmission lines. A further investigation is necessary to decide under which conditions such a measurement could be useful. A possible challenge is the time needed for performing a scan of the magnetic field around a transmission line, during which the transmission line load could change significantly.

3.2.2 Measurements using current transformer secondary currents

Measuring currents at the secondary side of the current transformers has some practical advantages over the measurement of the primary currents. For instance, current probes can be installed and removed without taking the circuit out of service. There is also the possibility to directly probe the zero-sequence current by installing a single probe around all three secondary leads coming from the current transformers at the same time. The remainder of this chapter will concentrate on measurement methods that make use of secondary currents to estimate zero-sequence currents in the primary circuit.

Figures 3.2 and 3.3 show the general principles of measurement of secondary currents. The three primary phase currents A , B and C are measured by the installed current transformers. The secondary leads from the current transformers are installed for use by secondary equipment, such as protection relays or measurement equipment. This secondary wiring can be probed by using current clamps, as shown in figure 3.3. In this chapter, we study three strategies to measure zero-sequence currents using secondary current. In the indirect and direct strategies, current clamps are used to measure secondary currents. These current clamps are connected to a recording device (in this case an oscilloscope). The recorded signals can be processed to calculate the sequence currents by extracting the 50 Hz component using a Fourier Transform [79]. In the PMU-strategy, the secondary wiring is connected to a PMU.

Current Transformers

In general, two types of current transformers can be identified at substations: measuring current transformers and protective current transformers. Ideal measuring current transformers have a linear transfer function between primary current and secondary currents, whereas an ideal protective current transformer has a fast response time, but not necessarily a linear transfer function between primary and secondary current. For our purposes, we will focus only on measuring current transformers.

Upper bounds for current transformer errors are described in the international norm series IEC 61869 [80], [81]. The mechanisms by which measurement errors are

introduced in current transformers are described by two parameters: the ratio error and the phase displacement.

The ratio error of a current transformer is defined by: *"the error which an instrument transformer introduces into the measurement and which arises from the fact that the actual transformation ratio is not equal to the rated transformation ratio"* [80], definition 3.4.3. The ratio error is defined as the following percentage [81]:

$$\epsilon = \frac{k_r I_s - I_p}{I_p} \times 100\%, \quad (3.1)$$

where ϵ is the ratio error, k_r is the rated transformation ratio, I_s is the measured secondary current and I_p is the actual primary current.

The phase displacement $\Delta\phi$ of a current transformer is defined by: *"difference in phase between the primary voltage or current and the secondary voltage or current phasors, the direction of the phasors being so chosen that the angle is zero for an ideal transformer"*, [80], definition 3.4.4. The phase displacement is expressed in centiradians or arcminutes.

As stated above, the values of the ratio error and phase displacement as stated in the IEC 61869-series are upper bounds. In practice, current transformers may have actual errors that are lower than these. The maximum ratio error and phase displacement as a function of the percentage of rated current for class 0.2S current transformers is shown in figure 3.1. For percentages larger than 20% of the rated current, the maximum ratio error is equal to 0.2%, hence the classification of this class.

Measuring zero-sequence currents using Phasor Measurement Units

PMUs are increasingly used in power systems to monitor the state of the system [82]. PMUs allow for the observation of voltage and current phasors (both amplitudes and phase angles), power system frequency and the rate of change of frequency. The measurements of the phase current phasors can be used for the calculation of the corresponding sequence components, as is shown in [83].

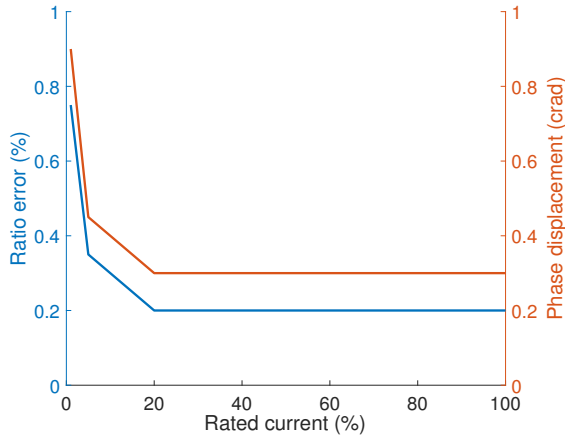


Figure 3.1: Upper bounds for the ratio error (in percentage) and phase displacement (in centiradians) as a function of the fraction of the rated current of the current transformer for class 0.2S, according to IEC 61869-1 [80]. For currents larger than 20% of the rated current, the ratio error is at most 0.2%, hence the class indication 0.2S.

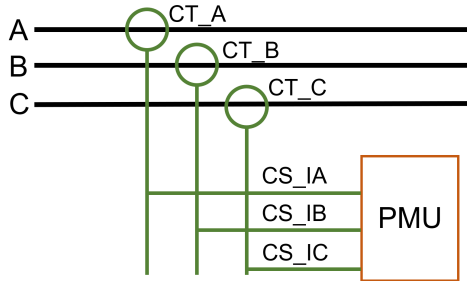


Figure 3.2: Schematic overview of the measurement of the phase currents using a Phasor Measurement Unit.

Measuring the zero-sequence current indirectly from secondary currents

When each phase current is measured separately using current clamps around the secondary wires from the current transformers, the ZSC can be calculated in the post-processing stage by combining the signals from each measurement channel, as is shown in Figure 3.3. This strategy is designated as the indirect strategy in this chapter. The advantage of this approach is that the ZSC can be measured even when secondary leads are not physically close together.

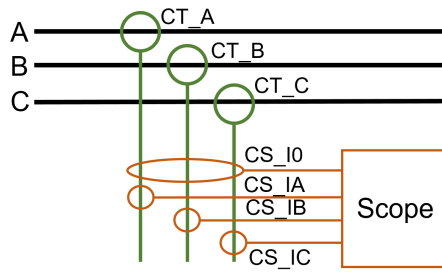


Figure 3.3: Schematic overview of the direct and indirect measurement of the zero-sequence current from secondary currents, including a dedicated probe that measures all three secondary currents simultaneously.

Measuring the zero-sequence current directly from secondary currents

Figure 3.3 also shows the principle of direct measurement of the ZSC from the secondary circuits, which is an alternative to the indirect measurement for ZSCs. One current sensor (CS_I0) is installed around the secondary circuits of all three current transformers of a single high-voltage branch. Since this sensor encloses the three phases simultaneously, it will sense the net current $I_A + I_B + I_C = 3 \times I_0$. In parallel to this, all secondary leads coming from the current transformers are also measured individually to be able to calculate the two remaining sequence currents.

The time-dependent signals from the current sensors in the indirect and direct strategies are recorded using an oscilloscope at a certain sampling frequency. This sampling frequency is chosen such that a reconstruction of the signal at the fundamental power frequency is possible. The magnitude and phase angle can be extracted using a Discrete Fourier Transform for the frequency of interest (e.g. 50 Hz).

3.3 Measurement uncertainty analysis of secondary current measurements

Evaluation of the measurement uncertainty is done in steps: firstly, the individual components within the measurement chain are analyzed individually. From this, the contribution of each component to the total measurement uncertainty of the measurement chain is determined. Next, the components are combined into the complete measurement chain. Many possible different measurement chains are

then simulated that have a certain component measurement errors that is inside the error bounds for that particular component. To this end, two methods of analysis are proposed in this work, namely: the analytical method, which determines the total measurement uncertainty algebraically and the stochastic method that uses MC simulations to estimate the total measurement uncertainty.

3.3.1 Assumptions

The analysis is based on a number of assumptions:

- The 50 Hz component is filtered out during the postprocessing stage of the measurement using a Digital Fourier Transform.
- The analysis starts with a known I_0 and I_1 to synthetically construct the phase currents, to be able to relate the outcome of the models to the 'true' value of I_0 and I_1 . In practice, the true values are evidently not known.
- In this research, the choice was made not to include negative-sequence currents in order to simplify the analysis. Therefore in this work, phase currents will only consist of a superposition of positive-sequence currents and zero-sequence currents. In practice, a non-zero negative-sequence current might be present, but the exclusion of negative-sequence currents in the present analysis does not influence the validity of the outcomes presented in this chapter. This has been verified by performing additional validation simulations.
- Phase current phasors are thus constructed from the known I_1 and I_0 by the following set of equations [20]:

$$\begin{cases} I_A = I_0 + I_1 \\ I_B = I_0 + \alpha \cdot I_1 \\ I_C = I_0 + \alpha^2 \cdot I_1 \end{cases}, \quad (3.2)$$

where $\alpha = \exp\left(\frac{2\pi}{3}j\right)$, i.e. a phasor rotation over $\frac{2\pi}{3}$.

- The different error sources are independent and uncorrelated. Therefore, the covariance between the errors of different error sources is equal to zero [84].

3.3.2 Error sources

Errors are modelled by assuming that each quantity of interest is uniformly distributed with the width equal to the maximum error value, according to the guidelines given in [85, section 6.4.2] and as determined in the relevant standard [80]. In the case of complex valued error sources, it is assumed that both the real and the imaginary part of the error are uniformly distributed with the corresponding widths.

Current Transformers

Instrumentation transformers are treated in the international norm IEC 61689 [80]. In particular, maximum measurement errors of current transformers (CTs) are determined within part 2 of this standard [81]. The maximum measurement errors depend on the class of the measurement transformer. We will assume the use CTs of class 0.2S, since the use of this class is usual practice in the high voltage system in the Netherlands. For these CTs, the upper limits for the ratio error and phase displacement are given as a function of the ratio between the current passing through the CT and rated current of the CT [81]. Relative errors decrease with increasing current [81]. More advanced approaches to the determination of instrument transformer errors exist [86], but these are out of scope of this study.

The ratio error is defined as the percentage difference of the measured secondary current times the current ratio with the primary current [81, Section 3.4.3]. The phase displacement is defined as the difference between the phase angle of the primary and secondary voltages [87, Section 3.4.4].

Current clamps and oscilloscope

The measurement accuracy of the current clamps that are connected to the secondary leads coming from the CTs can be found in the respective data sheet. For the direct ZSC measurement, it is advisable to use a current clamp with a high sensitivity (corresponding to the expected ZSC value of a few percent of the direct-sequence current). The data sheet of the current clamp will give the accuracy of the current clamp in a percentage of the rated current of the current clamp, depending on load impedance.

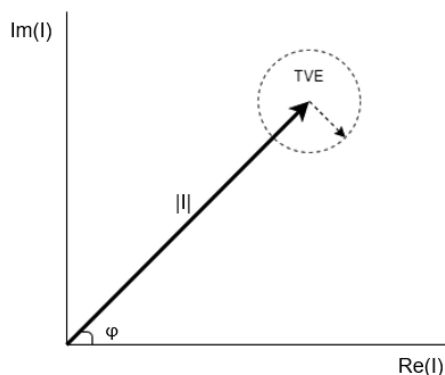


Figure 3.4: Schematic representation of the Total Vector Error of a PMU.

The digital oscilloscope that connects to the current clamp converts the analog signal into a digital signal, via an Analog-to-Digital converter. This conversion will lead to a quantization error [88]. Besides the quantization error, oscilloscopes also have a certain input uncertainty as a function of the full measurement scale.

PMU Total Vector Error

The measurement error of a PMU is defined by the Total Vector Error (TVE) [82]. The measured value of an observed vector is located within a disc described around the true value of the vector. The radius of this disc is equal to a certain percentage of the vector magnitude [82]. The TVE magnitude depends on the particular design of the PMU. Since the phase of the TVE-vector with respect to the measured vector is unknown (i.e. a uniform disc of uncertainty), the error magnitude in the analytical error expression is equal to half the magnitude of the TVE [89].

3.4 Analytical approach to error analysis

The real part of the standard measurement uncertainty of a complex quantity of interest z that is determined by a function of several variables $z = f(x_1, \dots, x_n)$ is

given by [90]:

$$u(\text{Re}(z)) = \left[\left(u(\text{Re}(x_1)) \left| \frac{\partial z}{\partial x_1} \right| \right)^2 + \dots + \left(u(\text{Re}(x_n)) \left| \frac{\partial z}{\partial x_n} \right| \right)^2 \right]^{\frac{1}{2}}, \quad (3.3)$$

where $u(\cdot)$ is the uncertainty associated with the respective variable. An analogous expression can be obtained for the uncertainty in the imaginary part of the variable, by inserting the imaginary part for the real part in (3.3) [84]. By constructing expressions for the measurement chains as described in section 3.2.2, we can determine analytical expressions for the total measurement errors of the measured positive-sequence currents and zero-sequence currents.

3.4.1 Measurement using current transformers, current clamps and an oscilloscope

The expression for the indirect determination of I_0 by means of three separate current clamps mounted on the secondary leads coming from the current transformers (see figure 3.3) is given by:

$$\tilde{I}_{0,\text{indirect}} = \frac{1}{3}(a_4 a_3 a_2 a_1 I_A + b_4 b_3 b_2 b_1 I_B + c_4 c_3 c_2 c_1 I_C), \quad (3.4)$$

where the following symbols signify the respective transfer coefficients: $\{a_1, b_1, c_1\}$ for the current transformers, $\{a_2, b_2, c_2\}$ for the current clamps, $\{a_3, b_3, c_3\}$ for the oscilloscope inputs and $\{a_4, b_4, c_4\}$ for the A/D-conversions inside the oscilloscope, respectively. The first three transfer coefficients are complex, the fourth is real. In this analysis, we will assume that the transfer coefficients have an expectation value of 1 and a standard deviation of σ_μ , with $\mu = 1 \dots 4$ (which is in general different for each type of transfer coefficient).

Similarly, an expression can be constructed for the direct determination by means of one single current clamp on all secondary leads coming from the current transformers:

$$\tilde{I}_{0,\text{direct}} = \frac{1}{3} a_4 a_3 a_2 \cdot (a_1 I_A + b_1 I_B + c_1 I_C). \quad (3.5)$$

The transfer coefficients are defined in a similar manner to the situation with three current clamps, with the difference that there is only one transfer coefficient for the current clamp (a_2 through a_4).

From the equations for the measurement chains, expressions can be found for the measurement uncertainty of the zero-sequence current. For the indirect measurement case, by applying (3.3), we get:

$$\begin{aligned} u(\operatorname{Re}(\tilde{I}_{0,\text{ind}}))^2 = & \frac{1}{9} [u(a_4)^2 + u(\operatorname{Re}(a_3))^2 + u(\operatorname{Re}(a_2))^2 + u(\operatorname{Re}(a_1))^2 + \dots \\ & u(b_4)^2 + u(\operatorname{Re}(b_3))^2 + u(\operatorname{Re}(b_2))^2 + u(\operatorname{Re}(b_1))^2 + \dots \\ & u(c_4)^2 + u(\operatorname{Re}(c_3))^2 + u(\operatorname{Re}(c_2))^2 + u(\operatorname{Re}(c_1))^2], \end{aligned} \quad (3.6)$$

and:

$$\begin{aligned} u(\operatorname{Im}(\tilde{I}_{0,\text{ind}}))^2 = & \frac{1}{9} [u(\operatorname{Im}(a_3))^2 + u(\operatorname{Im}(a_2))^2 + u(\operatorname{Im}(a_1))^2 + \dots \\ & u(\operatorname{Im}(b_3))^2 + u(\operatorname{Im}(b_2))^2 + u(\operatorname{Im}(b_1))^2 + \dots \\ & u(\operatorname{Im}(c_3))^2 + u(\operatorname{Im}(c_2))^2 + u(\operatorname{Im}(c_1))^2]. \end{aligned} \quad (3.7)$$

The uncertainty in the magnitude of I_0 is given by [84]:

$$u(|\tilde{I}_{0,\text{ind}}|) = \sqrt{u(\operatorname{Re}(\tilde{I}_{0,\text{ind}}))^2 + u(\operatorname{Im}(\tilde{I}_{0,\text{ind}}))^2}. \quad (3.8)$$

For the direct measurement we find similar expressions:

$$\begin{aligned} u(\operatorname{Re}(\tilde{I}_{0,\text{dir}}))^2 = & \frac{1}{9} [u(a_4)^2 + u(\operatorname{Re}(a_3))^2 + u(\operatorname{Re}(a_2))^2 + \dots \\ & u(\operatorname{Re}(a_1))^2 + u(\operatorname{Re}(b_1))^2 + u(\operatorname{Re}(c_1))^2], \end{aligned} \quad (3.9)$$

and:

$$\begin{aligned} u(\operatorname{Im}(\tilde{I}_{0,\text{dir}}))^2 = & \frac{1}{9} [u(\operatorname{Im}(a_3))^2 + u(\operatorname{Im}(a_2))^2 + \dots \\ & u(\operatorname{Im}(a_1))^2 + u(\operatorname{Im}(b_1))^2 + u(\operatorname{Im}(c_1))^2]. \end{aligned} \quad (3.10)$$

The uncertainty in the magnitude can be constructed according to (3.8). We designate the uncertainty parameters associated with this current clamp as $a_2 \dots a_4$, since only one current clamp is used.

As is evident from the comparison between (3.6) and (3.7) on one hand and (3.9) and (3.10) on the other side, the uncertainty in $\tilde{I}_{0,\text{dir}}$ will always be smaller than or equal to the uncertainty in $\tilde{I}_{0,\text{ind}}$, since all terms in the expressions are $\in \mathbb{R}_0^+$.

3.4.2 Measurement using current transformers and a PMU

The expression for the determination of I_0 using a PMU (as depicted in figure 3.2) can be made in an analogous way as in (3.4):

$$\tilde{I}_{0,PMU} = \frac{1}{3}(a_P a_1 I_A + b_P b_1 I_B + c_P c_1 I_C), \quad (3.11)$$

where $\{a_1, b_1, c_1\}$ and $\{a_P, b_P, c_P\}$ are the transfer coefficients of the current transformers and the PMU, respectively. Here, we also assume that the transfer coefficients have an expectation value of 1 and standard deviation σ_μ .

From this expression, we find the following analytical expression for the total measurement uncertainty of the PMU measurement chain:

$$\begin{aligned} u(\operatorname{Re}(\tilde{I}_{0,PMU}))^2 &= \frac{1}{9} [u(\operatorname{Re}(a_P))^2 + u(\operatorname{Re}(a_1))^2 + \dots \\ &\quad + u(\operatorname{Re}(b_P))^2 + u(\operatorname{Re}(b_1))^2 + \dots \\ &\quad + u(\operatorname{Re}(c_P))^2 + u(\operatorname{Re}(c_1))^2], \end{aligned} \quad (3.12)$$

and:

$$\begin{aligned} u(\operatorname{Im}(\tilde{I}_{0,PMU}))^2 &= \frac{1}{9} [u(\operatorname{Im}(a_P))^2 + u(\operatorname{Im}(a_1))^2 + \dots \\ &\quad + u(\operatorname{Im}(b_P))^2 + u(\operatorname{Im}(b_1))^2 + \dots \\ &\quad + u(\operatorname{Im}(c_P))^2 + u(\operatorname{Im}(c_1))^2]. \end{aligned} \quad (3.13)$$

The uncertainty in the magnitude is again given by:

$$u(|\tilde{I}_{0,PMU}|) = \sqrt{u(\operatorname{Re}(\tilde{I}_{0,PMU}))^2 + u(\operatorname{Im}(\tilde{I}_{0,PMU}))^2}. \quad (3.14)$$

The solutions found in (3.12) and (3.13) are largely analogous to the expressions of measurement uncertainty for the indirect measurement using current clamps in (3.6) and (3.7). The expressions give us insight into the standard measurement uncertainty that is associated with the different measurement approaches.

3.4.3 From standard measurement uncertainty to a confidence interval

To transform the standard uncertainty into a confidence interval, the standard uncertainty is multiplied by a two-dimensional coverage factor $k_{2,p}$, which depends

on the number of degrees of freedom and the desired coverage probability [89]. We use a two-dimensional coverage factor since the partial measurement uncertainties are complex. To compare the analytical method with the MC method that is described hereafter, we assume the number of degrees of freedom to be infinite ($\gg 1$) and the coverage probability to be 98% (in line with the number of simulations and probabilities used in the MC simulations). The expanded uncertainty is given by [89]:

$$U = k_{2,p}u, \quad (3.15)$$

where u is the standard uncertainty associated with a particular measurement approach. For our case, $k_{2,0.98} = 2.7971$. The confidence interval can then be established by: $[x - U, x + U]$, where x is the expected value of the measurand (in our case I_0) [89]. Coverage factors for other coverage probabilities can be found in [89]. It is assumed that the error is symmetrically distributed around x , as long as $x - U \geq 0$. If the latter expression is smaller than zero, $x - U$ is assumed to be zero.

Although the analytical method gives us expressions for the width of the confidence interval, it does not give us direct insight in the actual distribution of measurement outcomes. To this end, we have set up MC simulations for the three described measurement strategies.

3.5 Error analysis using Monte Carlo simulations

For the MC simulations, the measurement chains were modelled according to Sec. 3.2.2. For a given simulation run, a set of randomized errors was generated for each component in the measurement chain.

The current transformer errors are modelled as having a uniform distribution between the limits as stated in the standard [81]. The current clamp and oscilloscope input accuracies are also modelled as uniformly distributed errors. The quantization error that is caused by the A/D-conversion inside the oscilloscope is modelled by rounding the simulated value at the input of the oscilloscope to the nearest value inside the set of possible values given the limits of measurement and number of measurements. The magnitude of the PMU Total Vector Error is modelled as a uniform distribution between zero and the maximum TVE-percentage.

Table 3.1: Overview of the simulation parameters used in the MC simulations

Parameter	Value
I_1	100 . . . 1900 A (in steps of 100 A)
I_0	10 A
Current transformer class	0.2s
Current transformer rating	2000 A
Current clamp accuracy	1%
Oscilloscope input accuracy	0.2%
Oscilloscope bit rate	16 bit
Oscilloscope range ^a	-2000 . . . 2000 A
PMU Total Vector Error	1%
Number of simulations per (I_0, I_1) -value	10^5

^aEquivalent value given by the transfer function of the current clamp.

The TVE angle is modelled as a uniform distribution between 0 and 2π . The end point of the measured phasor is therefore within the disc as depicted in figure 3.4.

A measure of the measurement uncertainty is the width of the distribution of zero-sequence currents found for a particular known combination of I_1 and I_0 . We use the following metric for the width of the I_0 -distribution:

$$\mathcal{W}_{I_0} = \mathcal{I}_0^{0.99} - \mathcal{I}_0^{0.01}, \quad (3.16)$$

where \mathcal{W}_{I_0} is the width of the distribution and $\mathcal{I}_0^{0.99}$ and $\mathcal{I}_0^{0.01}$ are the 99th and 1st percentile of the I_0 -distribution, respectively.

For a given set of known positive-sequence currents and zero-sequence currents, 10^5 MC runs were generated. By means of these simulations, a distribution of the possible outcomes of the estimated zero-sequence currents is attained. As an example, figure 3.5 shows the dependence of the distribution width on the number of simulations. At 10^5 simulations, the distribution width yields a stable value, which is approximately 6 A for the chosen combination of I_0 and I_1 (respectively 10 A and 500 A). The outcome of the simulations are studied using statistical methods. Table 3.1 shows the input parameters for the MC simulations for all studied cases. We have chosen parameters that reflect the actual accuracy of instruments that one

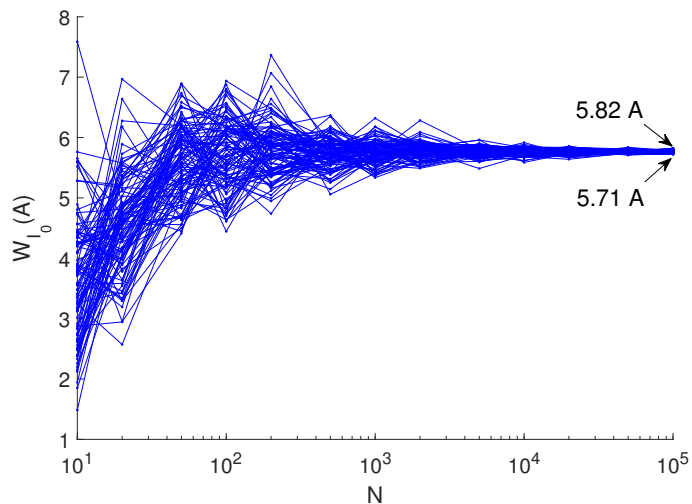


Figure 3.5: Ensemble of the zero-sequence current distribution widths (as defined in (3.16)) as a function of the number of simulations (PMU-case), at $I_1 = 500$ A and $I_0 = 10$ A. 100 repetitions were made of a range of different run numbers (ranging from 10^0 runs to 10^5 runs), at a single value for I_0 and I_1 . From 10^4 runs onwards, the widths converge to a single value, indicating outcome stability of the simulations. At 10^5 runs, all widths are within the interval (5.71, 5.82).

would encounter in practice and to provide the possibility to compare the accuracy of the different measurement strategies studied. For example, in practice one would be advised choose to use a current clamp with a higher accuracy for the simultaneous measurement of all phase currents or choose a PMU that has a smaller TVE value than described in this work. The developed methods allow easy adjustment to include the instrument parameters that one may use in their own measurements.

3.5.1 Simulated error distributions of the current clamps and oscilloscope method

Figure 3.6 shows the outcomes of the MC simulation for the measurement using current clamps and an oscilloscope, for both the direct and indirect method. The plot shows that, given the chosen uncertainty parameters, there is a clear distinction between the outcome distributions for the direct and indirect method: the direct measurement method leads to a tighter distribution around the true value of I_0 and therefore performs better than the indirect method for the parameters chosen. Furthermore, the mean values of the direct measurement distributions are equal to the input value of I_0 , whereas the mean values of the indirect measurement distributions increase with increasing I_1 .

3.5.2 Simulated error distributions for a PMU system

Figure 3.7 shows the outcomes of the MC simulations for the measurement strategy using a PMU. We observe that the width of the distribution varies between approximately 1.2% and 1% of I_1 , depending on I_1 , using the aforementioned accuracy values in the measurement chain. This means that for lower values of I_0 with respect to I_1 , the uncertainty about the measured value can become quite large (e.g. for a constant I_0 of 10 A, this amounts to a (1-99%)-distribution width of 24 A or 240% of I_0). The I_0 -distribution mean increases with increasing I_1 , similar to the simulations outcomes of the indirect measurement method. Since the lower value of the magnitude of I_0 cannot be smaller than 0 A, the lower bound of the distribution will be capped at 0. The upper bound can increase with increasing I_1 , which leads to the observed increase of the mean with increasing I_1 .

3.6 Comparison between the analytical method and the MC simulation method

Since MC simulations are relatively computationally expensive and time consuming to perform for each combination of I_0 and I_1 , it is worthwhile to compare the analytical expressions and the MC simulations, in order to study the mutual agreement between and validity of the applied methods of analysis in this particular and illustrative example. The comparisons in Figs. 3.6 and 3.7 show that the outcome

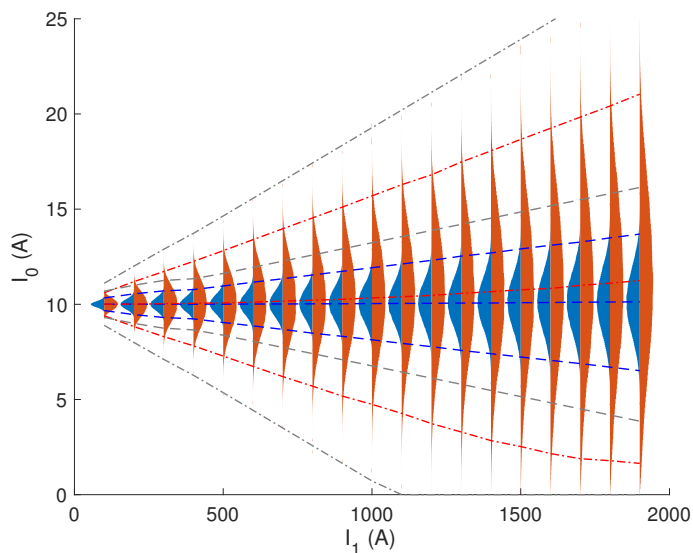


Figure 3.6: Simulation outcomes that show the measurement outcome bandwidths at a constant zero-sequence current of 10 A and the direct sequence current from 100 A to 2000 A in intervals of 100 A, measured using current clamps and oscilloscope. Distributions are plotted as a split violin plot. Both the direct method (left side violin, blue) and indirect method (right side violin, red) are shown. Also plotted are the distribution means, 1%-quantiles and 99%-quantiles. The dashed grey lines show the upper (99%) and lower (1%) bounds as predicted by the analytical model for the direct measurement, the grey dash-dot lines show the upper and lower bounds from the analytical model for the indirect measurement.

of the analytical method is in agreement with the I_0 distribution width from the MC simulations. Both the analytical method and the MC method show that the lower bound the I_0 -magnitude in case of the PMU-measurements and indirect oscilloscope measurements goes to zero at higher values of I_1 , since the minimum cannot be smaller than zero. In all cases, the analytical method predicts a higher value for the upper bound of the distribution and a lower value of the lower bound of the distribution.

In most practical applications, the analytical method is better suited to determine the confidence interval of a measurement than the MC-method, since the upper and lower bounds can be directly calculated for a given (I_0, I_1) combination. The MC method is computationally more expensive (due to the large number of

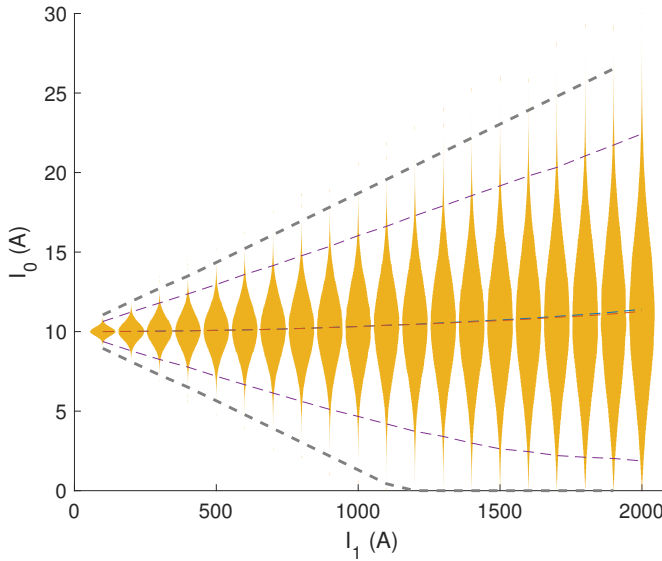


Figure 3.7: Simulation outcomes that show the measurement outcome bandwidths for a zero-sequence current of 10 A measured using a PMU. The figure shows double-sided violin plot for the outcomes of simulations at intervals of 100 A of the direct-sequence current. Also shown are the distribution means (in blue), medians (in red) and 1%-quantiles and 99%-quantiles (in purple). The dashed grey lines show the upper and lower bounds as predicted by the analytical model for the PMU-measurements.

simulations needed per combination of I_0 and I_1). The MC method can be implemented by means of a look-up table could be made to determine the upper and lower bounds for a certain range of I_0 and I_1 . If a more precise estimation of the confidence interval is necessary or the number of needed combinations of I_0 and I_1 is small, one could opt for the application of the MC method.

Table 3.2 shows the distribution widths of the various measurement strategies for different values of I_1 , based on the outcomes of the analytical method. Of the three strategies, the direct strategy leads to the smallest distribution widths. It is interesting to note that the distribution widths of the indirect strategy and PMU strategy are relatively similar at different values of I_1 .

Table 3.3 presents the uncertainty budgets (relative variances) for the studied

Table 3.2: Comparison of the I_0 -distribution width as a function of I_1 between the three studied strategies based on analytical calculations

I_1 (A)	Direct Oscilloscope \mathcal{W}_{I_0} (A)	Indirect Oscilloscope \mathcal{W}_{I_0} (A)	PMU \mathcal{W}_{I_0} (A)
100	1.4	2.2	2.1
500	3.2	9.3	8.7
1000	6.5	18.6	17.4
1500	9.7	23.9	23.1
1900	12.3	27.6	26.5

measurement strategies as a percentage of total variance per measurement strategy, using the analytical methods developed. The uncertainty budgets were determined at a positive-sequence current of 1000 A and a zero-sequence current of 10 A, with the measurement system parameters as described in table 3.1. Combining the outcomes of the I_0 -distribution widths and the outcome of the variance analysis, one may observe that the direct oscilloscope strategy is the most precise measurement method of the three studied measurement strategies. In this strategy, the current transformers constitute the largest source of uncertainty for the direct method (99.8% of the outcome variance). Therefore, if one used the direct method to measure zero-sequence currents during steady state operation, the best way to improve the measurement accuracy is to use well-calibrated current transformers. On the other hand, if one uses the PMU strategy, the most efficient way to improve zero-sequence current measurement accuracy is by using a PMU that has a Total Vector Error that is as low as possible, since in this case 86.2% of the outcome variance is the largest error source. An interesting observation is that the variance caused by the PMU Total Vector Error is very close to the sum of the variances "Current clamps", "Oscilloscope" and "A/D conversion" in the indirect oscilloscope strategy (86.2% versus 87.9%).

3.7 Validation measurements and simulations

To determine the validity of the analytical and MC models for the measurements using current clamps and an oscilloscope, validation measurements were carried out using a current source (Omicron CMC 356) that can put out three independent

Table 3.3: Comparison of the distribution of variances (as a percentage of total variance) for the studied measurement strategies, at $I_1 = 1000 \text{ A}$, $I_0 = 10 \text{ A}$.

Source of uncertainty	Direct Oscilloscope Strategy (%)	Indirect Oscilloscope Strategy (%)	PMU Strategy (%)
Current transformers	99.8	12.1	13.8
Current clamps	0.19	75.8	-
Oscilloscope	0.030	12.1	-
A/D conversion	0.021	0.0075	-
PMU Total Vector Error	-	-	86.2

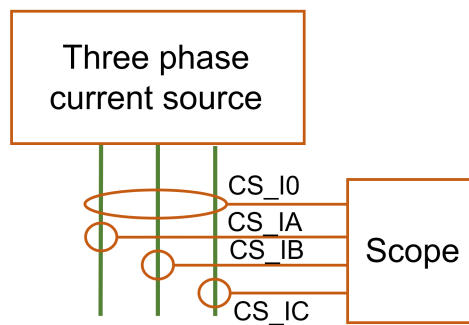


Figure 3.8: The measurement setup used for the validation measurements. Three independent phase currents were generated and measured using the direct and indirect measurement.

phase currents with arbitrarily chosen amplitudes and phase angles for each phase, which are in the same order as the currents in secondary circuits of current transformers. The current source was used to generate 19 different I_1 -values (equivalent to 100 A to 1900 A primary positive-sequence current) at a constant I_0 -value (equivalent to 10 A primary zero-sequence current), taking into account a primary CT ratio of 1:800. Three current clamps with a per-clamp accuracy of 2% were used to measure each individual phase current, in addition to a 16 bit oscilloscope with an input accuracy of 0.2% per channel. A fourth current clamp was used to measure the ZSC directly. To achieve variation within the measurements, the current clamps for the indirect measurements were placed around the phase conductors in all possible permutations, leading to six measurement outcomes per I_1 -value. Figure 3.8

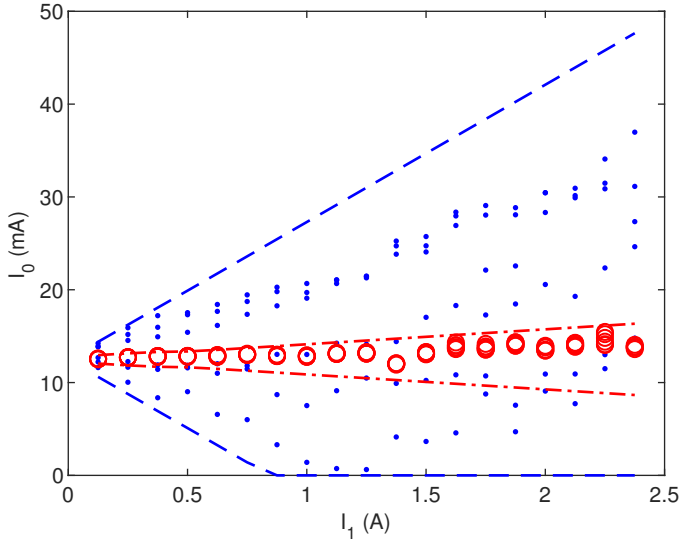


Figure 3.9: Overview of validation measurement outcomes (blue dots) and corresponding 1% and 99% error bounds (blue dashed lines), for the indirect measurements and measurement outcomes (red circles) and corresponding 1% and 99% error bounds (red dash-dot lines) for the direct measurements. Note that the current scale is different from the current scales in figures 3.6 and 3.7.

shows a schematic of the validation measurement setup.

Figure 3.9 shows the outcome of the validation measurements together with the predicted error bounds from the analytical model using the aforementioned parameters of the current clamps and an assumed 0.2% accuracy of the current source. Note that the current scale is different from the current scales in Figs. 3.6 and 3.7. The measurement outcomes show good agreement with the predictions of the analytical model.

Figure 3.10 shows the outcomes of validation simulations of PMU measurements in which the impact of the presence of a negative-sequence current in the current signal is studied. The simulations show that for small values of I_2 (in this case, $I_2 = I_0 = 10$ A), the presence of a negative-sequence current does not influence the simulated with of the zero-sequence current. When performing zero-sequence current measurements in the field, it is recommended to perform a measurement system validation as described here.

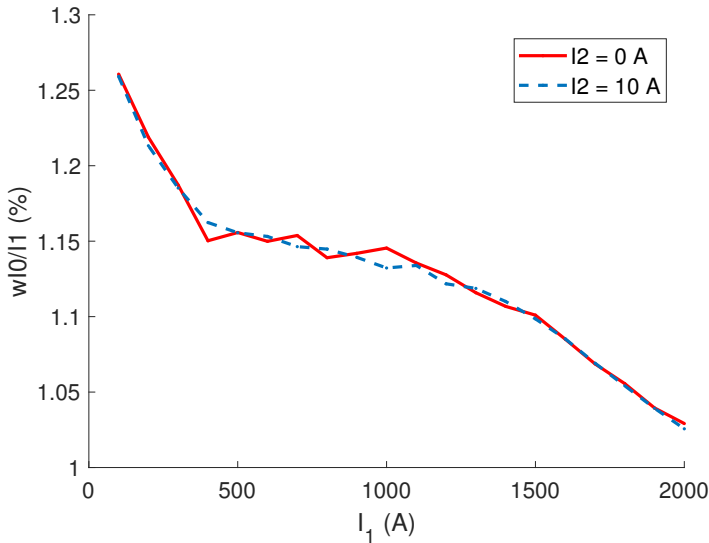


Figure 3.10: Relative width of the I_0 -distribution of a simulated PMU measurement relative to the input value of I_1 , with and without the presence of a negative-sequence current. The outcome shows that the simulated width of the I_0 -distribution is independent of the presence of a negative-sequence current in the current signal.

3.8 Summary and conclusions

A number of practical approaches to measuring ZSCs during normal operation is available. By defining the complete measurement chain and the different factors that contribute to measurement uncertainty, it is possible to analyze the total measurement uncertainty that is associated with the ZSC measurement. Three measurement strategies have been studied both analytically and by means of MC simulations. The advantage of the analytical method is that it is computationally much faster to determine the measurement uncertainty once the complete expression for the measurement error has been established. The MC method is more flexible in the use of different statistical distributions of the underlying measurement errors (e.g. non-uniformly distributed errors) and provides insight into the statistical distribution of total measurement uncertainty.

The direct strategy using current clamps connected to the secondary leads of

the current transformers is more accurate than the determination of the ZSC using a PMU, given comparable accuracy of the instruments used. We also observe a difference between the direct and indirect strategies of measurement. The direct measurement strategy is more precise than the indirect measurement. By using a single current sensor to measure the ZSC directly, the total measurement uncertainty in the determination of the ZSC in the branch will be smaller than by using three independent current sensors of the same accuracy. It however remains necessary to measure each phase individually (i.e. the indirect strategy) to be able to calculate the other sequence currents. Current transformer measurement errors are the dominant errors for the direct method. The PMU TVE is the dominant source of uncertainty for the PMU strategy. If there is a preference for the use of a PMU and there is the possibility to connect a current sensor that can measure all three phase currents simultaneously, this will increase the measurement accuracy.

A comparison between the analytical method and MC simulations shows that the outcomes of these methods are in agreement for all studied strategies. This is also supported by validation measurements for the direct and indirect strategies.

In this study, general values for the measurement errors of the different components were used, such as normalized values for the measurement errors of the current transformers. In practice these values are upper bounds for the measurement error and instruments inside the measurement chain might have better accuracy values. The methods that were developed in this chapter are general and are also applicable in such cases. Taking into account the actual tolerances of these measurement instruments may lead to a decrease of the total measurement error of the measurement chain.

Future work includes the application of the developed methods to assess ZSC measurement uncertainty in meshed power systems where several PMUs are installed. By using these methods, one can assess if measurements of ZSCs by independent PMUs are in agreement and the propagation of ZSCs in the meshed system can be studied in more detail.

Another interesting future line of research would be to apply Rogowski coils to directly measure primary currents around (isolated) primary conductors. When these devices are combined using an integrator circuit, this could result in improved

measurement accuracy by excluding the contribution of the primary current transformers to the measurement error. The measurement uncertainty of such a measurement setup could be analyzed by means of the same methods that were developed in this chapter.

Another possible measurement setup that could be used if the secondary leads from the current transformers are not physically close to each other is to connect the current sensors in series before connecting to the measurement device (such as an oscilloscope). The accuracy of such an setup could also be studied using the methods developed in this chapter.

Based on the results developed in this chapter, the following recommendations can be made for zero-sequence current measurement in practice:

- If there is a possibility to measure all three phase leads from the primary current transformers simultaneously, this leads to the most precise measurement of zero-sequence currents.
- To be able to measure the positive-sequence current and negative-sequence current, it is necessary to measure each phase lead independently.
- If a single probe is used for zero-sequence current measurements, it is advised to use a dedicated current probe with high sensitivity and to set the oscilloscope range to the proper range of values that can be expected (i.e. smaller than the nominal load of the transmission line). This provides better measurement accuracy, in particular when zero-sequence current levels are relatively low.
- To prevent possible influence of higher harmonics (such as the third harmonic), the 50 Hz component should be filtered out.
- Calibrating the primary current transformers can improve the measurement accuracy significantly, in particular for the direct measurement strategy.
- Other measurement equipment should be calibrated correctly before starting the measurement campaign.
- For the PMU measurement strategy, the best way to increase measurement accuracy is to use a PMU with a lower Total Vector Error.

Chapter 4

Zero-sequence current measurements in the 150 kV grid using the direct method

4.1 Introduction

Performing field measurements on in-service high voltage branches can serve to further understand the behavior of zero-sequence currents in high voltage systems during steady state conditions. Current literature lacks exhaustive information on the time-domain behavior of zero-sequence currents during these condition, as a function of the different parameters on which zero-sequence current levels depend. When zero-sequence current levels are reported in literature, only single (extreme) values are given, either based on field measurements or simulations. In reality, currents in high voltage systems are continually changing due to changing supply and demand. Reports of longer time series that show the dynamics of zero-sequence currents in time are however not available in current literature.

To address this lack of knowledge and to study the dynamics of zero-sequence currents in a real-life field setting for longer time periods, online field measurements were performed in two high-voltage branches connected to a single high voltage substation. The goal of this research is to obtain more insight into the behavior of zero-sequence currents through measurement. The two 150 kV branches (consisting

in part of overhead lines and in part of underground cables) were measured during a period of approximately 240 hours. The measurements were performed using the current transformer, current transducer and oscilloscope method as described in the preceding chapter. By means of the methods that were developed in Chapter 3, the measurement accuracy of the measurements that were performed could be determined, an aspect of zero-sequence current measurement that is currently also not developed in literature.

This chapter describes the measurements that were performed and expands upon the information that could be extracted from these measurements. Section 4.2 describes the situation that was studied including the relevant information on the local network properties. Next, section 4.3 describes the measurement setup that was used to perform the measurements. In section 4.4 the methods that were developed in chapter 3 were used to determine the measurement accuracy and errors based on the individual accuracy parameters of the measurement instruments in the measurements chains. Section 4.5 gives an overview of the measurement results and analyzes several phenomena that were observed in the data. Finally, section 4.6 summarizes the results found in the chapter and expands on the conclusions that were drawn.

4.2 A hybrid transposed transmission line in a meshed network

Field measurements were performed at a high voltage substation in the eastern part of the Netherlands. At this substation (indicated by the internal code ZV), the two connected 150 kV branches were studied. Figure 4.1 shows a schematic diagram of the 150 kV and 380 kV network in the vicinity of the branches that were studied by measurements at substation ZV, where the two branches under study are highlighted by thicker lines. Note that this is only part of a much larger surrounding network, in which several other sources of zero-sequence currents may be present. In addition, three 150/10 kV Y(N)d5 power transformers are present at substation ZV, as well as two two-phase 150 kV connections to a nearby customer, next to the two main 150 kV branches. These two-phase connections are connections in

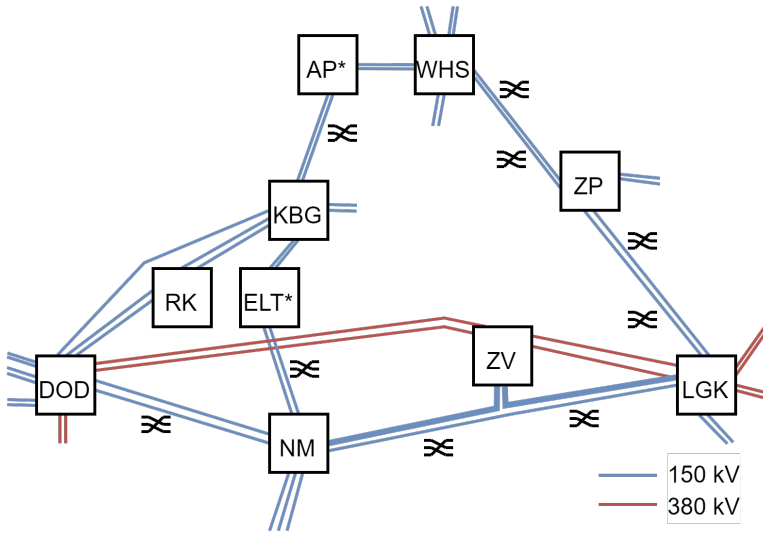


Figure 4.1: The high voltage network in the region around the 150 kV branches that were studied. The branches on which the measurement are performed are highlighted by the thicker lines. The network around the branches is highly meshed, which has a large influence on the way power flows through the network, depending on loads, available generation and possible outages of branches within the network. Substations where grounded transformer neutral points are present are indicated by an asterisk, locations of transpositions are indicated by a transposition symbol. Note that in some branches there is only a partial transposition present.

between phases. Since in this configuration (during normal operation) the outgoing current toward these connections is equal to the incoming current, the resulting zero-sequence current resulting from these connections is equal to zero. The negative-sequence current is however not equal to zero¹. This behavior has been validated by additional measurements that were performed on the currents of these customer connections.

The 150 kV branches connected to substation ZV are part of a meshed network of 150 kV and 380 kV branches. The schematic shown in figure 4.2 gives a more detailed overview of region in which the measurements were done. The additional lower voltages which are present at the substations is not shown for the sake of

¹Assume the outgoing current $I_A = I$, the incoming current $I_B = -I$ and $I_C = 0$. Then: $I_0 = \frac{1}{3}(I - I + 0) = 0$, $I_1 = \frac{1}{3}(I - \alpha I + 0) = \frac{1}{3}(1 - \alpha)I$ and $I_2 = \frac{1}{3}(I - \alpha^2 I + 0) = \frac{1}{3}(1 - \alpha^2)I$. Furthermore: $m_{I_2} = \left| \frac{I_2}{I_1} \right| \times 100\% = 100\% \forall I$

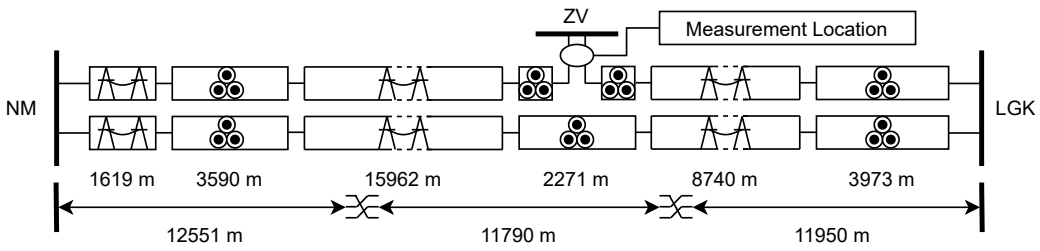


Figure 4.2: Overview of the system under study: 150kV NM-ZV-LGK. The upper part of the figure shows the configuration as a function of length: overhead line or underground cable. For the part of the branches that consist of overhead lines, the parallel branches are installed on the same tower. The lower part of the figure shows the locations of transposition towers within the branches.

simplicity. The branches in this network consist of a mixed combination of overhead lines and underground cables.

The system under study is schematically shown in figure 4.2. The two measured branches form a coupled system with a third 150 kV branch, which connects substation NM directly with substation LGK. Starting at substation NM, the branches first cross the Waal river via overhead lines for 1619 m, after which the branches consist out of cables for 3590 m. Following this, there is a section of 15962 m of overhead lines, followed by a cable section of in total 2271 m. In this cable section, two of the three branches (NM-ZV150 and LGK-ZV150 are connected to substation ZV at approximately the middle point. Towards substation LGK the branches consist again of an overhead line section (8740 m) and a final cable section (3973 m). The branch NM-LGK150, which connects substations NM and LGK directly is parallel to the other two branches of the full lengths of these branches.

In the branches transposition towers are present at two locations one at 12551 m from substation NM and one at 11950 m from substation LGK. The transposition tower divide the branches in roughly three equal parts from substation LGK to substation NM (taking lengths of the branches NM-ZV150 and LGK-ZV150 together).

4.3 Measurement setup

To perform the measurements, we designed a measurement chain that consists of both equipment that was already installed at the substation as well as equipment

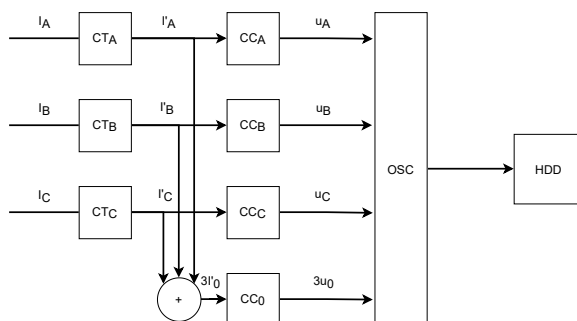


Figure 4.3: Measurement diagram for the oscilloscope measurements.

that was purposefully installed for the measurements.

Figure 4.3 shows a schematic of the measurement chain for one 150 kV branch, which is identical to the current clamp and oscilloscope measurement strategy described in Chapter 3. As the primary currents I_A , I_B and I_C pass through the current transformers, secondary currents I'_A , I'_B and I'_C are generated. Four current clamps were installed around the secondary leads coming from the current transformers: three current clamps for each current transformer, as well as a single current clamp that enclosed all three phases at once (the "direct probe"). The current clamps transform the currents inside their perimeters into voltages. Each current clamp was connected to a four-channel digital oscilloscope. This ensured that all signals could be synchronized with each other to construct the respective symmetrical components I_0 , I_1 and I_2 . The signals from the current clamps were recorded using a USB oscilloscope and stored for subsequent analysis.

The accompanying accuracy and measurement errors of each measurement instrument within the measurement chain and the combined measurement accuracy of the complete measurement chain is further discussed in section 4.4.

4.3.1 Measurement data post-processing

After the data are recorded to a hard drive, the data could be processed for further analysis. Each data channel was broken up in equal lengths. For each length, the 50 Hz amplitude and phase angle was determined using a Fast Fourier Transform. From the amplitude and phase angle, three phasors can be determined for

Component	Parameter	Value
Current transformers	<i>Class</i>	0.2s
	<i>Rated transformation ratio</i>	1000:1
	<i>Rated current</i>	2000 A
Current clamps	<i>Accuracy</i>	2 %
	Oscilloscope	<i>Input accuracy</i>
		<i>Bit rate</i>

Table 4.1: Overview of the individual accuracy values of the components in the measurement chain.

each phase current and one phasor can be determined for the zero-sequence current from the direct probe. Using these phasors, the positive-sequence component, zero-sequence component and negative-sequence component (if necessary) can be determined and analyzed for the particular time period.

4.4 Measurement chain accuracy

Using the methods developed in chapter 3, we can determine the measurement accuracy of the measurement chain described in the preceding section. To this end, this section first describes the errors associated to all elements within the measurement chain and consequently combines these errors to determine the total measurement error of the whole chain. Table 4.1 presents the relevant parameters of the components in the measurement chain.

4.4.1 Current transformers

The installed current transformers at substation ZV are class 0.2S current transformers with a ratio of 1000 between the primary and secondary current and a rating of 2000 A. Figure 3.1 shows the upper bounds for the ratio error and phase displacement as a function of the rated current.

4.4.2 Current clamps

The precision of a current clamp is given by the manufacturer as a function of the output range of the instrument. The current clamps that were used for the measurement have a precision of 2%.

4.4.3 Oscilloscope

The accuracy of a digital oscilloscope is determined by two factors: the input accuracy and the error introduced by rounding an analog value to the closest available digital value.

The USB-oscilloscope that was used for the measurements has an input accuracy of 0.2%. The signal was converted to a digital signal with 16 bit resolution. In the post-processing stage, the 50 Hz component for each measured current channel was determined using a Discrete Fourier Transform.

Before the measurement, the current clamps and oscilloscope were calibrated in a laboratory environment using a calibrated three-phase current source.

4.4.4 Combined measurement accuracy

The analytical method developed in Chapter 3 for direct oscilloscope measurement was used to determine the width of the confidence interval for the measurements of zero-sequence currents. Figure 4.4 shows the combined measurement accuracy (expressed as the 1-99% distribution width of I_0) for the measurement setup within the parameter space of the measurement outcomes. The outcomes are the result of calculations of the I_0 -distribution width as a function of a known combination of (I_1, I_0) and the measurement system parameters as mentioned. For instance, at the point (250,5) in the (I_1, I_0) -parameter space, the width of the distribution is equal to 2 A, meaning that a I_0 measurement outcome can be expected in the interval (4,6) A. The figure shows that for zero-sequence currents larger than approximately 2 A, the distribution width is mostly dependent on the primary-sequence current: in this part of the parameter space, the isolines are oriented close to vertical. For smaller currents, a kink is visible in the isolines, which is caused by the lower part of the I_0 -distribution reaching 0 A, which is the lower bound of the zero-sequence current magnitude by definition.

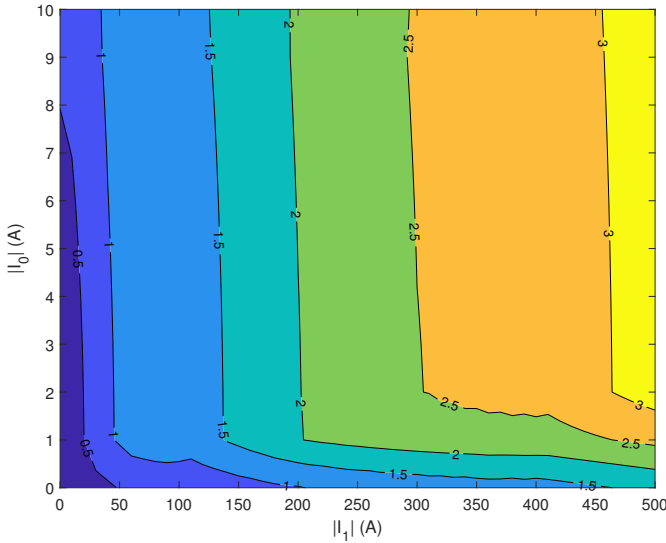


Figure 4.4: Width of the I_0 -distribution of the direct measurement method within the parameter space of the measurement outcomes at ZV.

4.5 Measurement results and analysis

Figures 4.5 and 4.6 show the measurement outcomes plotted as a time series for both branches over the full measurement period. The figures show both the measured zero-sequence current (from the direct measurements of the zero-sequence current) as well as the positive-sequence current. For the zero-sequence current, the outcome of the direct measurements is shown together with the associated 1-99% confidence interval. Since the uncertainty associated with the indirect measurements is much larger (see chapter 3), the outcome of the indirect is not shown.

Figure 4.7 presents the data in an alternative way: by showing a scatter plot of (I_1, I_0) for both branches, downsampled to a total of 1000 data points over the full measurement period. During the measurement period, the mean zero-sequence current and positive-sequence current is lowest in the NM-ZV150 branch. This is due to the fact that during the measurement period, power flows mainly from the LGK-substation in the direction of ZV and NM, since substation LGK is a coupling point between the 150 kV and 380 kV networks. Part of the load coming from substation LGK is present at substation ZV. Another observation is that both datasets

show a relatively constant value of I_0 with respect to I_1 and the data appear to be clustered and homogeneous. A distinctive cluster in the LGK-ZV150-data can be observed around $I_1 = 200$ A and $I_0 = 7.5$ A. This cluster corresponds to the time period around 144 hours, when one of the branches (NM-ZV150) was brought out of service due to planned maintenance. The corresponding cluster for the NM-ZV150-branch can therefore be observed near the origin.

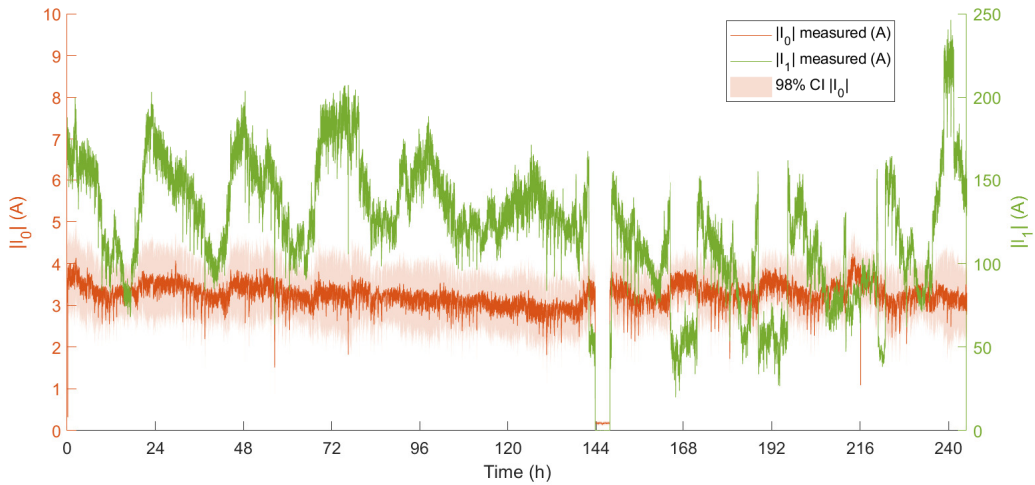


Figure 4.5: Time series of the measured magnitudes of $|I_0|$ (in orange, left y-axis) and $|I_1|$ (in green, right y-axis) for the full measurement period for the branch NM-ZV150.

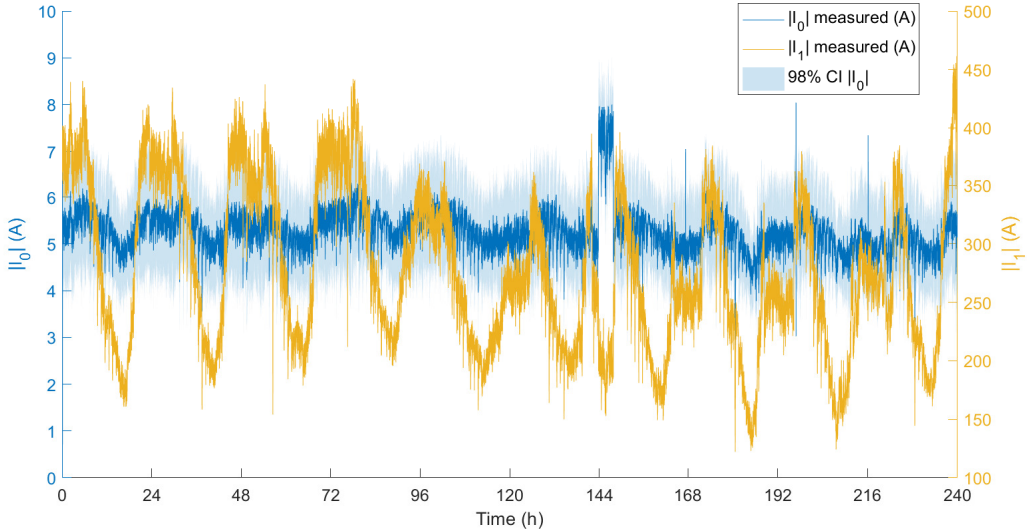


Figure 4.6: Time series of the measured magnitudes of $|I_0|$ (in blue, left y-axis) and $|I_1|$ (in yellow, right y-axis) for the full measurement period for the branch LGK-ZV150.

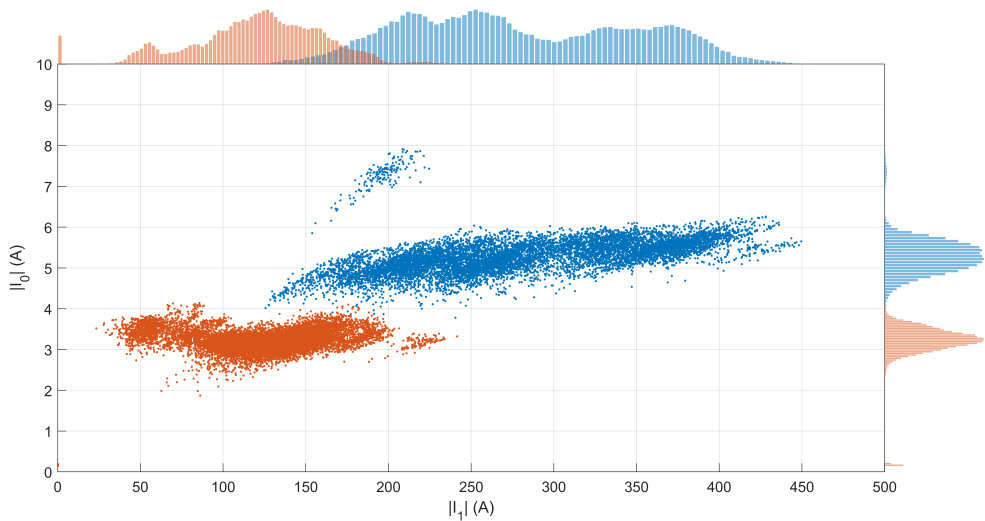


Figure 4.7: The scatter plot of $|I_1|$ and $|I_0|$ for the full measurement series, downsampled to 10 000 samples per branch. The histograms of the respective $|I_0|$ and $|I_1|$ distributions are also shown.

During the measurement period, several modes of operation can be distinguished:

- Between 0 and 143 hours, the positive sequence current fluctuates on a daily basis.
- Around 144 hours, branch NM-ZV150 is brought offline because of a planned outage. In consequence, the positive-sequence current in branch LGK-ZV-150 decreases. Branch NM-ZV150 is brought online again around 152 hours.
- Between 164 to 245 hours, there are several large fluctuations in the positive-sequence current due to sudden load changes in the network.

In the remainder of this section, each mode of operation is studied in more detail.

4.5.1 Daily fluctuations

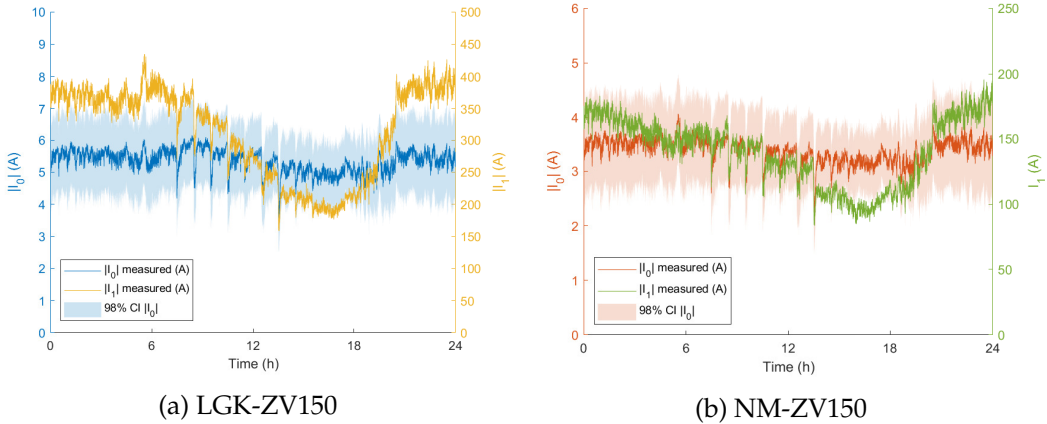


Figure 4.8: Time series of measured $|I_0|$ and $|I_1|$ in both branches on day 2, which was a day with normal daily fluctuations in the network.

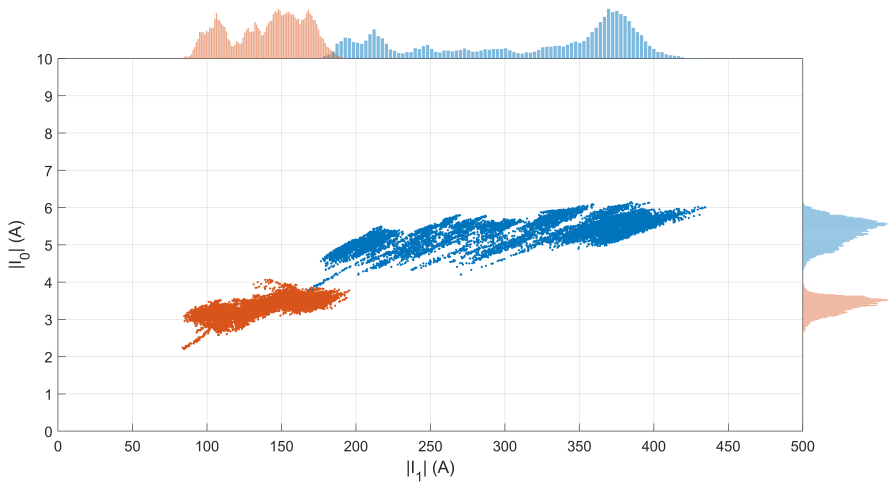


Figure 4.9: The scatter plot of $|I_1|$ and $|I_0|$ for day 2, downsampled to 10 000 samples per branch. Also shown are the histograms for $|I_0|$ and $|I_1|$ for both branches.

Figures 4.8a and 4.8b show the time series of zero-sequence currents and positive sequence currents for the second 24 hours of measurement for both branches. Figure 4.9 shows the same data, as a $|I_0|$, $|I_1|$ scatter plot. Several observations can

be made on the basis of the data: while the positive sequence current shows a clear distinction in magnitude between different parts of the day, this distinction is not clearly present in the zero-sequence current magnitude. The zero-sequence current magnitude is therefore not strongly dependent on the positive sequence current magnitude. Note that the time designation does not correspond with the hour of day, but rather with the start of the measurement series, which was started at approximately 10:00 AM on day 1.

During normal daily operation, the positive-sequence current and the zero-sequence current fluctuate throughout the day and mostly follows the direction of the positive-sequence current: when the positive-sequence current increases, the zero-sequence current also increases, however within the bounds of the measurement accuracy. The dynamic range (the ratio between minimum and maximum value in a given time period, e.g. 24 hours) is smaller for the zero-sequence current than for the positive-sequence current. For instance, for the first 24 hours in branch LGK-ZV150, the dynamic range for the zero-sequence current is 1.2, whereas the dynamic range for the positive-sequence current is 2.5 during this time period. The difference in dynamic range between $|I_0|$ and $|I_1|$ is larger for the branch LGK-ZV150, which could be caused by the meshed network connected to substation LGK.

Another observation that can be made are the repeated drops in both the positive sequence current and the zero-sequence current in both branches, starting from approximately 7.5 hours in the measurement time and continue until 15.5 hours. The drops occur with a constant return rate of 1 hour. The most likely cause of this is a change in supply and demand due to trading. The measured drop rate of the first drop at 7.5 hours of the primary-sequence current is approximately -2.2 A/s, whereas the drop rate of the zero-sequence current is approximately -0.03 A/s.

4.5.2 Scheduled outage

Around 144 hours of measurement time, one of the circuits (NM-LGK150) was temporarily taken out of service because of a scheduled outage, see figures 4.10a, 4.10b and 4.11. After 4 hours, (shortly before 148 hours) the circuit was put into service again. We observe a number of interesting points around these phenomena.

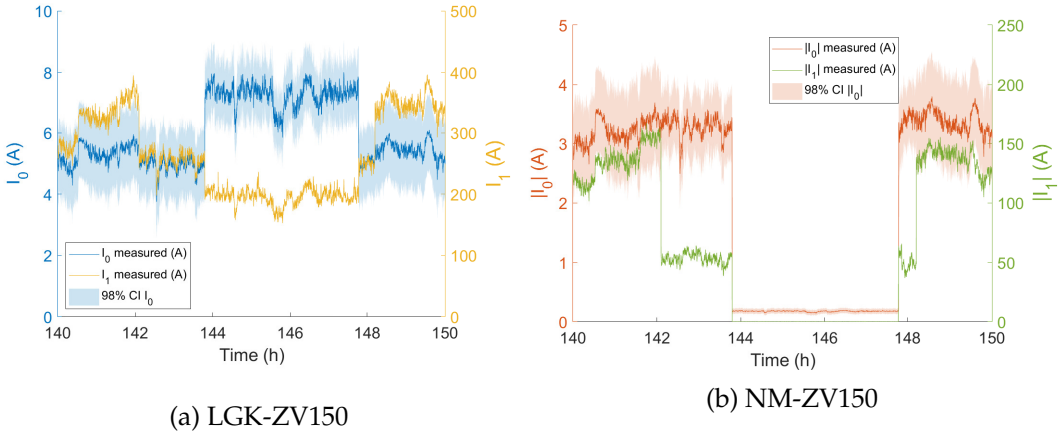


Figure 4.10: Time series of measured $|I_0|$ and $|I_1|$ in both branches during the scheduled outage of branch NM-ZV150.

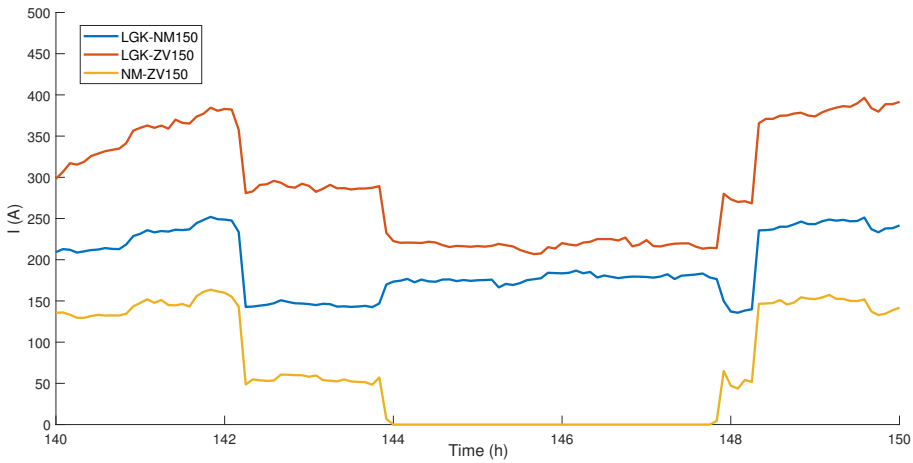


Figure 4.11: 5 minute average phase current magnitude in the three branches within the combination of branches LGK-ZV-NM. Data retrieved from the Energy Management System (EMS). Note that these data are the signals from one of the three current transformers per branch and are not equal to the positive-sequence currents in the respective branches.

Firstly, the load is not brought to 0 A in one step. Approximately 1.7 hours before the branch is brought out of service, the primary-sequence current is lowered by approximately 100 A. This drop is observed in all three branches ² (see figure 4.11). In consequence however, the zero-sequence current does not decrease significantly in branch NM-ZV150. The zero-sequence current in the branch LGK-ZV150 however does decrease slightly, albeit within the measurement bandwidth.

After the first part of the load decreased, branch NM-ZV150 is brought out of service and the positive-sequence reduces from approximately 57 A to 0 A. Furthermore, the positive-sequence current in branch LGK-ZV150 decreases by approximately 69 A. The positive-sequence current in branch LGK-NM150 increases by approximately 31 A. The difference between the decrease in load in the branches NM-ZV-LGK150 and the increase in load in branch NM-LGK150 is caused by other branches within the network carrying part of the load, due to the network's meshed configuration. A detailed analysis of the actual load flows in the complete 150/380 kV network is out of scope of this work.

When we observe the behavior of the zero-sequence current in branch LGK-ZV150 at the moment of switching off branch NM-ZV150, we observe an interesting phenomenon: where zero-sequence current is normally positively correlated to the positive-sequence current (as can be seen in the daily fluctuations), here the zero-sequence current *increases* while the positive sequence current decreases. This can be explained by analyzing the system design in figure 4.2: because the branch LGK-ZV is for the longest part untransposed (in total 11950 m of the total length of 13850 m, or 86%), there is a relatively strong magnetic coupling between the branches LGK-ZV150 and LGK-NM150 in the section where these branches are parallel to each other. Therefore, the increase in positive-sequence current in branch LGK-NM150 leads to an increase in the zero-sequence current in branch LGK-ZV150, while the positive-sequence current in the latter branch is actually decreasing. The outage period can also be observed in the scatter plot in Figure 4.7. Whereas there normally is an almost horizontal linear relation between I_1 and I_0 , a small cluster is visible through which a line through the origin can be drawn. Since there is no full transposition in the branches during the outage of NM-LGK150, there appears

²Note that the data recorded in the Energy Management System (EMS) are the phase current signals from one of the three current transformers installed at the respective substations. Only one phase current per circuit is currently stored in the EMS to limit the amount of data that needs to be stored.

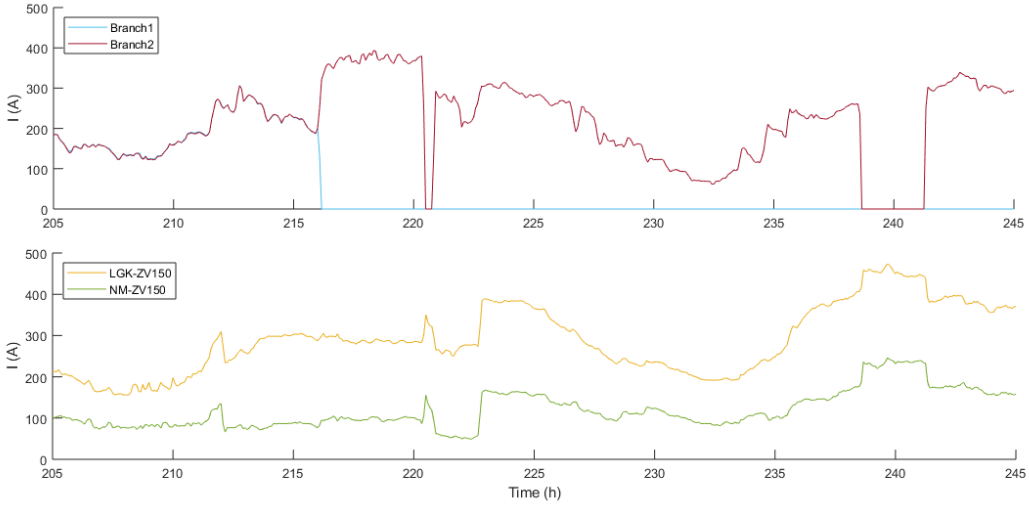


Figure 4.12: Measured currents from the EMS in branches 1 and 2 (one of which encountered a sudden loss of load during the storm) and the measured single-phase currents in EMS in branches LGK-ZV150 and NM-ZV150 during the same time period.

a linear relationship between I_1 and I_0 during this period.

During planned switching operation, one may observe that the measured value of the zero-sequence component does not go to zero when the positive-sequence component does in circuit A-C. This can be attributed due to the noise floor of the measurement chain.

4.5.3 Sudden load changes

In the period between 163 and 245 hours, a number of step phenomena due to sudden load switching occur: the currents in circuits LGK-ZV150 and NM-ZV150 decrease sharply at approximately 164, 188 and 220 hours and increase sharply at approximately 172, 196 and 223 hours. In this section, we will focus on the sudden load changing events that occurred between approximately 215 and 240 hours measurement time.

On January 18, 2018, the Netherlands were hit by a small but powerful storm. This storm also had an influence on the high voltage network, notably leading to the failure (i.e. a short circuit fault) in one of the overhead lines in the vicinity of

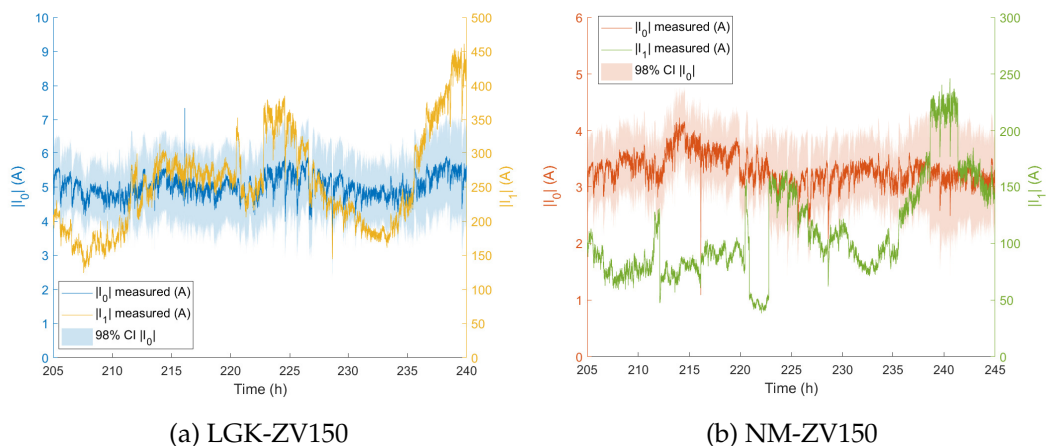


Figure 4.13: Time series of measured $|I_0|$ and $|I_1|$ in both branches during a day with many sudden load changes.

the branches under study at approximately 216 hours measurement time. The 5-minute averaged current of four branches is shown in figure 4.12. The current in one of the branches (indicated as Branch1) suddenly decreases from 200 A to 0 A. In consequence, the current in the other branch (Branch2) almost doubles. Shortly after 220 hours, Branch2 is taken out of service for a short period of time. In reaction, the current in branches LGK-ZV150 and NM-ZV150 first increases and then decreases. Around 238 hours, Branch2 is taken offline again and it is switched back on around 242 hours. The compensatory increase and decrease in current is also visible in branches LGK-ZV150 and NM-ZV150.

This failure can also be observed in the behavior of the zero-sequence currents in the branches that were studied. Around the time of the failure (at approximately 216 hours), a sharp peak is observed in both branches. Between approximately 221 hours and 223 hours, sudden decreases and increases in positive sequence current can be observed in both branches. In contrast, the sudden increases and decreases in positive-sequence current due to the sudden load switching do not have a measurable effect on the measured zero-sequence current, as can be seen in figures 4.13a and 4.13b. The same phenomenon occurs in reverse between approximately 238 hours and 241 hours in branch NM-ZV150: the positive-sequence current suddenly increases and decreases. The zero-sequence current however does not change significantly during the same time period.

4.6 Summary and conclusions

This chapter provides an overview of a measurement campaign that measured both positive-sequence currents and zero-sequence currents in two hybrid 150 kV high voltage branches in a meshed network for approximately 240 hours. These measurement series provide insight into the dynamical behavior of zero-sequence currents in these branches during normal operation in a meshed network and include the uncertainty associated with the measurement of zero-sequence currents. The high voltage branches that were studied are part of a meshed network of 150 kV and 380 kV branches within the eastern part of the Netherlands. The studied branches consist in part of overhead lines and partly of underground cables. Furthermore, the branches are transposed at two locations. A third 150 kV branch is present in parallel to the two measured 150 kV branches.

The methods that were developed in the preceding chapter were utilized to assess the measurement accuracy of the measurements. It is important to know the measurement accuracy, since the zero-sequence currents that are present are small with respect to the per-phase currents in the studied branches. A presentation of zero-sequence current measurement results that includes the associated measurement accuracy is currently lacking in literature.

During daily fluctuations, we observe that positive-sequence currents and zero-sequence currents are positively correlated, but the dynamic range of the positive-sequence currents is larger than the zero-sequence currents. This shows that in transposed hybrid high voltage branches that partly consists out of overhead lines and partly out of underground cables, the coupling between positive-sequence current and zero-sequence current remains weak. One planned switching event of one of the studied branches was observed during the measurement series, in which this branch was brought offline for approximately 4 hours. After this branch was taken offline, we observe a decrease in the positive-sequence current of the other studied branch, but an increase in the measured zero-sequence current and an increased coupling between positive-sequence current and zero-sequence current. This increase is due to the increased current in the third, parallel, branch in combination with the untransposed nature of the longest part of the branch that was kept in service. During several instances of sudden changes in load, we have observed that the positive-sequence current can increase or decrease dramatically, but this change

is not observed in the zero-sequence current.

Chapter 5

Zero-sequence currents and unbalance factors: two case studies

5.1 Introduction

An increasing number of grid operators use Phasor Measurement Units (PMUs) for the monitoring and control of their assets [82]. A PMU allows the user to measure both the amplitude and the phase angle (i.e. the phasor) of a measurand under interest, in particular the voltage or current. For example, a PMU can measure the phasor of the phase currents in a transmission line. To accurately measure the phase angle of a phasor, a PMU uses a precise clock signal that is available worldwide: the satellite-based Global Position System (GPS) [82]. The inputs from the different measurement instruments at the substation (such as voltage transformers and current transformers) are combined with the GPS timing signals to provide synchronized phasors (i.e. *synchrophasors* [82]) that can be compared between PMU systems at different locations. Because of the high accuracy of measuring phasors as a function of time, PMU systems are also able to measure power frequency as a function of time (the first time derivative of the phasor angle) and the Rate of Change of Frequency (ROCOF, the second time derivative of the phasor angle) and differences in phase angle in different parts of the network.

Since both phasor magnitude and phase angle are available from PMU data, it is possible to determine the symmetrical components associated with a set of three

phasors, such as the three phase currents measured from a transmission line. This chapter studies the observed phenomena in several 380 kV transmission lines in the Netherlands, where PMUs are installed. In particular, phenomena regarding the zero-sequence current and positive-sequence current, zero-sequence current unbalance factors and the associated measurement uncertainties are studied. In the current literature, no analysis of measurement campaigns of zero-sequence currents using PMU data, that includes an analysis of measurement uncertainty, is found.

This chapter studies two separate and representative cases within the high voltage grid in the Netherlands, where circulating zero-sequence currents and through zero-sequence currents play a role. Measurement data from these cases were analyzed and in the analysis, the techniques to assess measurement uncertainty as developed in Chapter 3 are applied to the measurement data. The phenomena that were observed during measurements are discussed.

This chapter is organized as follows: section 5.2 describes the measurement setups at the substations that have PMUs installed; in section 5.3 the measurement accuracy of the measurement setups are discussed, using the methods developed in chapter 3; in the two following sections (5.4, 5.5), the different field case studies are discussed; finally, section 5.6 summarizes the chapter and discusses the conclusions.

5.2 Measurement setup

The PMU measurement data was obtained from pre-installed PMU systems at two 380 kV substations at different locations in the Netherlands: one double-circuit branch in between two substations and two branches in a meshed network connect to two other substations. In the latter case, a new substation was built within the existing network after the first measurement period. The influence of the inclusion of the new substation (after which the measured branches were operated in parallel between the substations), with measurement data from a later period is also studied. All measured branches fully consist out of overhead lines.

5.2.1 Measurement chain

Figure 5.1 shows the PMU measurement chain. Current transformers measure the primary currents I_A , I_B and I_C . The secondary leads from the current transformers are directly connected to the PMU relays. In this measurement setup, there is no

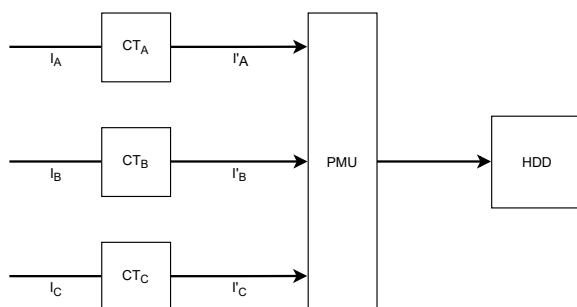


Figure 5.1: Measurement diagram for the PMU measurements

probe present for the direct measurement of zero-sequence currents (i.e. a simultaneous measurement of all three phase current signals). The measurement errors associated with the PMU measurement chain are discussed in the next section.

5.2.2 Measurement data post-processing

The analog signal from the current transformers is processed inside the PMU. At set time intervals, the amplitude and phase angle is recorded by the PMU. By using time stamps which are synchronized using GPS technology, it is possible to accurately determine the phasors at these time stamps.

5.3 Measurement chain accuracy

Using the methods developed in Chapter 3, the measurement chain accuracy for PMU measurements can be determined. It is important to have insight into the accuracy of the measurements, since without knowledge about the measurement uncertainty, the measurements lack value. Table 5.1 gives an overview of the relevant measurement system parameters that give a contribution to the total measurement uncertainty. The description of current transformer measurement accuracy can be found in Chapter 3.

5.3.1 PMU accuracy

The accuracy of a PMU is determined by its Total Vector Error (TVE), as Chapter 3 describes in more detail. The total vector area defines a circular region in the

Component	Parameter	Value
Current transformers		
	Class	0.2s
	Rated current	2500 A
PMU		
	Total Vector Error	1 %

Table 5.1: Overview of the individual accuracy values of the components in the PMU measurement chain.

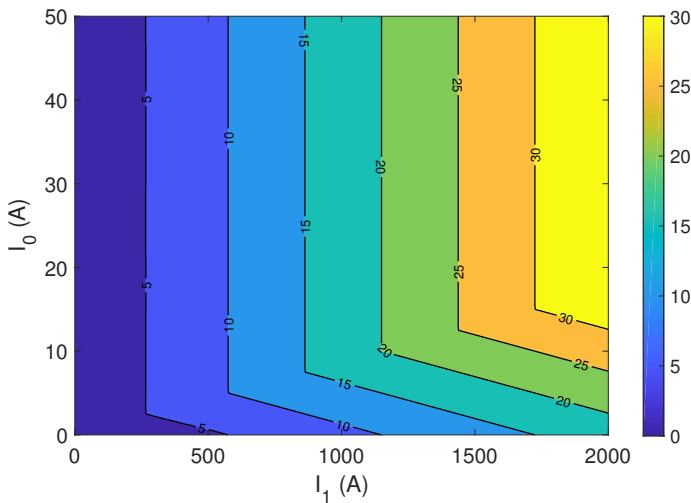


Figure 5.2: The width of the $|I_0|$ distribution (in A) of the PMU measurements within the parameter space of the measurements. Shown here are the distribution widths for current transformers with a rating of 2500 A. The difference in distribution between this rating and a current transformer with a rating of 4000 A is negligible.

$(\text{Re}(I_0), \text{Im}(I_0))$ -plane, which is expressed as a percentage of the vector magnitude. In our measurements, PMUs were used that have a TVE of 1%¹.

5.3.2 Combined measurement accuracy

Figure 5.2 shows $|I_0|$ distribution width as a function of $|I_0|$ and $|I_1|$, as determined by the analytical expressions developed in Chapter 3 (compare with figure 4.4. Two

¹Siemens SIMEAS R-PMU

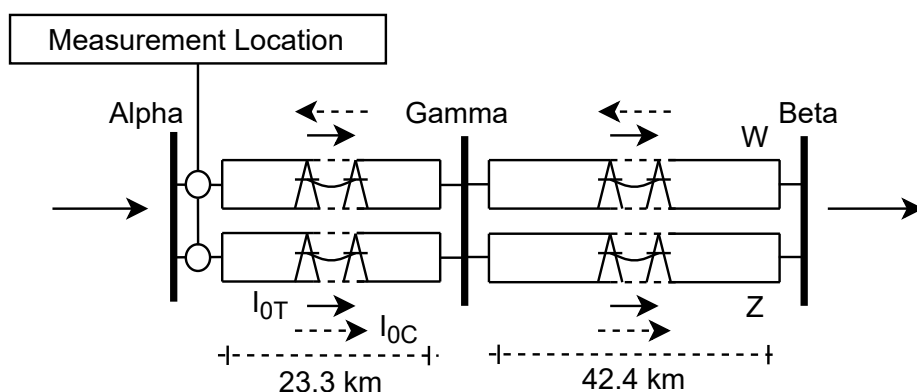


Figure 5.3: Overview of the high voltage branch studied in the first case study. Circuits W and Z connect substations Alpha and Beta, with a branched-off connection at substation Gamma at approximately 23.3 km from substation Alpha, the complete length of the branch is 65.7 km. The circulating zero-sequence current (dashed arrows) and through zero-sequence currents (solid arrows) per circuit are schematically shown.

distinct areas can be observed in the distribution plot: for higher values of $|I_0|$, the isolines of constant distribution width are vertical, meaning that in this part of the parameter space the distribution width is only dependent on the value of $|I_1|$. At lower $|I_0|$ values, an inflection point can be observed in the distribution widths, after which the isolines are slanted. This is caused by the fact that the lower bound of the I_0 magnitude distribution cannot be smaller than 0 A, since a magnitude by definition cannot be smaller than 0. In this region, the measured zero-sequence current is of the same order as the measurement error and caution should be taken in drawing conclusions based on measured zero-sequence current values.

5.4 Circulating and through zero-sequence currents in parallel circuits

Figure 5.3 shows the first study case, which is a double circuit overhead transmission line that connects substations Alpha and Beta (note that substation names in this chapter have been made anonymous). At approximately 23.3 km from substation Alpha, both circuits are connected to substation Gamma via a branch-off construction: the conductors from substations Alpha and Beta are directly connected to

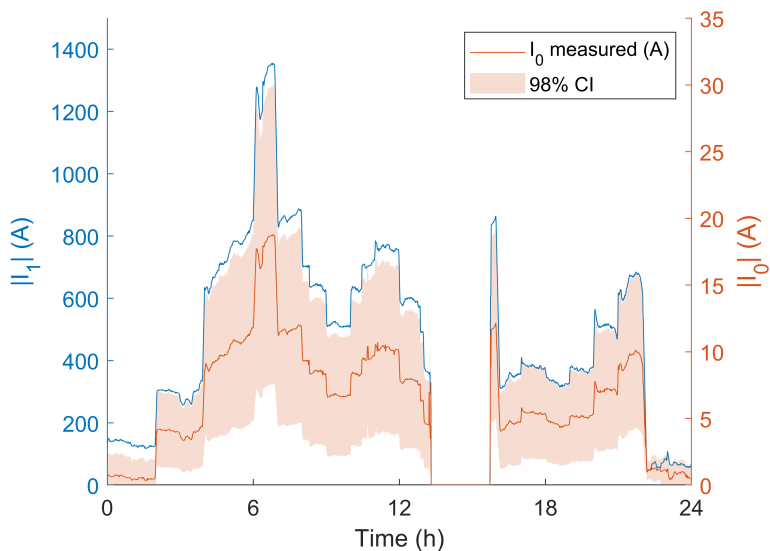
each other and to the conductors that connect to the busbar at substation Gamma. Since the power transformers at substation Gamma are ungrounded at one side (cf. section 2.6), there will no contribution to the measured zero-sequence current at substation Alpha from loads connected to the secondary side of the power transformers at substation Gamma. The total length of the high voltage branch from substation Alpha to substation Beta is 65.7 km. The circuits are untransposed over the length of the high voltage branch and have a rated current capacity of 4000 A per conductor. PMUs are installed at substation Alpha to measure current and voltage phasors. A dataset of one month in 2018 with a recording frequency of 10 Hz was available for analysis.

Figures 5.4a and 5.4b show $|I_1|$ and $|I_0|$ as a function of time during one day of measurement, including the calculated measurement uncertainty around $|I_0|$. At approximately 13.3 hours, circuit W was switched off. At approximately 15.7 hours, the circuit was brought back online. During the switching off of circuit W, a clear increase in both $|I_1|$ and $|I_0|$ in circuit Z can be observed, which compensated for the loss of capacity of circuit W.

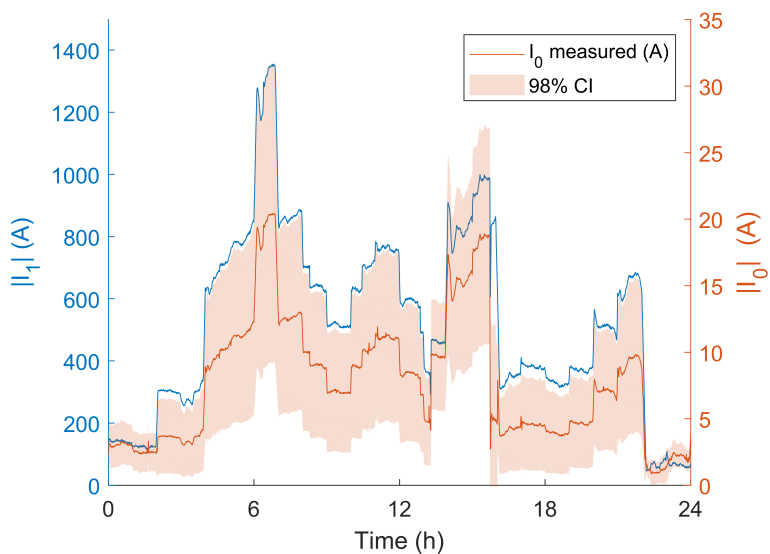
Due to the layout of the circuits, it is possible to study circulating and through zero-sequence currents in the branch, as described in section 2.1. Figure 5.5 shows the circulating and through zero-sequence currents as a function of time. At the time of switching off of circuit W (indicated by the dashed lines in the plot), the calculated circulating and through zero-sequence currents are identical². However, one may argue that if one of the circuits is switched off, the definition of a ‘circulating’ zero-sequence current is no longer valid, since this current cannot circulate in both circuits at all times. Only in case the switched off circuit is grounded at both ends, a current can flow through its conductors due to inductive coupling with the other circuit within the same branch. In practice in the Netherlands, this is always the case to mitigate the risk of induced voltages at the ungrounded end points of the circuit and to create a safe working environment. In case the circuit is grounded at one side, no significant current will run through the circuit and a maximum induced voltage is to be expected at the other side of the circuit.

In general, the observed magnitude of the circulating zero-sequence current is larger than the through zero-sequence current. Besides the absolute magnitudes of

²Since $|I_{0W} - I_{0Z}| = |I_{0W} + I_{0Z}|$ if $I_{0W} = 0$, where I_{0W} and I_{0Z} are the measured zero-sequence currents in circuits W and B, respectively.



(a) Circuit W



(b) Circuit Z

Figure 5.4: Time series of measured $|I_1|$ (left axes, in blue) and $|I_0|$ (right axes, in red) in both circuits on a single day, which featured a short duration switch-off event in one of the circuit.

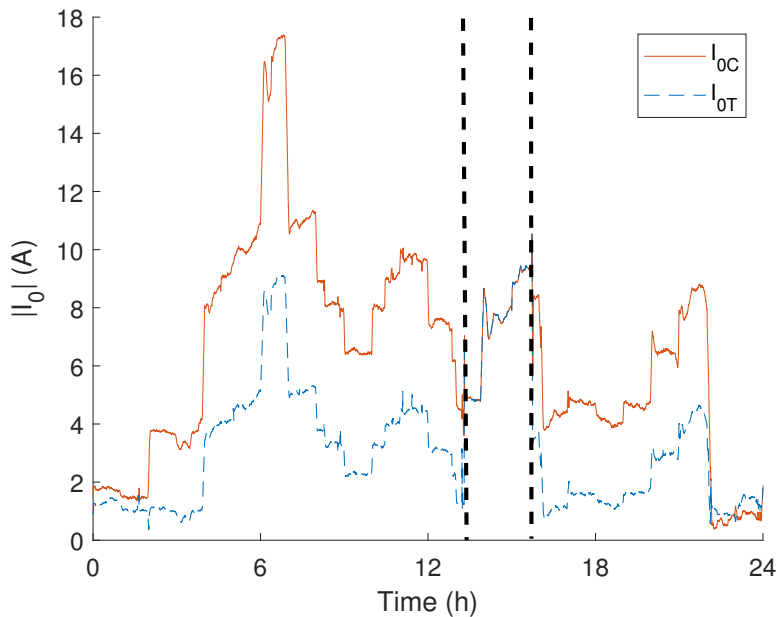


Figure 5.5: Measured circulating (solid, red) and through (dashed, blue) zero-sequence currents in the branch Alpha-Gamma-Beta. The dashed lines indicate the period when circuit W was temporarily switched off.

the circulating and through zero-sequence current, it is worthwhile to study these zero-sequence current components relative to the positive-sequence currents in the circuits. Figure 5.6 shows the zero-sequence current circulating and through unbalance factors that were introduced in section 2.1. It can be observed that the circulating unbalance factor is constant as a function of time (having a value of approximately 1.3%), i.e. the ratio between the circulating zero-sequence current and the sum of the positive-sequence currents in both circuits is constant and there is a linear relationship between these quantities. This was however not the case when circuit W was brought out of service.

A basic (radial) model of the transmission line was developed in EMTP-ATP and implemented to calculate the circulating zero-sequence current factor numerically, using the conductor properties and transmission geometry, as a function of the average measured positive-sequence current in the transmission line. More information on the design of the model can be found in Appendix E. Using a lookup

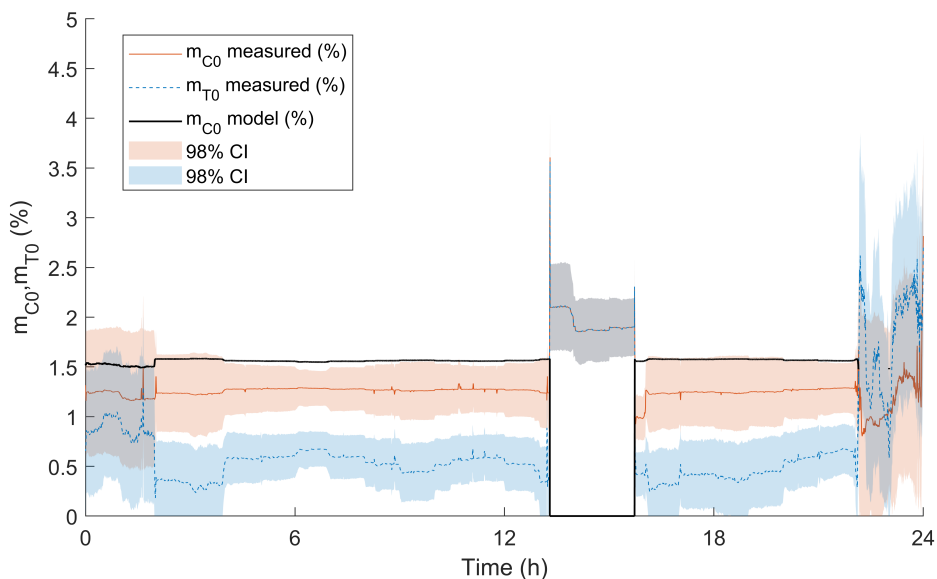


Figure 5.6: Circulating and through unbalance factors in the branch Alpha-Gamma-Beta, including the model prediction based on the calculated impedance matrix of the transmission line.

script, the modeled circulating zero-sequence current unbalance factor was determined on the measured average positive-sequence current in both circuits. Figure 5.6 shows that the model prediction is of the same order of magnitude as the measurement outcomes and shows the same behavior as the measured m_{C0} as a function of the positive-sequence current, taking into the uncertainty in certain model parameters, such as the assumed resistivity of the ground (which in practice will not be a constant value along the length of the transmission line). Between 22h and 24h of measurement time, the measured positive-sequence currents were too low to match the model and no model outcomes were available. The radial model predicts a nonzero lower limit to positive-sequence currents due to capacitive loading currents. In practice, the transmission line is part of a meshed system, where generators and loads are dispersed throughout the system.

The through unbalance factor is found not to be constant in time (observed values between approximately 0.5% and 2%) and is determined by factors outside the branch itself. Since the power transformers at substation Gamma are only grounded

on one side, there is no contribution to the measured zero-sequence current at substation Alpha from loads connected at a lower voltage level at the intermediate substation Gamma.

Figure 5.6 also shows the confidence interval bands (at the 98%-level) around the measured unbalance factors. The derivation of the expressions to compute these confidence intervals has been developed and can be found in Appendix F. In the final two hours of measurement, both the circulating and through unbalance factors show large fluctuations. This coincides with a relatively low level of positive-sequence currents at this time period. Because of the low positive-sequence current level, the uncertainty bounds increase, as can be observed in the figure.

5.5 A newly included substation in the existing network

The second study case is that of a double-circuit 380 kV high voltage branch that connected from one substation to two other substations, see figure 5.7a for a schematic representation. Substation Delta was connected to substation Epsilon (circuit length: 98.9 km) and substation Zeta (circuit length: 45.8 km). In turn, substations Epsilon and Zeta were also connected through a circuit with a length of 67.3 km. All branches fully consist out of overhead lines and no transpositions are present in the branches under study. In 2018-2019, a new substation (indicated as substation Eta) was built in this part of the network. The situation after the inclusion of this substation is shown in figure 5.7b, together with the corresponding circuit lengths. An interesting component of the network at this location is the presence of a phase shifter [91] at substation Zeta. The function of this component is to regulate the flow of real power through the network by changing the phase angles of the three phase voltages [91].

It is worthwhile to study the effect of the inclusion of the substation on the zero-sequence current behavior in the network. One could hypothesize that in the situation after inclusion there will be a constant circulating zero-sequence current factor measured at the circuits between substations Delta and Eta, since the circuits are connected to the same substations at both sides, as was the case in the first case study. This hypothesis will be tested in this section.

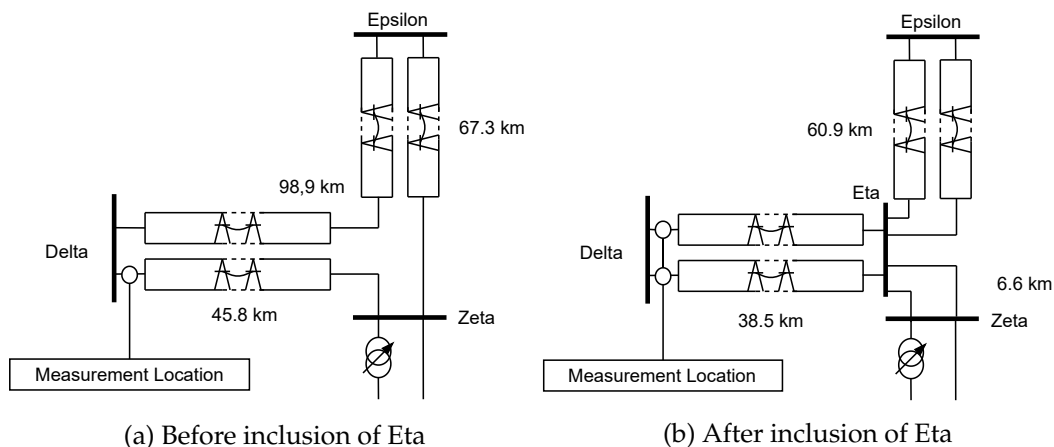


Figure 5.7: Schematic overview of the 380 kV network before and after the inclusion of the intermediate substation Eta. Note the presence of a phase shifting transformer at substation Zeta. The lower circuit that connects to substation Delta is designated as the "southern" circuit, whereas the other circuit is designated as the "northern" circuit.

5.5.1 Before inclusion of the intermediate substation

For the period preceding the inclusion of substation Eta, a PMU measurement dataset of 1 month in 2018 was available only for the circuit between substations Delta and Zeta. The data were stored at a recording frequency of 10 Hz.

Figures 5.8 and 5.9 show the time-series plots of $|I_1|$ and $|I_0|$ and the scatter plot of $|I_1|$ and $|I_0|$ in the circuit Delta-Zeta, respectively. The measurement outcomes show that positive-sequence current and zero-sequence current are not always correlated with each other. In particular, in the lower left quadrant of the scatter plot the relation between $|I_1|$ and $|I_0|$ appears to be uncorrelated. In the upper right quadrant, there does appear to be a linear relationship between $|I_1|$ and $|I_0|$. This quadrant is associated with the time period between approximately 20:00 and 24:00 during this day.

In the next subsection, the influence of the inclusion of a new substation between the existing substations Delta and Zeta will be studied and it will be discussed if the behavior mentioned above is still present after this inclusion.

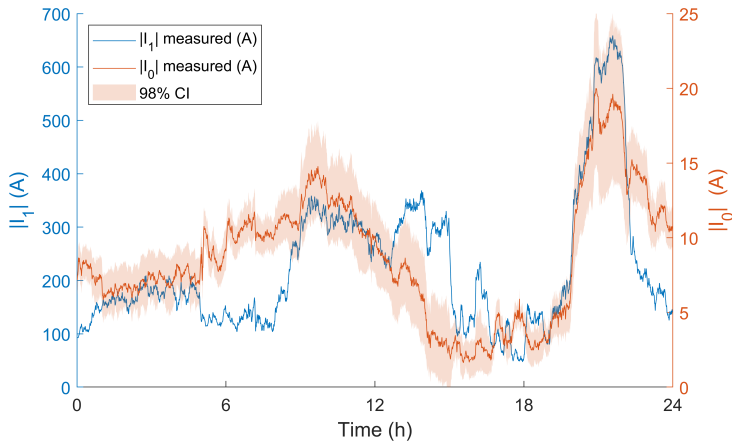


Figure 5.8: $|I_1|$, $|I_0|$ and the 98% confidence interval around $|I_0|$ for one day of measurement for circuit Delta-Zeta.

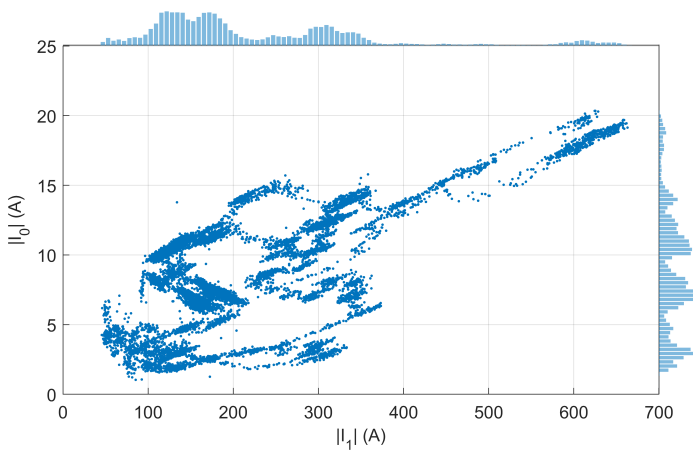


Figure 5.9: The scatter plot of $|I_1|$ and $|I_0|$ in the circuit Delta-Zeta for the chosen day of measurement. Also shown are the histograms of $|I_1|$ and $|I_0|$, respectively. The data set of the set is downsampled to 10 000 samples.

5.5.2 After inclusion of the intermediate substation

A dataset of 3 months in 2020 (after the inclusion of substation Eta) was made available for analysis. The data in this dataset were stored at a recording frequency of 1 Hz. Measurement data was available for both branches from substation Delta to

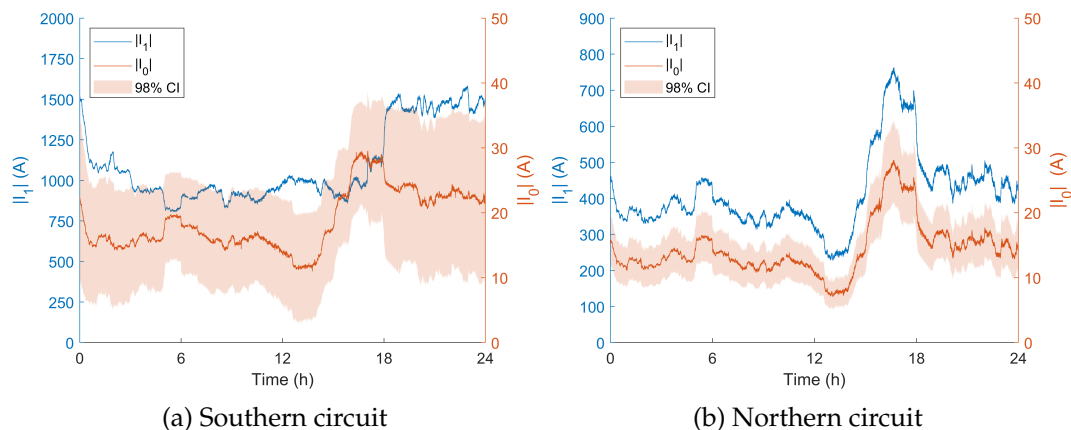


Figure 5.10: $|I_0|$ and $|I_1|$ during one day of measurement in the southern and northern circuit of the branch between substations Delta and Eta.

substation Eta, as shown in figure 5.7b.

Figures 5.10a and 5.10b show $|I_1|$ and $|I_0|$ as a function of time for one day of measurement within the dataset. The layout of the southern circuit is largely identical to the circuit Delta-Zeta in the situation before inclusion of substation Eta, except for the part of the circuit between the location of substation Eta and substation Zeta (which is approximately 6.6 km in length). While $|I_1|$ and $|I_0|$ are strongly correlated within the northern circuit, this is not the case in the southern circuit, where $|I_1|$ and $|I_0|$ are less correlated, comparable to the behavior that was observed before the inclusion of substation Eta. It may also be observed that the positive-sequence current in the southern circuit during this day is much larger than the positive-sequence current in the northern circuit. The zero-sequence currents in both circuits are of the same order, although the measurement uncertainty around the zero-sequence current in the southern circuit is much larger than in the northern circuit. This is due to the larger positive-sequence current in the southern circuit, which increases measurement uncertainty in the zero-sequence current in this circuit, as is shown in Chapter 3.

Figure 5.11 shows the circulating and through zero-sequence current unbalance factors for the two circuits as a function of time of the selected day of measurement, as well as the corresponding confidence intervals. A nonstationary circulating zero-sequence current factor between approximately 1% and 3% was observed, as well

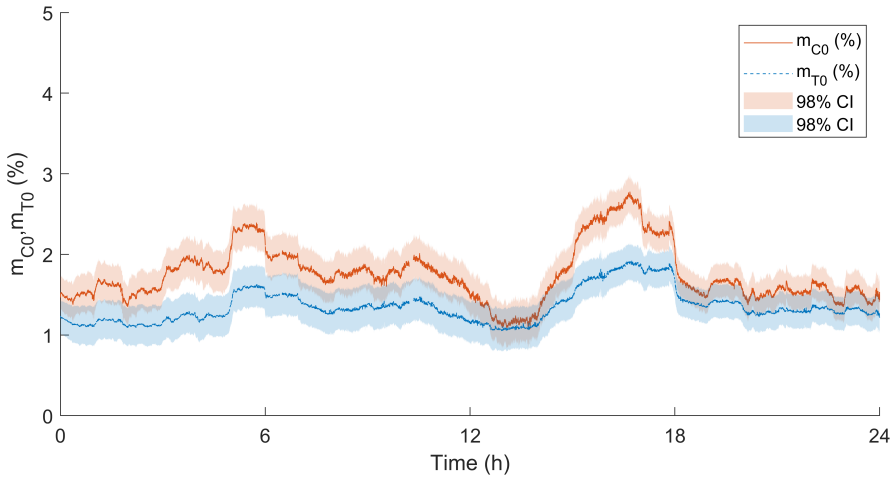


Figure 5.11: m_{C0} and m_{T0} as a function of time during the selected measurement day after inclusion of substation Eta.

as a nonstationary through zero-sequence current factor between approximately 1% and 2%. Here it can be concluded that both the through unbalance factor as well as the circulating unbalance factor are not constant as a function of time. In contrast to the first studied case, it is particularly interesting to observe that the latter (circulating) unbalance factor is not stationary (cf. figure 5.6). The hypothesis that the inclusion of the intermediate substation leads to a constant circulating zero-sequence current factor is therefore rejected. A possible explanation for the observed behavior is that the northern and southern circuit were not connected to the same busbar at substation Eta during the measurement, since high voltage substations are designed with multiple busbars to allow for redundancy during maintenance or faults. This explanation is also supported by the fact that the positive-sequence currents in both circuits are not equal: one would expect that if the circuits were connected to the same busbars at both ends, the positive-sequence current would be distributed equally among both circuits, since both circuits are of equal length and design. Figures 5.10a and 5.10b however show that this is not the case.

Although the circulating unbalance factor is determined by (2.6) and this value can be calculated for any combination of two high-voltage circuits carrying zero-sequence and positive-sequence currents, it may be argued that the nomenclature is not valid in this case. The "circulating" path in this case is evidently not trivial

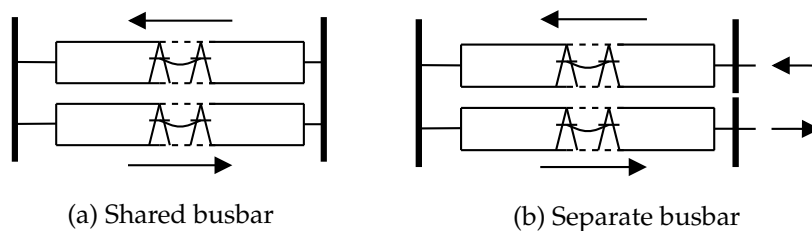


Figure 5.12: Example single-line diagrams of high voltage branches in which both circuits are connected to the same busbar (on the left) and in which each circuit connects to a separate busbar (on the right). The 'circulating' zero-sequence current flows are also depicted in both situations.

when both circuits are not connected to the same busbars at both ends (see Figure 5.12): since the circulating zero-sequence current does not simply follow a path in both circuits only, it closes through a different, a priori unknown path outside the branch and through the whole network. The concept of a "circulating" zero-sequence current is in this case therefore not valid and a more general proposal would be to indicate this concept as a differential zero-sequence current or differential zero-sequence current unbalance factor within the high voltage branch.

5.6 Summary and conclusions

This chapter provides an overview the measurement setup for zero-sequence currents using a PMU and of a number of PMU-measurements that have been made in several 380 kV branches in the Netherlands, which were measured and recorded using pre-installed Phasor Measurement Units. The methods developed in Chapter 3 were applied to determine the measurement accuracy for the different measurements.

Based on the measurements in the first study case, it is shown that the circulating zero-sequence current during normal operation of both circuits within the branch is constant relative to the total positive-sequence current in the branch as a function of time. a circulating zero-sequence current factor of approximately 1.3% was observed. Measurement outcomes are in agreement with a basic numerical model, taking into account measurement uncertainty and model input parameter uncertainty. The through zero-sequence current was however found not to be constant

as a function of time. The measured zero-sequence current factors are in agreement with values found in literature.

The second case study entails a situation where a new substation was built in an existing part of the network. Although the measured branches share the same right-of-way after inclusion of the new substation, the circulating zero-sequence current in this case is not constant relative to the total positive-sequence current as a function of time. This was caused by the fact that both circuits were not connected to the same busbars at both ends, in particular at substation Eta. This also explains why the positive-sequence currents in both circuits are not (close to) equal to each other, since both circuits between Delta and Eta share the same right-of-way. The measured zero-sequence current factors are in agreement with values found in literature.

In case when both circuits are not connected to the same busbar at both ends, the concept of a *circulating* zero-sequence current within the branch is not a completely accurate description anymore. In this case, it would be more accurate if the circulating zero-sequence current would be designated as a differential zero-sequence current, in analogy to the well-known differential mode in EMC literature. This is also the case when one of the parallel circuits within a single branch is taken out of service and it is not possible for current to pass through the switched-off circuit.

When a double circuit line is connected on both ends at the busbars, the circulating zero-sequence current can in principle be modelled by determining the total impedance matrix of the transmission line. The through zero-sequence current in a meshed network is however much more difficult to model, since this depends on factors that are outside of the transmission line, such as the presence of unbalanced loads and the zero-sequence impedance of the whole network.

Chapter 6

Conclusions, contribution and further research

Zero-sequence currents in high-voltage power systems during normal operation can provide a significant contribution to electromagnetic interference with other nearby infrastructures, despite the relatively low levels with respect to positive-sequence current levels. This dissertation provides an overview of the current state of the art related to zero-sequence currents during normal operation, as well as the measurement of these. Measurement of zero-sequence currents during normal operation is challenging because of the relatively low levels in combination with the inherent measurement uncertainty associated with measurement in high-voltage systems. Three measurement strategies have been analyzed utilizing two methods of analysis. The developed measurement uncertainty analysis has been applied to two measurement campaigns: firstly, a measurement campaign in two transposed 150 kV branches that consist of a combination of underground cables and overhead transmission lines; secondly, a measurement campaign in several untransposed 380 kV branches that consist fully out of overhead lines, where the unbalance factors were studied including the quantification of the measurement uncertainty of these. The order of magnitudes of zero-sequence currents that were found during the measurements agrees with values that are presented in literature. These specific conclusions relate to the observed behavior during field measurements. Care must be

taken if one wants to generalize these conclusions in a different scenario. In principle, the results from the field measurements are only pertinent to the observed scenarios.

6.1 Conclusions

Zero-sequence current unbalance during normal operation

Zero-sequence currents in transmission lines that consist of multiple parallel circuits can be decomposed into circulating zero-sequence currents and through zero-sequence currents.

Two main causes of zero-sequence currents during normal operation are identified: geometric unbalance between conductors in transmission lines (both overhead as well as underground systems) and unbalanced loads. In some cases, zero-sequence currents can propagate between different voltage levels. This depends of the specific design of the transformer that transforms one voltage into another voltage and the locations of grounded transformer neutral points.

The phase positions of conductors and the presence of lightning wires in transmission lines can have a significant influence on the circulating and through zero-sequence currents in this transmission line and therefore on the resulting magnetic field surrounding the transmission line.

Zero-sequence current measurement uncertainty during normal operation

Three practically applicable zero-sequence current measurement strategies were studied using two methods of analysis. The first two strategies entail the application of a dedicated measurement system that utilizes the secondary circuitry of the current transformers present at a high-voltage substation, which in turn is measured by current measuring devices connected to a recording device, such as an oscilloscope. A distinction is made between the indirect measurement strategy, in which all phases are measured separately and the direct measurement strategy, in which the three secondary leads are measured simultaneously utilizing a single current measuring device. The third studied strategy utilizes PMUs which may have been pre-installed at the substation. The two applied methods of analysis are analytical expressions for measurement uncertainty and Monte Carlo simulations of the

measurement chains. The outcomes of the two methods of analysis agree with each other. The direct and indirect methods were also validated using lab experiments.

Computationally, the analytical method is preferable to the Monte Carlo method to determine measurement uncertainty as a function of the measurement accuracy parameter of the measurement system. On the other hand, the Monte Carlo method provides insight into the actual statistical distributions of measurement outcomes and is more flexible in regard to the application of more advanced measurement error distributions of the different elements in the measurement chain.

The measurement uncertainty analyses show that comparatively, the direct strategy is the most precise measurement strategy, since it utilizes a single current measuring clamp to measure the secondary leads from the current transformers. In practice however, it might not be possible to physically combine the three phase current leads from the current transformers and the indirect strategy or PMU strategy might be another possibility in these cases.

Zero-sequence current measurements in the 150 kV grid using the direct method

Zero-sequence current measurements in two transposed 150 kV branches that consist out of a combination of overhead lines and underground cables show that a nonzero zero-sequence current is present in these branches, taking into account measurement uncertainty. Note that it was not possible to distinguish between circulating and through zero-sequence currents in this case, since only two circuits out of the three circuits that make up the transmission line could be measured.

During the measurement series, several modes of operation were observed (see figures 4.5 and 4.6): firstly, during daily fluctuations, positive-sequence currents and zero-sequence currents are positively correlated, however the dynamic range of the zero-sequence current signal is smaller than the dynamic range of the positive-sequence current; secondly, during planned outage of one of the two measured branches, it was observed that the zero-sequence current in the branch that remained in service increased significantly, because part of the current that ran through the branch that was brought out of service was carried by the third branch that runs parallel to the measured branches; thirdly and finally, during several instances of sudden load changes, large fluctuations in positive-sequence currents were observed, whereas these fluctuations were not observed in the zero-sequence current.

Zero-sequence currents and unbalance factors: two case studies in 380 kV transmission lines

Zero-sequence currents in several 380 kV overhead transmission lines that were measured and recorded using PMUs were studied, including an analysis of the measurement errors using the methods developed in Chapter 3.

The first studied case entailed a untransposed double-circuit overhead transmission line. A decomposition into circulating zero-sequence currents and through zero-sequence currents shows that the circulating zero-sequence current factor is constant as a function of time within measurement accuracy while both parallel branches are in service. This is in accordance with a numerical model prediction, taking into account measurement uncertainty and model parameter uncertainty. A constant circulating zero-sequence current factor equates to a linear relationship between the circulating zero-sequence current between the branches and the total positive-sequence current in both branches. By definition, no circulating zero-sequence current is present when one of the two branches is taken out of service. The through zero-sequence current factor is shown not to be constant as a function of time.

The second studied case considers a situation in which a new substation is connected to several existing 380 kV branches. After commissioning of the substation, it was observed that the circulating zero-sequence current factor was not constant as a function of time, even though both branches are connected to the same substations at both ends. A possible explanation for this is that both parallel branches are not connected to the same busbars on both sides, which means that the 'circulating' zero-sequence current takes a more convoluted path through the (meshed) network. In this case, nonstationary through zero-sequence current factors were observed.

6.2 Dissertation contribution

The main contributions of this dissertation are the following:

- A comprehensive description of the current state of the art in literature concerning zero-sequence currents during steady state operation was developed.
- Measurement uncertainty associated with three practically applicable strategies to measure zero-sequence currents during steady state operation has been

analyzed using two complementary methods: by developing analytical expressions and by designing Monte Carlo simulations that simulate error propagation in the respective measurement chains.

- The developed models for measurement uncertainty were validated by means of measurements performed in a laboratory setting.
- The developed measurement uncertainty analysis methods were applied to field measurements in 150 kV branches that were measured using a dedicated measurement system and in 380 kV branches where pre-installed PMUs were installed.
- During the measurement campaigns, several types of zero-sequence current behavior during steady state operation were observed.

6.3 Recommendations for future research

Although this dissertation provides insight into several practically applicable measurement strategies to measure zero-sequence currents during normal operation, other measurement strategies may be designed that provide a greater accuracy, depending on the goal of the measurement. In particular, a method that would apply Rogowski coils installed directly around (isolated) primary conductors in combination with an integrator circuit that combines the signals from all three phase current could provide a greater measurement accuracy by excluding the role of the primary current transformers. The measurement uncertainty associated with such a measurement setup could be analyzed using the methods developed in this dissertation.

An alternative approach to measuring zero-sequence currents during normal operation would be to construct a map of the magnetic field in a 2D-plane around a transmission line, for example by drone measurements. The advantage of this approach is that it does not need access to a high voltage substation to perform the measurements. The challenge in this approach is that it entails solving the *inverse* problem of reconstructing the current distribution in all relevant conductors from the measured magnetic field. This evidently also places requirements on the

measurement accuracy of the magnetic field, as well as the accuracy of position determination of the measurement device. In the past years, some efforts were made on this problem and the preliminary results out of these are promising.

Recent research has shown that power swings that can occur in power systems can have a significant influence on distance protection relays [60], [92]. Power swings can be both symmetric (consisting only of positive-sequence or negative-sequence currents) or asymmetric (also consisting of zero-sequence currents). It is imperative that these relays operate correctly to prevent maloperation. Since zero-sequence currents are associated with asymmetric power swings, it is important to assess measurement uncertainty of zero-sequence currents during these power swings.

Experience from the field shows that there may be an increase in unbalanced loads in future three-phase power systems at the medium voltage level, due to several causes, such as photovoltaic installations or other power electronic devices. If there is no intermediate transformer present that interrupts the zero-sequence current path, zero-sequence currents will return through the connecting cable's earth return conductor (in case the cable earth conductors are fully bonded) in case of an unbalanced load. Since earth return conductors are normally not designed to carry large (zero-sequence) currents in proportion to the current in the cable's main conductor, this may lead to thermal failure of the cable system.

6.4 Practical recommendations for measurement and modeling of zero-sequence currents

Concerning the measurement of zero-sequence currents in practice, the following practical aspects are recommended:

- If there is a possibility to measure three phase leads simultaneously, this leads to the most precise measurement of zero-sequence currents.
- To be able to measure the positive-sequence current and negative-sequence current, it is necessary to measure each phase lead independently.

- If a single probe is used for zero-sequence current measurements, it is advised to use a dedicated current probe with high sensitivity and to set the oscilloscope range to the proper range of values that can be expected (i.e. smaller than the nominal load of the transmission line).
- Calibrating the primary current transformers can improve the measurement accuracy significantly, in particular for the direct measurement strategy.
- To prevent possible influence of higher harmonics (such as the third harmonic), the 50 Hz component should be filtered out.
- Other measurement equipment should be calibrated correctly before starting the measurement campaign.
- For the PMU measurement strategy, the best way to increase measurement accuracy is to use a PMU with the lowest possible Total Vector Error.

Concerning the modeling of (circulating) zero-sequence currents, it is recommended that all conductors are included in the numerical model, including grounded conductors, such as lightning wires.

Appendix A

OHL zero-sequence impedance expressions for several situations

Single circuit

Below, the expressions are given for zero-sequence impedances of single-circuit and double-circuits overhead lines with zero, one or two earth wires. The expressions are given in [27].

No earth wire

$$Z'_{0S} = R'_0 + jX'_0 = \frac{R'_1}{n_2} \frac{3}{8} \omega \mu_0 + j \frac{\omega \mu_0}{2\pi} \left(3 \cdot \ln \frac{\delta}{\sqrt[3]{r_B D_M^2}} + \frac{\mu_T}{4n} \right) \quad (\text{A.1})$$

One earth wire

$$Z'_{0S1E} = Z'_{0S} - 3 \frac{(Z'_{CE})^2}{Z'_{EE}} \quad (\text{A.2})$$

where Z'_{CE} is the mutual impedance between phase conductors and the earth wire:

$$Z'_{CE} = \frac{1}{8} \omega \mu_0 + j \frac{\omega \mu_0}{2\pi} \ln \left(\frac{\delta}{D_{ME}} \right) \quad (\text{A.3})$$

and Z'_{EE} is the self-impedance of the earth wire:

$$Z'_{EE} = R'_E + \frac{1}{8}\omega\mu_0 + j\frac{\omega\mu_0}{2\pi} \left(\ln \left(\frac{\delta}{r_E} \right) + \frac{\mu_E}{4} \right) \quad (\text{A.4})$$

Two earth wires

$$Z'_{0S2E} = Z'_{0S} - 3 \frac{(Z'_{C2E})^2}{Z'_{E1E2}} \quad (\text{A.5})$$

where Z'_{C2E} is the mutual impedance between the phase conductors and earth wires (in case of a symmetric arrangement of the earth wires around the center of the circuit):

$$Z'_{CE2} = \frac{1}{8}\omega\mu_0 + j\frac{\omega\mu_0}{2\pi} \ln \left(\frac{\delta}{D_{M2E}} \right) \quad (\text{A.6})$$

and Z'_{E1E2} is the mutual impedance between the earth wires:

$$Z'_{E1E2} = R'_E/2 + \frac{1}{8}\omega\mu_0 + j\frac{\omega\mu_0}{2\pi} \left(\ln \left(\frac{\delta}{D_{E1E2}} \right) + \frac{\mu_E}{8} \right) \quad (\text{A.7})$$

The symbols in the expressions above have the following meaning, as far as they are not discussed in Chapter 2:

R'_1	phase conductor resistance [Ω/km]
n_2	number of subconductors (in case of a bundled conductor)
r_B	bundle conductor equivalent radius
D_M	geometric mean distance $= \sqrt[3]{D_{AB} \cdot D_{BC} \cdot D_{CA}}$
μ_T	relative permeability of phase conductor, $\mu_T = 1$ for non-ferromagnetic materials
δ	skin depth of the earth at ground resistivity ρ_E $= \frac{1.85}{\sqrt{\omega\mu_0/\rho_E}}$
D_{ME}	geometric mean distance from the phase conductors to the earth wire $= \sqrt[3]{D_{AE} \cdot D_{BE} \cdot D_{CE}}$
R'_E	earth wire resistance [Ω/km]
μ_E	relative permeability of an earth wire, $\mu_T = 1$ for non-ferromagnetic materials
r_E	earth wire radius
D_{M2E}	geometric mean distance from the phase conductors to the two earth wires $= \sqrt[6]{D_{AE1} \cdot D_{BE1} \cdot D_{CE1} \cdot D_{AE2} \cdot D_{BE2} \cdot D_{CE2}}$

Double circuit

No earth wire

$$Z'_{0D} = Z'_{0S} + 3Z'_{C1C2} \quad (\text{A.8})$$

where

$$Z'_{C1C2} = \frac{1}{8}\omega\mu_0 + j\frac{\omega\mu_0}{2\pi} \ln\left(\frac{\delta}{\sqrt{D_{M1}D_{M2}}}\right) \quad (\text{A.9})$$

One earth wire

$$Z'_{0D1E} = Z'_{0D} - 6\frac{(Z'_{CE})^2}{Z'_{EE}} \quad (\text{A.10})$$

Two earth wires

$$Z'_{0D2E} = Z'_{0D} - 6\frac{(Z'_{CE1E2})^2}{Z'_{E1E2}} \quad (\text{A.11})$$

where

$$Z'_{CE1E2} = \frac{1}{8}\omega\mu_0 + j\frac{\omega\mu_0}{2\pi} \ln\left(\frac{\delta}{D_{M2E}}\right) \quad (\text{A.12})$$

The symbols in the expressions above have the following meaning, as far as they are not discussed before:

$$\begin{aligned} D_{M1} &= \sqrt[3]{D_{Aa} \cdot D_{Bb} \cdot D_{Cc}} \\ D_{M2} &= \sqrt[3]{D_{Ab} \cdot D_{Ac} \cdot D_{Bc}} \\ D_{M2E} &= D_{ME} \end{aligned}$$

Appendix B

Earth return currents according to Carson

John R. Carson [30] described the impedances with earth return of conductors placed above ground, both their self-impedance as well as mutual impedance. To get to the solution of this problem, Carson divides the (x, y) -plane into two half-spaces: the part above ground ("the dielectric") and the part in the ground, see figure B.1. Carson gives the following general expression for the solution of the differential equation (2.23) for the electric field strength caused by a current I passing through a conductor at height h_1 above ground:

$$E_Z(x, y) = -j \frac{\omega \mu_0 I}{\pi} \int_0^{\infty} \frac{e^{-sh_1}}{\sqrt{s^2 - k^2} + s} \cdot e^{y\sqrt{s^2 - k^2}} \cdot \cos(xks) ds - j \frac{\omega \mu_0 I}{2\pi} \ln \left(\frac{D}{d} \right) - \frac{\partial V}{\partial z}. \quad (\text{B.1})$$

In this equation, the first term (containing the indefinite integral) represents the contribution of the ground current, the second term represents the contribution of the secondary conductor P and the third term represents the electrostatic contribution to the field. According to Carson, the x - and y -components of the electric field in the earth are negligible, so only the z -component of the electric field will be present.

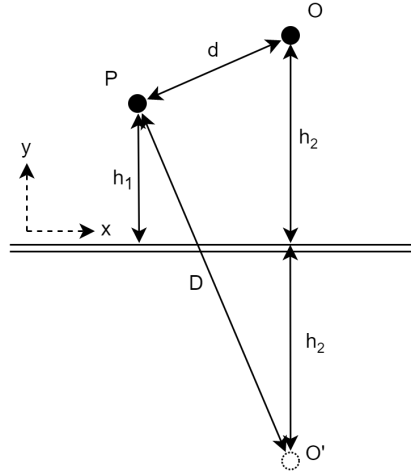


Figure B.1: The geometry as defined by Carson. O and P are conductors above ground, O' is the mirror conductor of conductor O .

Using the expression for the electric field, Carson derives the following expression for the self-impedance of a conductor with ground return:

$$Z_{self} = z + j\frac{\omega\mu_0}{2\pi} \ln\left(\frac{2h}{a}\right) + \frac{\omega\mu_0}{\pi} \int_0^{\infty} \left(\sqrt{s^2 + k^2} - s\right) \cdot e^{-2jhks} ds. \quad (\text{B.2})$$

Where z is the internal impedance of the conductor, a is the conductor's radius and h is the height above ground of the conductor. The second term can be interpreted as the contribution to the impedance when the earth would be regarded as a perfect conductor, whereas the third term is the correction due to the earth being an imperfect conductor with a finite conductivity.

The expression for mutual impedance is as follows:

$$Z_{mutual} = j\frac{\omega\mu_0}{2\pi} \ln\left(\frac{D}{d}\right) + \frac{\omega\mu_0}{\pi} \int_0^{\infty} \left(\sqrt{s^2 + k^2} - s\right) \cdot e^{-j(h_1+h_2)ks} \cos xks ds. \quad (\text{B.3})$$

The indefinite integrals in both expressions do not have a closed-form analytical solution. The indefinite integrals in (B.2) and (B.3) can be expressed in general for both self-impedance and mutual-impedance as:

$$J(p, q) = \int_0^{\infty} \left(\sqrt{s^2 + j} - s \right) \cdot e^{-ps} \cos qsd s. \quad (\text{B.4})$$

Where $p = 2j\hbar k$ and $q = 0$ for self-impedance and $p = j(h_1 + h_2)k$ and $q = xk$ for mutual impedance.

This integral can be expressed as a pair of infinite series $J = P + jQ$, where P and Q are functions of $r = \sqrt{p^2 + q^2}$ and $\theta = \tan^{-1}(q/p)$. P and Q are given by [30]:

$$P(r, \theta) = \frac{\pi}{8}(1 - s_4) + \frac{1}{2} \left(\ln \frac{2}{\gamma r} \right) s_2 + \frac{1}{2} \theta s_2' - \frac{1}{\sqrt{2}} \sigma_1 + \frac{1}{2} \sigma_2 + \frac{1}{\sqrt{2}} \sigma_3, \quad (\text{B.5})$$

$$Q(r, \theta) = \frac{1}{4} + \frac{1}{2} \left(\ln \frac{2}{\gamma r} \right) (1 - s_4) + \frac{1}{2} \theta s_4' - \frac{1}{\sqrt{2}} \sigma_1 + \frac{\pi}{8} s_2 + \frac{1}{\sqrt{2}} \sigma_3 - \frac{1}{2} \sigma_4, \quad (\text{B.6})$$

where $\ln \gamma$ is Euler's constant (0.57721...) and $s_2, s_4, s_2', s_4', \sigma_1, \sigma_2, \sigma_3, \sigma_4$ are infinite series, which are dependent on r and θ . The definitions of these series are given in appendix D.

r can be regarded as a normalized distance between a conductor and its mirror image (for the self-impedance case) or between a conductor and the mirror image of the other conductor (in the mutual impedance case). The distance is normalized by the skin depth of the earth ($1/\sqrt{\omega\mu_0\sigma}$). θ is the angle between the lines OO' and PO' in figure B.1.

For small values of r ($r \leq 1/4$), P and Q can be approximated by:

$$P = \frac{\pi}{8} - \frac{1}{3\sqrt{2}} r \cos \theta + \frac{r^2}{16} \cos 2\theta \left(0.6728 + \ln \frac{2}{r} \right) + \frac{r^2}{16} \theta \sin 2\theta, \quad (\text{B.7})$$

$$Q = -0.0386 + \frac{1}{2} \ln \left(\frac{2}{r} \right) + \frac{1}{3\sqrt{2}} r \cos \theta. \quad (\text{B.8})$$

The numerical values 0.6728 and -0.0386 in equations (B.7) and (B.8) can be derived from the full definitions of P and Q and are defined by:

$$0.6728 = -\ln \gamma + \frac{5}{4},$$

and

$$-0.0386 = \frac{1}{4} - \frac{1}{2} \ln \gamma.$$

Appendix C

Earth return currents according to Pollaczek

The calculation of impedances with earth return related to underground cables is treated by Felix Pollaczek [31], [32]. Three cases were treated in these works:

1. the self-impedance with ground return for underground cables;
2. the mutual impedance between two separate underground cables;
3. the mutual impedance between an underground cable and an overhead conductor.

For these cases, the following expressions were given by Pollaczek [32]:

$$Z_{self} = \frac{j\omega\mu_0}{2\pi} \cdot \left[K_0 \left(\frac{R}{p} \right) - K_0 \left(\frac{2h}{p} \right) + J_{self} \right], \quad (C.1)$$

$$Z_{Muu} = \frac{j\omega\mu_0}{2\pi} \cdot \left[K_0 \left(\frac{d}{p} \right) - K_0 \left(\frac{D}{p} \right) + J_{Muu} \right], \quad (C.2)$$

$$Z_{Mu0} = \frac{j\omega\mu_0}{2\pi} \cdot [J_{Mu0}]. \quad (C.3)$$

The respective geometric terms (R , h , $h_{1,2}$, x , d and D) are shown in figure C.1. The K_0 -terms in these equations are the zero-order modified Bessel functions

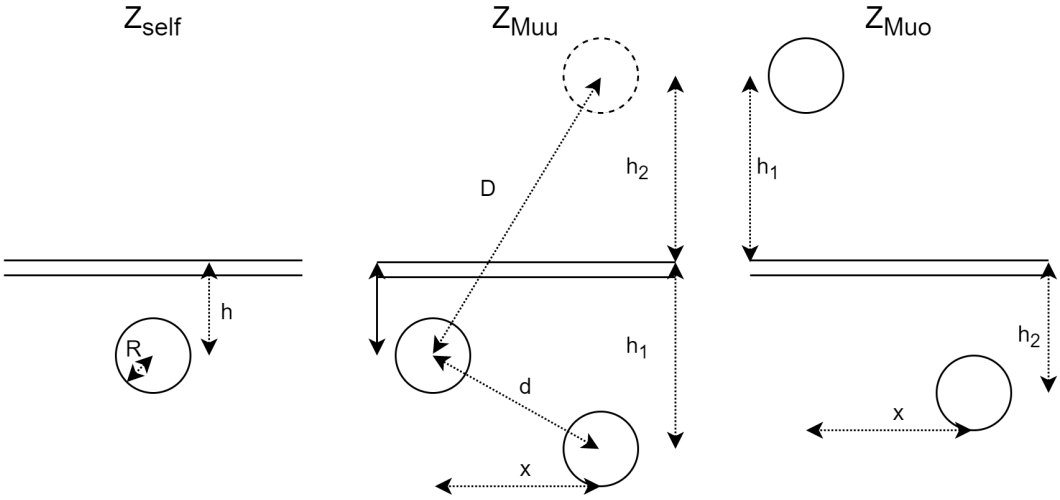


Figure C.1: Schematic representation of the geometric parameters used in Pollaczek's models for impedance with earth return. For the underground-underground model (middle situation), the distance to the image of the secondary conductor is used to calculate the mutual impedance.

of the second kind [93] and J_{self} , J_{Muu} and J_{Mu0} are the *Pollaczek integrals* for self-impedance, underground-underground mutual impedance and underground-overhead mutual impedance, respectively:

$$J_{self} = -2j \cdot \int_{-\infty}^{\infty} \frac{e^{-2h \cdot \sqrt{\beta^2 + 1/p^2}}}{|\beta| + \sqrt{\beta + 1/p^2}} \cdot e^{j\beta R} d\beta, \quad (C.4)$$

$$J_{Muu} = \int_{-\infty}^{\infty} \frac{e^{-(h_1+h_2) \cdot \sqrt{\beta^2 + 1/p^2}}}{|\beta| + \sqrt{\beta + 1/p^2}} \cdot e^{j\beta x} d\beta, \quad (C.5)$$

$$J_{Mu0} = \int_{-\infty}^{\infty} \frac{e^{-h_1 \cdot |\beta|} \cdot e^{-h_2 \cdot \sqrt{\beta^2 + 1/p^2}}}{|\beta| + \sqrt{\beta + 1/p^2}} \cdot e^{j\beta x} d\beta, \quad (C.6)$$

where $p = 1/\sqrt{j\omega\mu_0\sigma}$ is the complex skin depth of the earth and β is an integration variable. The Pollaczek integrals are difficult to solve analytically, due to their oscillatory nature [94]. Pollaczek gives infinite series approximations for the integral solutions. In addition, multiple numerical and analytical approximations for particular applications were developed [33], [94].

Appendix D

Carson series definitions

The infinite series in Carson's equations are given by [30]:

$$s_2 = \frac{1}{1!2!} \left(\frac{r}{2}\right)^2 \cos 2\Theta - \frac{1}{3!4!} \left(\frac{r}{2}\right)^6 \cos 6\Theta + \dots, \quad (\text{D.1})$$

$$s'_2 = \frac{1}{1!2!} \left(\frac{r}{2}\right)^2 \sin 2\Theta - \frac{1}{3!4!} \left(\frac{r}{2}\right)^6 \sin 6\Theta + \dots, \quad (\text{D.2})$$

$$s_4 = \frac{1}{2!3!} \left(\frac{r}{2}\right)^2 \cos 4\Theta - \frac{1}{4!5!} \left(\frac{r}{2}\right)^6 \cos 8\Theta + \dots, \quad (\text{D.3})$$

$$s'_4 = \frac{1}{2!3!} \left(\frac{r}{2}\right)^2 \sin 4\Theta - \frac{1}{4!5!} \left(\frac{r}{2}\right)^6 \sin 8\Theta + \dots, \quad (\text{D.4})$$

$$\sigma_1 = \frac{r \cos \Theta}{3} - \frac{r^5 \cos 5\Theta}{3^2 \cdot 5^2 \cdot 7} + \frac{r^9 \cos 9\Theta}{3^2 \cdot 5^2 \cdot 7^2 \cdot 9^2 \cdot 11} + \dots, \quad (\text{D.5})$$

$$\sigma_3 = \frac{r^3 \cos 3\Theta}{3^2 \cdot 5} - \frac{r^7 \cos 7\Theta}{3^2 \cdot 5^2 \cdot 7^2 \cdot 9} + \frac{r^{11} \cos 11\Theta}{3^2 \cdot 5^2 \cdot 7^2 \cdot 9^2 \cdot 11^2 \cdot 13} + \dots, \quad (\text{D.6})$$

$$\sigma_2 = \left(1 + \frac{1}{2} - \frac{1}{4}\right) \frac{1}{1!2!} \left(\frac{r}{2}\right)^2 \cos 2\Theta - \left(1 + \frac{1}{2} + \frac{1}{3} + \frac{1}{4} - \frac{1}{8}\right) \frac{1}{3!4!} \left(\frac{r}{2}\right)^6 \cos 6\Theta + \dots$$

$$\left(\approx \frac{5}{4}s_2\right), \quad (\text{D.7})$$

$$\begin{aligned}
 \sigma_4 = & \left(1 + \frac{1}{2} + \frac{1}{3} - \frac{1}{6}\right) \frac{1}{2!3!} \left(\frac{r}{2}\right)^4 \cos 4\Theta \\
 & - \left(1 + \frac{1}{2} + \frac{1}{3} + \frac{1}{4} + \frac{1}{5} - \frac{1}{10}\right) \frac{1}{4!5!} \left(\frac{r}{2}\right)^8 \cos 8\Theta + \dots \\
 & \left(\approx \frac{5}{3}s_4\right). \quad (\text{D.8})
 \end{aligned}$$

Appendix E

EMTP model of parallel circuit transmission line

The transmission line that was studied in the first case study of Chapter 5 was modeled as an EMTP-ATP model using the software ATPDraw (Version 7.2) using ATP version WATATP01. The transmission line was modeled as a Line Constants model with the following input parameters:

- Length: 23.3 km (between substation Alpha and Gamma) and 42.4 km (between substations Gamma and Beta).
- Phase conductor type: AMS620.
- Phase conductor bundling: 4 bundled conductors, 10 cm separated.
- Lightning wire type: HAWK.
- Transpositions: No.
- Geometry: See figure E.1, according to specifications transmission line owner.
- Phase ordering: See figure E.2, according to specifications transmission line owner.
- Ground resistivity: 20 Ωm .
- Model type: PI model.

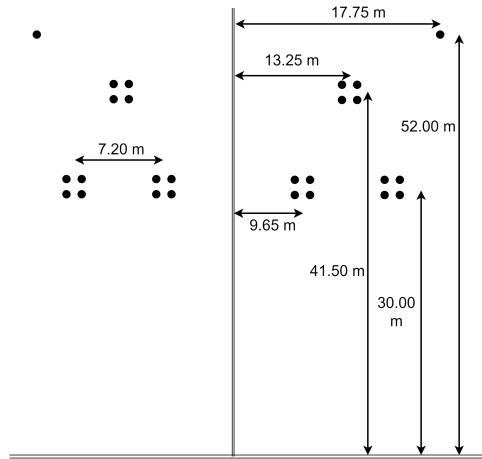


Figure E.1: Geometry of the transmission line used as input for the EMTP model. Note that the phase conductors have been modeled as four-bundles.

- Frequency: 50 Hz.
- Voltage: 380 kV RMS phase-to-phase
- Positive-sequence current: 100 A - 2500 A.

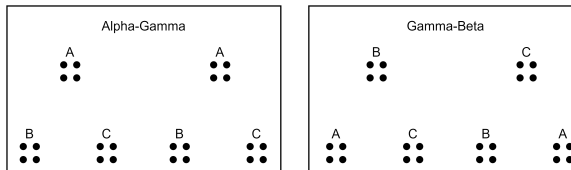


Figure E.2: Phase ordering of the transmission line used as input for the EMTP model between substations Alpha en Gamma (left side) and Gamma and Beta (right side).

Figure E.3 shows the implementation of the model in the ATPDraw application. The model makes the following assumptions:

- The busbar at the intermediate substation does not connect both circuits.
- There is no load present at the intermediate substation.
- The generator is an ideal balanced three-phase voltage generator.

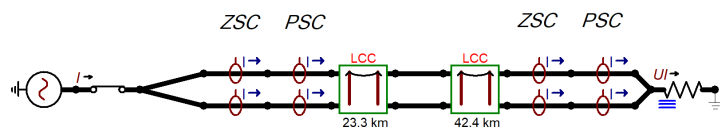


Figure E.3: Implementation of the model in ATPDraw

- The load is an ideal balanced three-phase resistive load of which the impedances are matched to lead to the desired positive-sequence currents.
- Insulator lengths: 6.00 m
- Conductor sag: 10.00 m

Note that no positive-sequence currents smaller than 100 A could be modeled due to the capacitive current in the transmission line in the radially modeled configuration.

The different positive-sequence currents were simulated by varying the loads at the receiving side of the model. A lookup table was made that establishes the relationship between the average positive-sequence current in the transmission line with the associated circulating zero-sequence current unbalance factor. This way, a model prediction of circulating zero-sequence current unbalance can be made on the basis of measured positive-sequence currents.

Appendix **F**

Error propagation in unbalance factors

The measurement uncertainty in the unbalance factors m_{0c} and m_{0t} can be determined from the definitions of these factors [21]:

$$m_{c0} = |\tilde{m}_{c0}| = \left| \frac{I_0^I - I_0^{II}}{I_1^I + I_1^{II}} \right| \times 100\%, \quad (\text{F.1})$$

and

$$m_{t0} = |\tilde{m}_{t0}| = \left| \frac{I_0^I + I_0^{II}}{I_1^I + I_1^{II}} \right| \times 100\%, \quad (\text{F.2})$$

where \tilde{m}_{c0} and \tilde{m}_{t0} are the complex-valued outcomes of the respective divisions.

Since the zero-sequence and positive-sequence current terms in these expressions are complex numbers, the expressions for measurement uncertainty of complex-valued functions will need to be used [90]:

$$u(\text{Re}(\tilde{m}_{c0}))^2 = u(\text{Re}(I_0^I))^2 \cdot \left| \frac{\partial \tilde{m}_{c0}}{\partial I_0^I} \right|^2 + u(\text{Re}(I_0^{II}))^2 \cdot \left| \frac{\partial \tilde{m}_{c0}}{\partial I_0^{II}} \right|^2 + \\ u(\text{Re}(I_1^I))^2 \cdot \left| \frac{\partial \tilde{m}_{c0}}{\partial I_1^I} \right|^2 + u(\text{Re}(I_1^{II}))^2 \cdot \left| \frac{\partial \tilde{m}_{c0}}{\partial I_1^{II}} \right|^2. \quad (\text{F.3})$$

A similar expression can be constructed for the uncertainty about the imaginary part of \tilde{m}_{c0} and the uncertainty about the real and imaginary parts of \tilde{m}_{t0} .

The partial derivatives in F.3 are as follows:

$$\left| \frac{\partial \tilde{m}_{c0}}{\partial I_0^I} \right| = \left| \frac{\partial \tilde{m}_{c0}}{\partial I_0^{II}} \right| = \frac{1}{|I_1^I + I_1^{II}|} \times 100\%, \quad (\text{F.4a})$$

$$\left| \frac{\partial \tilde{m}_{c0}}{\partial I_1^I} \right| = \left| \frac{\partial \tilde{m}_{c0}}{\partial I_1^{II}} \right| = \frac{|I_0^I - I_0^{II}|}{|I_1^I + I_1^{II}|^2} \times 100\%. \quad (\text{F.4b})$$

However, since during normal operation the fraction $\frac{|I_0^I - I_0^{II}|}{|I_1^I + I_1^{II}|^2} \ll 1$, the third and fourth terms in (F.3) contribute a negligible amount to the total uncertainty in m_{c0} and m_{t0} and can therefore be neglected.

The uncertainty about the magnitude of m_{c0} can be expressed as [84]:

$$u(m_{c0}) = u(|\tilde{m}_{c0}|) = \sqrt{u(\text{Re}(\tilde{m}_{c0}))^2 + u(\text{Im}(\tilde{m}_{c0}))^2}. \quad (\text{F.5})$$

We can now collect all the terms in this expression and use (F.5) to determine the final expression for the uncertainty about m_{c0} and m_{t0} :

$$u(m_{c0}) = u(m_{t0}) = \sqrt{u(|I_0^I|)^2 \cdot \frac{1}{|I_1^I + I_1^{II}|^2} + u(|I_0^{II}|)^2 \cdot \frac{1}{|I_1^I + I_1^{II}|^2}} \times 100\%, \quad (\text{F.6})$$

where $u(|I_0^I|)$ and $u(|I_0^{II}|)$ are the outcomes of the expressions for the uncertainties about $|I_0|$ as developed in chapter 3.

Bibliography

- [1] S. Rinaldi, J. Peerenboom, and T. Kelly, "Identifying, understanding, and analyzing critical infrastructure interdependencies", *IEEE Control Systems Magazine*, vol. 21, no. 6, pp. 11–25, Dec. 2001, ISSN: 1941-000X. DOI: [10.1109/37.969131](https://doi.org/10.1109/37.969131).
- [2] M. Nijhuis, M. Gibescu, and J. F. G. Cobben, "Assessment of the impacts of the renewable energy and ICT driven energy transition on distribution networks", *Renewable and Sustainable Energy Reviews*, vol. 52, pp. 1003–1014, Dec. 2015, ISSN: 1364-0321. DOI: [10.1016/j.rser.2015.07.124](https://doi.org/10.1016/j.rser.2015.07.124).
- [3] L. Tawney, R. Greenspan Bell, and M. Ziegler, *High Wire Act - Electricity Transmission Infrastructure and Its Impact on the Renewable Energy Market*. Washington, DC: World Resources Institute, 2011, ISBN: 978-1-56973-764-4.
- [4] International Energy Agency, "The Power of Transformation: Wind, Sun and the Economics of Flexible Power Systems", Paris, Tech. Rep., 2014.
- [5] H. Priemus, "Development and Design of Large Infrastructure Projects: Disregarded Alternatives and Issues of Spatial Planning", *Environment and Planning B: Planning and Design*, vol. 34, no. 4, pp. 626–644, Aug. 2007, ISSN: 0265-8135. DOI: [10.1068/b32109](https://doi.org/10.1068/b32109).
- [6] H. W. Ott, *Electromagnetic Compatibility Engineering*. John Wiley & Sons, Ltd, 2009.
- [7] Coenen, M.J., Goedbloed, J.J., and Integrated Circuits, *Electromagnetic Compatibility*. Mybusinessmedia B.V., 2010.

- [8] M. Grau Novellas, "On-chip interference studies from a propagative perspective: Implications of technology choices on the EMC performance of ICs", PhD Thesis, Eindhoven University of Technology, Eindhoven, 2018.
- [9] J. van Waes, "Safety and EMC aspects of grounding: Experimental studies in high-power systems", PhD Thesis, Eindhoven University of Technology, Eindhoven, 2003.
- [10] IEC, "IEC 61000-1-1 Electromagnetic Compatibility (EMC)", Standard IEC 61000-1-1.
- [11] F. Provoost, "Intelligent Distribution Network Design", PhD Thesis, Eindhoven University of Technology, Eindhoven, 2009.
- [12] M. Ovaere, E. Heylen, S. Proost, G. Deconinck, and D. Van Hertem, "How detailed value of lost load data impact power system reliability decisions", *Energy Policy*, vol. 132, pp. 1064–1075, Sep. 2019, ISSN: 0301-4215. DOI: [10.1016/j.enpol.2019.06.058](https://doi.org/10.1016/j.enpol.2019.06.058).
- [13] A. E. Shadare, M. N. Sadiku, and S. M. Musa, "Electromagnetic compatibility issues in critical smart grid infrastructure", *IEEE Electromagnetic Compatibility Magazine*, vol. 6, no. 4, pp. 63–70, 2017, ISSN: 2162-2272. DOI: [10.1109/MEMC.0.8272283](https://doi.org/10.1109/MEMC.0.8272283).
- [14] S. Nauta, R. Serra, B. Baum, and M. van Riet, "Towards an integral EMC test of intelligent Ring Main Units", in *CIGRE 2019*, Madrid, 2019, ISBN: 978-2-9602415-0-1. DOI: <http://dx.doi.org/10.34890/576>.
- [15] Cigré Working Group 36.02, "Guide on the Influence of High Voltage AC Power Systems on Metallic Pipelines", Paris, Cigré Technical Brochure TB95, 1995.
- [16] CIGRE/CIGRE JWG C4.2.02, "AC Corrosion on Metallic Pipelines Due to Interference from AC Power Lines", Paris, Cigré Technical Brochure TB290, 2006.
- [17] R. M. Paulussen and R. Koopal, "Increasing EMC on International Conventional Railways: A Practical Implementation", in *2018 International Symposium on Electromagnetic Compatibility (EMC EUROPE)*, Aug. 2018, pp. 248–250. DOI: [10.1109/EMCEurope.2018.8485017](https://doi.org/10.1109/EMCEurope.2018.8485017).

- [18] C. A. Marshman, "EMC in railways", in *IET 13th Professional Development Course on Electric Traction Systems*, Nov. 2014, pp. 1–8. DOI: [10.1049/cp.2014.1440](https://doi.org/10.1049/cp.2014.1440).
- [19] R. D. White, "Managing infrastructure EMC", in *2009 IET Seminar on EMC in Railways*, Feb. 2009, pp. 1–25. DOI: [10.1049/ic.2009.0110](https://doi.org/10.1049/ic.2009.0110).
- [20] C. L. Fortescue, "Method of Symmetrical Co-Ordinates Applied to the Solution of Polyphase Networks", *Transactions of the American Institute of Electrical Engineers*, vol. XXXVII, no. 2, pp. 1027–1140, Jul. 1918, ISSN: 0096-3860. DOI: [10.1109/T-AIEE.1918.4765570](https://doi.org/10.1109/T-AIEE.1918.4765570).
- [21] M. H. Hesse, "Circulating Currents in Paralleled Untransposed Multicircuit Lines: II - Methods for Estimating Current Unbalance", *IEEE Transactions on Power Apparatus and Systems*, vol. PAS-85, no. 7, pp. 812–820, Jul. 1966, ISSN: 0018-9510. DOI: [10.1109/TPAS.1966.291709](https://doi.org/10.1109/TPAS.1966.291709).
- [22] "Electromagnetic compatibility (EMC) - Part 3-13: Limits - Assessment of emission limits for the connection of unbalanced installations to MV, HV and EHV power systems", Standard IEC 61000-3-13:2008, 2008.
- [23] J. C. Das, *Understanding Symmetrical Components for Power System Modeling*, English, ser. IEEE Press Series on Power Engineering. Wiley-IEEE Press, 2017, ISBN: 978-1-119-22689-5.
- [24] J. J. Grainger and W. D. Stevenson, *Power System Analysis*. McGraw-Hill, 1994.
- [25] P. Anderson, *Analysis of Faulted Power Systems*, ser. IEEE Press Series on Power Engineering 11. 1995.
- [26] A. Kalyuzhny and G. Kushnir, "Analysis of Current Unbalance In Transmission Systems With Short Lines", vol. 22, May 2007. DOI: [10.1109/TPWRD.2006.883011](https://doi.org/10.1109/TPWRD.2006.883011).
- [27] F. Kiessling, P. Nefzger, J. Nolasco, and U. Kaintzyk, *Overhead Power Lines - Planning, Design, Construction*, ser. Power Systems. Springer, 2003.
- [28] A. Hochrainer, *Symmetrische Komponenten in Drehstromsystemen*. Springer-Verlag, 1957.
- [29] J. R. Carson, "Ground return impedance: Underground wire with earth return", *The Bell System Technical Journal*, vol. 8, no. 1, pp. 94–98, Jan. 1929, ISSN: 0005-8580. DOI: [10.1002/j.1538-7305.1929.tb02307.x](https://doi.org/10.1002/j.1538-7305.1929.tb02307.x).

- [30] J. R. Carson, "Wave propagation in overhead wires with ground return", *The Bell System Technical Journal*, vol. 5, no. 4, pp. 539–554, Oct. 1926, ISSN: 0005-8580. DOI: [10.1002/j.1538-7305.1926.tb00122.x](https://doi.org/10.1002/j.1538-7305.1926.tb00122.x).
- [31] F. Pollaczek, "Über das Feld einer unendlich langen wechselstromdurchflossenen Einfachleitung", *Elektrische Nachrichten Technik*, vol. 3, pp. 339–359, 1926.
- [32] —, "Über die induktionswirkungen einer wechselstrom-einfachleitung", *Elektrische Nachrichten Technik*, vol. 4, no. 1, pp. 18–30, 1927.
- [33] O. Saad, G. Gaba, and M. Giroux, "A closed-form approximation for ground return impedance of underground cables", *IEEE Transactions on Power Delivery*, vol. 11, no. 3, pp. 1536–1545, Jul. 1996, ISSN: 1937-4208. DOI: [10.1109/61.517514](https://doi.org/10.1109/61.517514).
- [34] D. Woodhouse, "On the theoretical basis of Carson's equations", in *2012 IEEE International Conference on Power System Technology (POWERCON)*, Oct. 2012, pp. 1–6. DOI: [10.1109/PowerCon.2012.6401356](https://doi.org/10.1109/PowerCon.2012.6401356).
- [35] D. Woodhouse, W. Tocher, and M. Bale, "How does current flow in the ground?", in *2016 Down to Earth Conference (DTEC)*, Sep. 2016, pp. 1–7. DOI: [10.1109/DTEC.2016.7731304](https://doi.org/10.1109/DTEC.2016.7731304).
- [36] R. Rüdtenberg, *Transient Performance of Electric Power Systems: Phenomena in Lumped Networks*. McGraw-Hill, 1950.
- [37] M. H. Hesse, "Circulating Currents in Paralleled Untransposed Multicircuit Lines: I - Numerical Evaluations", *IEEE Transactions on Power Apparatus and Systems*, vol. PAS-85, no. 7, pp. 802–811, Jul. 1966, ISSN: 0018-9510. DOI: [10.1109/TPAS.1966.291708](https://doi.org/10.1109/TPAS.1966.291708).
- [38] B. Li, J. He, Y. Li, and Y. Zheng, "Multi-circuit transmission lines", in *Protection Technologies of Ultra-High-Voltage AC Transmission Systems*, Elsevier, 2020, pp. 189–213, ISBN: 978-0-12-816205-7. DOI: [10.1016/B978-0-12-816205-7.00011-X](https://doi.org/10.1016/B978-0-12-816205-7.00011-X).
- [39] B. Li, X. Li, and Z. Bo, "Unbalanced Circulating Current of Double-Circuit Transmission Lines", in *2011 Asia-Pacific Power and Energy Engineering Conference*, Mar. 2011, pp. 1–4. DOI: [10.1109/APPEEC.2011.5748643](https://doi.org/10.1109/APPEEC.2011.5748643).

- [40] B. Li, F. Guo, X. Li, and Z. Bo, "Circulating Unbalanced Currents of EHV/UHV Untransposed Double-Circuit Lines and Their Influence on Pilot Protection", *IEEE Transactions on Power Delivery*, vol. 29, no. 2, pp. 825–833, Apr. 2014, ISSN: 0885-8977. DOI: [10.1109/TPWRD.2013.2286092](https://doi.org/10.1109/TPWRD.2013.2286092).
- [41] S. Song, J. Shi, C. Huang, L. Gao, Q. Bu, and Y. Yuan, "Method for estimating unbalanced currents in untransposed double-circuit lines on the same tower", in *International Conference on Renewable Power Generation (RPG 2015)*, Oct. 2015, pp. 1–6. DOI: [10.1049/cp.2015.0321](https://doi.org/10.1049/cp.2015.0321).
- [42] J. Zhou, D. You, S. Lu, and Z. Shu, "Analysis of unbalanced current in a 220kV short double-circuit line", in *2015 5th International Conference on Electric Utility Deregulation and Restructuring and Power Technologies (DRPT)*, Nov. 2015, pp. 306–311. DOI: [10.1109/DRPT.2015.7432247](https://doi.org/10.1109/DRPT.2015.7432247).
- [43] T. Gönen and M. S. Haj-Mohamadi, "Electromagnetic Unbalance Of Untransposed And Transposed Transmission Lines With "N" Overhead Ground Wires", *COMPEL - The international journal for computation and mathematics in electrical and electronic engineering*, vol. 7, no. 3, pp. 107–122, Jan. 1988, ISSN: 0332-1649. DOI: [10.1108/eb010043](https://doi.org/10.1108/eb010043).
- [44] J. Švec and J. Ehrenberger, "Analysis of current unbalance in meshed transmission system", in *2015 16th International Scientific Conference on Electric Power Engineering (EPE)*, May 2015, pp. 320–324. DOI: [10.1109/EPE.2015.7161081](https://doi.org/10.1109/EPE.2015.7161081).
- [45] J. Ehrenberger and J. Švec, "Evaluation of overhead lines current unbalance in meshed grids and its reduction", *Journal of Modern Power Systems and Clean Energy*, pp. 1–9, Mar. 2018, ISSN: 2196-5625, 2196-5420. DOI: [10.1007/s40565-018-0387-3](https://doi.org/10.1007/s40565-018-0387-3).
- [46] W. A. Thue, *Electrical Power Cable Engineering*, ser. Power Engineering Vol. 7. New York: CRC Press, 1999, ISBN: 978-0-8247-9976-2.
- [47] A. Ametani, "A General Formulation of Impedance and Admittance of Cables", *IEEE Transactions on Power Apparatus and Systems*, vol. PAS-99, no. 3, pp. 902–910, May 1980, ISSN: 0018-9510. DOI: [10.1109/TPAS.1980.319718](https://doi.org/10.1109/TPAS.1980.319718).
- [48] J. D. Jackson, *Classical Electrodynamics*, Third. John Wiley & Sons, Inc, 1999.

- [49] W. A. Lewis and G. D. Allen, "Symmetrical-Component Circuit Constants and Neutral Circulating Currents for Concentric-Neutral Underground Distribution Cables", *IEEE Transactions on Power Apparatus and Systems*, vol. PAS-97, no. 1, pp. 191–199, Jan. 1978, ISSN: 0018-9510. DOI: [10.1109/TPAS.1978.354469](https://doi.org/10.1109/TPAS.1978.354469).
- [50] H. Nakanishi, H. Inoguchi, I. Hashimoto, Y. Ito, H. Takehana, N. Nagaoka, and A. Ametani, "A study of zero-sequence current induced in a cable system", *IEEE Transactions on Power Delivery*, vol. 6, no. 4, pp. 1352–1358, Oct. 1991, ISSN: 0885-8977. DOI: [10.1109/61.97663](https://doi.org/10.1109/61.97663).
- [51] G. Karady, C. Nunez, and R. Raghavan, "The feasibility of magnetic field reduction by phase relationship optimization in cable systems", *IEEE Transactions on Power Delivery*, vol. 13, no. 2, pp. 647–654, Apr. 1998, ISSN: 1937-4208. DOI: [10.1109/61.660956](https://doi.org/10.1109/61.660956).
- [52] G. L. Skibinski, B. Brown, and M. Christini, "Effect of Cable Geometry on Induced Zero Sequence Ground Currents with High Power Converters", in *2006 Record of Conference Papers - IEEE Industry Applications Society 53rd Annual Petroleum and Chemical Industry Conference*, Sep. 2006, pp. 1–11. DOI: [10.1109/PCICDN.2006.359703](https://doi.org/10.1109/PCICDN.2006.359703).
- [53] A. Hafner, M. Luz, and W. Carpes Jr, *Impedance and Admittance Calculations of a Three-Core Power Cable by the Finite Element Method*. Jun. 2015. DOI: [10.13140/RG.2.1.4873.5848](https://doi.org/10.13140/RG.2.1.4873.5848).
- [54] G. Johnson, M. Schroeder, and G. Dalke, "A Review of System Grounding Methods and Zero Sequence Current Sources", in *2008 61st Annual Conference for Protective Relay Engineers*, Apr. 2008, pp. 35–71. DOI: [10.1109/CPRE.2008.4515046](https://doi.org/10.1109/CPRE.2008.4515046).
- [55] A. D. Kolagar, P. Hamedani, and A. Shoulaie, "The effects of transformer connection type on voltage and current unbalance propagation", in *2012 3rd Power Electronics and Drive Systems Technology (PEDSTC)*, Feb. 2012, pp. 308–314. DOI: [10.1109/PEDSTC.2012.6183346](https://doi.org/10.1109/PEDSTC.2012.6183346).
- [56] L. Fekih-Ahmed, "Necessary and sufficient conditions for load balance in three-phase power systems", in *1996 IEEE International Symposium on Circuits*

- and Systems. Circuits and Systems Connecting the World. ISCAS 96*, vol. 1, May 1996, 645–648 vol.1. DOI: [10.1109/ISCAS.1996.540030](https://doi.org/10.1109/ISCAS.1996.540030).
- [57] M. Pokorny, “Analysis of unbalance due to asymmetrical loads”, *Iranian Journal of electrical and computer engineering*, vol. 4, no. 1, pp. 50–56, Jan. 2005.
- [58] D. J. Griffiths, *Introduction to electrodynamics*. Pearson, 1999, ISBN: 978-0-321-85656-2.
- [59] T. A. Papadopoulos, G. C. Christoforidis, D. D. Micu, and L. Czumbil, “Medium-voltage cable inductive coupling to metallic pipelines: A comprehensive study”, in *2014 49th International Universities Power Engineering Conference (UPEC)*, Sep. 2014, pp. 1–6. DOI: [10.1109/UPEC.2014.6934713](https://doi.org/10.1109/UPEC.2014.6934713).
- [60] J. G. Rao and A. K. Pradhan, “Accurate Phasor Estimation During Power Swing”, *IEEE Transactions on Power Delivery*, vol. 31, no. 1, pp. 130–137, Feb. 2016, ISSN: 1937-4208. DOI: [10.1109/TPWRD.2015.2441132](https://doi.org/10.1109/TPWRD.2015.2441132).
- [61] S. M. Hashemi and M. Sanaye-Pasand, “Distance Protection During Asymmetrical Power Swings: Challenges and Solutions”, *IEEE Transactions on Power Delivery*, vol. 33, no. 6, pp. 2736–2745, Dec. 2018, ISSN: 1937-4208. DOI: [10.1109/TPWRD.2018.2816304](https://doi.org/10.1109/TPWRD.2018.2816304).
- [62] D. D. Micu, G. C. Christoforidis, and L. Czumbil, “AC interference on pipelines due to double circuit power lines: A detailed study”, *Electric Power Systems Research*, vol. 103, no. Supplement C, pp. 1–8, Oct. 2013, ISSN: 0378-7796. DOI: [10.1016/j.epsr.2013.04.008](https://doi.org/10.1016/j.epsr.2013.04.008).
- [63] K. Dasgupta and S. A. Soman, “Estimation of zero sequence parameters of mutually coupled transmission lines from synchrophasor measurements”, *Transmission Distribution IET Generation*, vol. 11, no. 14, pp. 3539–3547, 2017, ISSN: 1751-8695. DOI: [10.1049/iet-gtd.2017.0057](https://doi.org/10.1049/iet-gtd.2017.0057).
- [64] M. Asprou, E. Kyriakides, and M. M. Albu, “Uncertainty Bounds of Transmission Line Parameters Estimated From Synchronized Measurements”, *IEEE Transactions on Instrumentation and Measurement*, vol. 68, no. 8, pp. 2808–2818, Aug. 2019, ISSN: 1557-9662. DOI: [10.1109/TIM.2018.2867966](https://doi.org/10.1109/TIM.2018.2867966).

- [65] M. Asprou, E. Kyriakides, and M. Albu, "The effect of PMU measurement chain quality on line parameter calculation", in *2017 IEEE International Instrumentation and Measurement Technology Conference (I2MTC)*, May 2017, pp. 1–6. DOI: [10.1109/I2MTC.2017.7969757](https://doi.org/10.1109/I2MTC.2017.7969757).
- [66] D. Ritzmann, P. S. Wright, W. Holderbaum, and B. Potter, "A Method for Accurate Transmission Line Impedance Parameter Estimation", *IEEE Transactions on Instrumentation and Measurement*, vol. 65, no. 10, pp. 2204–2213, Oct. 2016, ISSN: 1557-9662. DOI: [10.1109/TIM.2016.2556920](https://doi.org/10.1109/TIM.2016.2556920).
- [67] A. Mingotti, L. Peretto, R. Tinarelli, and K. Yiğit, "Simplified Approach to Evaluate the Combined Uncertainty in Measurement Instruments for Power Systems", *IEEE Transactions on Instrumentation and Measurement*, vol. 66, no. 9, pp. 2258–2265, Sep. 2017, ISSN: 1557-9662. DOI: [10.1109/TIM.2017.2677620](https://doi.org/10.1109/TIM.2017.2677620).
- [68] P. A. Pegoraro and S. Sulis, "Robustness-Oriented Meter Placement for Distribution System State Estimation in Presence of Network Parameter Uncertainty", *IEEE Transactions on Instrumentation and Measurement*, vol. 62, no. 5, pp. 954–962, May 2013. DOI: [10.1109/TIM.2013.2243502](https://doi.org/10.1109/TIM.2013.2243502).
- [69] A. Xue, F. Xu, K. E. Martin, H. You, J. Xu, L. Wang, and G. Wei, "Robust Identification Method for Transmission Line Parameters That Considers PMU Phase Angle Error", *IEEE Access*, vol. 8, pp. 86 962–86 971, 2020, ISSN: 2169-3536. DOI: [10.1109/ACCESS.2020.2992247](https://doi.org/10.1109/ACCESS.2020.2992247).
- [70] F. Messina, P. Marchi, L. R. Vega, C. G. Galarza, and H. Laiz, "A Novel Modular Positive-Sequence Synchrophasor Estimation Algorithm for PMUs", *IEEE Transactions on Instrumentation and Measurement*, vol. 66, no. 6, pp. 1164–1175, Jun. 2017, ISSN: 1557-9662. DOI: [10.1109/TIM.2016.2637578](https://doi.org/10.1109/TIM.2016.2637578).
- [71] V. Milojević, S. Čalija, G. Rietveld, M. V. Ačanski, and D. Colangelo, "Utilization of PMU Measurements for Three-Phase Line Parameter Estimation in Power Systems", *IEEE Transactions on Instrumentation and Measurement*, vol. 67, no. 10, pp. 2453–2462, Oct. 2018, ISSN: 1557-9662. DOI: [10.1109/TIM.2018.2843098](https://doi.org/10.1109/TIM.2018.2843098).

- [72] C. Wang, V. A. Centeno, K. D. Jones, and D. Yang, "Transmission Lines Positive Sequence Parameters Estimation and Instrument Transformers Calibration Based on PMU Measurement Error Model", *IEEE Access*, vol. 7, pp. 145 104–145 117, 2019, ISSN: 2169-3536. DOI: [10.1109/ACCESS.2019.2944818](https://doi.org/10.1109/ACCESS.2019.2944818).
- [73] H. Zhou, X. Zhao, D. Shi, H. Zhao, and C. Jing, "Calculating sequence impedances of transmission line using PMU measurements", in *2015 IEEE Power Energy Society General Meeting*, Jul. 2015, pp. 1–5. DOI: [10.1109/PESGM.2015.7285981](https://doi.org/10.1109/PESGM.2015.7285981).
- [74] M. Zhou, V. Centeno, J. S. Thorp, and A. G. Phadke, "Calibrating Instrument Transformers with Phasor Measurements", *Electric Power Components and Systems*, vol. 40, no. 14, pp. 1605–1620, Oct. 2012, ISSN: 1532-5008. DOI: [10.1080/15325008.2012.707290](https://doi.org/10.1080/15325008.2012.707290).
- [75] P. Chatterjee, A. Pal, J. S. Thorp, J. D.L. R. Lopez, and V. A. Centeno, "Error reduction of phasor measurement unit data considering practical constraints", *IET Generation, Transmission & Distribution*, vol. 12, no. 10, pp. 2332–2339, Feb. 2018, ISSN: 1751-8695. DOI: [10.1049/iet-gtd.2017.1359](https://doi.org/10.1049/iet-gtd.2017.1359).
- [76] S. Ziegler, R. C. Woodward, H. H. Iu, and L. J. Borle, "Current Sensing Techniques: A Review", *IEEE Sensors Journal*, vol. 9, no. 4, pp. 354–376, Apr. 2009. DOI: [10.1109/JSEN.2009.2013914](https://doi.org/10.1109/JSEN.2009.2013914).
- [77] S. Lin, P. Gao, and W. Xu, "Zero sequence power line current measurement by using magnetic field sensor array", *International Transactions on Electrical Energy Systems*, vol. 25, no. 9, pp. 1685–1696, 2015, ISSN: 2050-7038. DOI: [10.1002/etep.1916](https://doi.org/10.1002/etep.1916).
- [78] —, "Zero sequence power line current measurement by using magnetic field sensor array", *International Transactions on Electrical Energy Systems*, vol. 25, no. 9, pp. 1685–1696, Sep. 2015, ISSN: 2050-7038. DOI: [10.1002/etep.1916](https://doi.org/10.1002/etep.1916).
- [79] S. Nauta, R. Serra, M. van Riet, J. van Waes, P. Jansen, and R. Koopal, "Zero-sequence currents in the high-voltage grid in the Netherlands", *Cigré Session 2018*, 2018.
- [80] "Instrumentation Transformers", International Electrotechnical Commission, Standard IEC 61869, 2007.

- [81] “Instrument Transformers - Part 2: Additional requirements for current transformers”, International Electrotechnical Commission, Standard IEC 61869-2:2012, 2012.
- [82] A. G. Phadke and J. S. Thorp, *Synchronized Phasor Measurements and Their Applications*, ser. Power Electronics and Power Systems. Springer International Publishing, 2017, ISBN: 978-3-319050584-8.
- [83] S. Nauta, J. van Waes, K. Koreman, F. Provoost, M. van Riet, and R. Serra, “Measurement and analysis of zero sequence current levels during normal operation”, *25th International Conference and Exhibition on Electricity Distribution*, 2019.
- [84] K. Yhland and J. Stenarson, “A Simplified Treatment of Uncertainties in Complex Quantities”, in *2004 Conference on Precision Electromagnetic Measurements*, Jun. 2004, pp. 652–653. DOI: [10.1109/CPEM.2004.305464](https://doi.org/10.1109/CPEM.2004.305464).
- [85] BIPM, IEC, IFCC, ILAC, ISO, IUPAC, IUPAP, and OIML, “Evaluation of measurement data - Supplement 1 to the “Guide to the expression of uncertainty in measurement” - Propagation of distributions using a Monte Carlo method”, JCGM 101:2008, 2008.
- [86] M. Faifer, A. Ferrero, C. Laurano, R. Ottoboni, S. Toscani, and M. Zanoni, “An Innovative Approach to Express Uncertainty Introduced by Voltage Transformers”, *IEEE Transactions on Instrumentation and Measurement*, vol. 69, no. 9, pp. 6696–6703, Sep. 2020, ISSN: 1557-9662. DOI: [10.1109/TIM.2020.2990392](https://doi.org/10.1109/TIM.2020.2990392).
- [87] “Instrument Transformers - Part 1: General requirements”, International Electrotechnical Commission, Standard IEC 61869-1:2007, 2007.
- [88] M. Pelgrom, *Analog-to-Digital Conversion*. Springer, 2017, ISBN: 978-3-319-44971-5.
- [89] B. Hall, “Notes on complex measurement uncertainty: Part 1”, Measurements Standards Laboratory of New Zealand, Lower Hutt, New Zealand, Technical Report 2483, Nov. 2010, p. 36.
- [90] S. G. Rabinovich, *Measurement Errors and Uncertainties*. Springer Science and Media, Inc., 2005, ISBN: 978-0-387-29143-7.

-
- [91] J. Verboomen, D. V. Hertem, P. H. Schavemaker, W. L. Kling, and R. Belmans, "Phase shifting transformers: Principles and applications", in *2005 International Conference on Future Power Systems*, Nov. 2005, pp.1–6. DOI: [10.1109/FPS.2005.204302](https://doi.org/10.1109/FPS.2005.204302).
- [92] S. M. Hashemi and M. Sanaye-Pasand, "Distance Protection During Asymmetrical Power Swings: Challenges and Solutions", *IEEE Transactions on Power Delivery*, vol. 33, no. 6, pp. 2736–2745, Dec. 2018, ISSN: 1937-4208. DOI: [10.1109/TPWRD.2018.2816304](https://doi.org/10.1109/TPWRD.2018.2816304).
- [93] G. B. Arfken, H. J. Weber, and F. E. Harris, "Chapter 14 - Bessel Functions", en, in *Mathematical Methods for Physicists (Seventh Edition)*, G. B. Arfken, H. J. Weber, and F. E. Harris, Eds., Boston: Academic Press, Jan. 2013, pp. 643–713, ISBN: 978-0-12-384654-9. DOI: [10.1016/B978-0-12-384654-9.00014-1](https://doi.org/10.1016/B978-0-12-384654-9.00014-1).
- [94] X. Legrand, A. XÉmard, G. Fleury, P. Auriol, and C. A. Nucci, "A Quasi-Monte Carlo Integration Method Applied to the Computation of the Pollaczek Integral", *IEEE Transactions on Power Delivery*, vol. 23, no. 3, pp. 1527–1534, Jul. 2008, ISSN: 1937-4208. DOI: [10.1109/TPWRD.2007.909050](https://doi.org/10.1109/TPWRD.2007.909050).

List of Publications

Journal Publications

2021

S. Nauta, R. Serra, "Zero-Sequence Current Measurement Uncertainty in Three-Phase Power Systems During Normal Operation" Manuscript accepted for publication in IET Generation, Transmission & Distribution. <https://dx.doi.org/10.1049/gtd2.12254>

Conference Contributions

2020

S. Nauta, P. Kropman, F. Provoost, M. van Riet. "Experimental Investigation of Ground Return Currents and Mutual Induction in Extruded Cables" Cigré Session Paper C4-327_2020, 2020.

2019

S. Nauta, J.B.M. van Waes, K. Koreman, F. Provoost, M. van Riet, R. Serra. "Measurement and analysis of zero sequence current levels during normal operation" 25th International Conference and Exhibition on Electricity Distribution, (CIRED 2019), IFEMA, Madrid, Spain, 2019. <https://doi.org/10.34890/577>

S. Nauta, M. van Riet, B. Baum, R. Serra. "Towards an integral EMC test of intelligent Ring Main Units" 25th International Conference and Exhibition on Electricity Distribution, (CIRED 2019), IFEMA, Madrid, Spain, 2019. <https://dx.doi.org/10.34890/576>

2018

S. Nauta, R. Serra, M. van Riet, J.B.M. van Waes, P. Jansen, R. Koopal. "Zero-sequence currents in the high voltage grid in the Netherlands" Cigré Session Paper C4-103_2018, 2018.

2012

S. Nauta, M. Bosch-Rekvelde, H. Mooij. "Project Complexity in the Semiconductor Industry: A Case Study Approach" Paper presented at PMI Research and Education Conference, Limerick, Munster, Ireland. Newtown Square, PA: Project Management Institute, 2012.

2011

Y. Bilevych, V. Blanco Carballo, M. van Dijk, M. Fransen, H. van der Graaf, F. Hartjes, N. Hessey, W. Koppert, S. Nauta, M. Rogers, A. Romaniouk, R. Veenhof, "Angular resolution of the gaseous micro-pixel detector Gossip" Nuclear Physics B - Proceeding Supplements Volume 215, Issue 1, June 2011, Pages 51-55, 2011. <https://doi.org/10.1016/j.nuclphysbps.2011.03.132>

Acknowledgements

I started my PhD project in March 2016. What a journey it has been. I am proud to have reached the moment to write these acknowledgements. So, let's start. This PhD project would not have existed without the generous support of my employer Alliander. Moreover, TenneT: thanks for providing the data for Chapter 5.

Ramiro, muchas gracias for your indispensable role as supervisor and endless support throughout the years. I got to know you as a committed and passionate researcher with a lot of care for his students. I appreciated this very much. Our weekly meetings on Mondays created a rhythm and were a joy. You taught me to be an independent researcher and have always challenged me to bring out the best in myself. The plots were not always in the right color combination, but luckily this combination did not make it to the front cover. I appreciate that your door was always open when I was stuck and needed help to continue. I could not have wished for a better supervisor. You are a true hero.

Guus, many thanks for introducing me to the Eindhoven part of the research team and all that you have done as my promotor.

Sjef, Frank, Marjan, Jeroen and Wouter, thanks for your insightful feedback to the manuscript and willingness to be part of the manuscript committee.

To all the colleagues in the EES group, thanks for welcoming me in your midst during my "Eindhoven days". I appreciated all the social moments. While we worked on diverging projects, there was one thing we all agreed on: the mediocre coffee.

Dear TenneT and Prorail colleagues, you helped me to put my research findings into perspective. You showed me the practical implications of my research.

Maarten, without you this project would not have existed. Your endless energy to pursue innovation within the industry is contagious and inspiring. I admire your ability to spot talent and give people a large amount of autonomy and responsibility to achieve their goals and dreams. This gave me the opportunity to pursue my dream to obtain a PhD degree. It is my sincere hope that we will carry on this “Maarten van Riet-spirit”, since it is essential to create a sustainable energy system. The Cabernet performances were the highlight of my Cigré weeks.

Frans, George V will never be the same. Thank you for keeping us company during the conferences in Paris and Madrid. Thanks for your well-grounded feedback and valuable observations.

Dear EC colleagues, your questions about how I was doing seemed like a small favor, but meant the world to me. Your support during the harder times was immensely valuable. Michiel, thank you for your support and for the philosophical insights on science and life during our walks. Pieter, almost eight years ago we began our “beïnvloedingsberekeningen”-journey together, which ultimately led to the take-off of this trip and a number of interesting field experiments. Even if this meant driving to the Noordoostpolder of all places in the middle of the night. Thank you for starting on this journey together and for your listening ear. Let’s cheers with our own brew soon!

Kelian, Rob, Clemens, Adriaan, Huug, Jeroen, Nick: you were the backstage heroes during the field experiments and data collection. Thanks!

Willem, Mohamed, Harm, Bert Jan: it was a pleasure to supervise your bachelor end projects and graduation project.

Freek, dankjewel dat je mijn paranimf wilt zijn. In tijden van nood bel ik jou, maar we vieren ook de mooie momenten. Ook jij bent bijna aan het einde gekomen van je PhD-reis. Laten we gauw proosten op dr.ir. Pols en dr.ir. Nauta, want proosten is een goede traditie die we in ons eerste studiejaar startten. P.S. Wanneer krijg ik nou eens het recept van jouw Soto Ajam?

Hendrik/Dana, mijn favoriete Brabo: dankjewel voor al jouw ondersteuning door de jaren heen, voor onze fietstochtjes en voor alle slechte grappen waar we dan veel te hard om hebben moeten lachen. Jules, ik houd van onze filosofische bespiegelingen op Italië, literatuur en koffie. Volgend jaar gaan we meer fietsen – en ja Dana, jij mag ook mee – en hoor ik hopelijk alles over jouw promotie.

Lieve Gerard en Margo, lieve papa en mama, eigenlijk staat alles wat ik jullie wil zeggen op pagina V. Jullie zijn een voorbeeld voor mij. Renske, ik ben trots dat jij mijn lieve zus bent. Colin, Elsa, Amélie en Hugo, dank voor jullie liefde. Ik ben heel blij dat jullie weer dichtbij ons zijn. Kirsten, bedankt voor alle kaarten, tekeningen en telefoontjes.

Finally, the love of my life, partner in crime and de allerliefste: Anouk. Het moment is eindelijk daar gekomen dat ik "nu" kan antwoorden op de vraag die jij mij al een paar jaar stelt. Omdat jij ditzelfde proces hebt doorgemaakt, heb ik op jou kunnen steunen als Dora the Explorer. Ik ben je daar eeuwig dankbaar voor. Jouw kritische blik heeft mij geholpen om het beste uit mijzelf te halen en je hebt mij er bovenop geholpen op de momenten dat ik niet meer zag hoe het verder moest. Het einde van deze reis betekent het begin van een nieuwe reis met zijn drieën. Samen kunnen wij de wereld aan. Ik hou van jou.

Thanks to all my family, friends, colleagues and everyone else who was involved in this project (I have undoubtedly forgotten someone here)!

MANY THANKS!

Curriculum Vitae

Sjoerd Nauta was born on May 9, 1986 in Delft, the Netherlands. He finished his secondary education (VWO at Christelijk Lyceum Veenendaal) in 2004. After this, he started studying Applied Physics at Delft University of Technology. He received his M.Sc. degrees in Applied Physics and Management of Technology in 2010 and 2011, respectively. His final M.Sc. projects were performed at NIKHEF Amsterdam (the Dutch institute for subatomic physics) and at NXP in Nijmegen.

In 2012, he joined the Dutch grid operator Alliander as a technical trainee and since 2014 he has been working as a technical consultant with Qirion (part of Alliander), specializing in underground cable systems and in Electromagnetic Compatibility (EMC) problems in high voltage systems.

In 2016, Sjoerd Nauta started as a part-time Ph.D. candidate in the Electrical Energy Systems group at Eindhoven University of Technology. His research interest is in EMC of large scale infrastructure, with an emphasis on zero-sequence currents in high-voltage systems during normal operation. During his Ph.D. project, he presented his research at two CIGRÉ sessions in Paris, as well as at CIRED in Madrid. He is a participating member of CIGRÉ, being a member of the national committees B1 (cable systems) and C4 (system technical performance). He also supervised several bachelor theses during this period.

It is Sjoerd Nauta's ambition to continue his research work on EMC topics in large infrastructures.

